Modelling and simulation of bifacial PV modules by implementing the ray tracing technique.

by

Jobert Louw

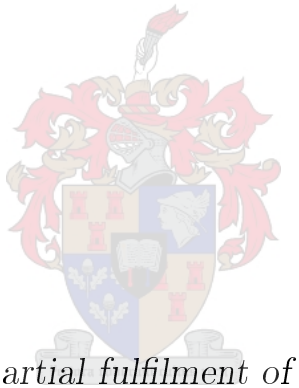

Thesis presented in partial fulfilment of the requirements for the degree of Master of Engineering (Electrical & Electronic) in the Faculty of Engineering at Stellenbosch University

Supervisor: Dr. A.J. Rix

March 2020

Declaration

By submitting this thesis electronically, I declare that the entirety of the work contained therein is my own, original work, that I am the sole author thereof (save to the extent explicitly otherwise stated), that reproduction and publication thereof by Stellenbosch University will not infringe any third party rights and that I have not previously in its entirety or in part submitted it for obtaining any qualification.

Date: March 2020 .....

Abstract

Modelling and simulation of bifacial PV modules by implementing the ray tracing technique.

J.A. Louw

Department of Electrical and Electronic Engineering,
University of Stellenbosch,
Private Bag X1, Matieland 7602, South Africa.

Thesis: MEng (E & E)

March 2020

This thesis shows how ray tracing can serve as an accurate irradiance mod-elling technique for bifacial PV modules. The electrical behaviour of bifacial modules is also modelled through investigation and development of two electri-cal models. Bifacial PV modules can increase the power output per unit area when compared to monofacial PV modules. This is made possible by exposing the PV cells of a bifacial module to the incident irradiance on the front and the rear side. This potential increase in power output allows bifacial PV to be an important role player in the growth of PV technology in the renewable energy market. In order to advance bifacial PV as the primary technology in the solar market, it is necessary to accurately model and simulate bifacial mod-ules. Existing bifacial PV simulation software mostly implements view factors which proves to be ineffective in accurately modelling the rear side irradiance of modules. There are some uncertainties regarding the electrical performance of bifacial PV, which can be significantly reduced once an accurate model is established for the technology.

An irradiance model is developed by implementing ray tracing to model the front and rear side irradiance of bifacial modules. The irradiance model is verified by comparing modelled irradiance with irradiance measurements from an experimental bifacial PV installation. Two one-diode electrical models are implemented for bifacial modules. The two models are verified by comparing modelled power with measured power of a single bifacial module in a bifacial installation. The bifacial PV simulation software is developed by integrating the irradiance and electrical models with the *python* development language.

After verification, the simulation software is used to simulate the effects of tilt angles, tracking, module height, albedo and row spacing on energy performance and bifacial gain of bifacial modules. A comparison is also done with existing commercial simulation software in order to determine the difference in accuracy between view factor and ray tracing models.

Uittreksel

Modellering en simulasie van tweesydige PV modules met implementasie van die ray tracing tegniek.

("Modelling and simulation of bifacial PV modules by implementing the ray tracing technique.")

J.A. Louw

Departement Elektriese en Elektroniese Ingenieurswese,
Universiteit van Stellenbosch,
Privaatsak X1, Matieland 7602, Suid Afrika.

Tesis: MIng (E & E)

Maart 2020

Hierdie tesis toon hoe 'raytracing'kan dien as 'n akkuratebestralingsmodel-lering tegniek vir tweesydigePV modules. Die elektriesegedrag van tweesy-digemodules word ook gemodelleer deur ondersoek en ontwikkelingvan twee elektriese modelle. TweesydigePV modules kan die krag uittreeper eenheid area vermeerder in vergelykingmet eensydige PV modules. Dit word moont-lik gemaakdeur die PV selle van 'n tweesydigemodule bloot te stel aan die inkomende bestralingvan byde die voor en agterkant.Hierdie potensiële ver-meerderingin krag uittree veroorsaakdat tweesydigePV modules 'n belangrikerol speel in die groei van PV tegnologie in die hernubare energie mark. Om sodoende tweesydigePV te vestigas die primêre tegnologie in die son ener-gie mark, word akkuratesimulasieen modellering van tweesydigePV modules benodig. Bestaandetweesydige PV simulasie sagtewareimplementeermeestal 'viewfactors'wat bewys dat dit oneffektiefis in die akkuratemodellering van die agterkantse bestraling.Daar is ook 'n reeks onsekerhede rakende die elek-triesegedrag van tweesydigePV modules, wat aansienlikverminder kan word sodra 'n akkuratemodel gevestig word.

'n Bestralingsmodel word ontwikkel deur gebruik te maak van 'ray tracing'om die voorste en agterste bestraling van tweesydige PV modules te modelleer. The bestralings model word geverifieer deur die gemodelleerde bestraling te vergelyk met bestraling soos gemeet op 'n tweesydige PV installasie. Twee een-diode elektriese modelle word geimplementeer vir tweesydige PV modules. Die twee modelle word geverifieer deur gemodelleerde krag uittreete vergelyk

met gemete krag uittree van 'n enkele tweesydige PV module in 'n tweesydige PV installasie. Die tweesydige PV simulasie sagteware word ontwikkel deur die integrasie van die bestralings en elektriese modelle met behulp van die *python* ontwikkelings taal. Na verifiëring, word die simulasie sagteware gebruik om die effekte te simuleer van kantel hoeke, opsporing, module hoogte, albedo en ry spasiëring op energie opwekking en tweesydige aanwins. 'n Vergelyking word ook getref met bestaande kommersiële simulasie sagteware om sodoende die verskil in akkuraatheid tussen 'view factor' en 'ray tracing' modelle vas te stel.

Acknowledgements

I would like to express my sincere gratitude to the following people and organisations:

Dr. Arnold Rix for leading and supporting throughout the duration of my research. Your diligence and knowledge in the field of electrical engineering and more specifically PV technology, was very helpful and much appreciated. I will be forever grateful for giving me the opportunity to complete my postgraduate studies in engineering.

Armand du Plessis for sharing his knowledge and time whenever it was needed. Ian Reischauer for his help in gathering the much needed data for this project. Thank you to the whole PV lab team for the two years of working together and sharing some fond memories.

My parents, Joos and Marian Louw, for providing me with the privilege of studying and completing an under- and postgraduate degree. I will be forever grateful and hope to make you proud in everything I pursue. To my wife, Linda Louw, you have been my pillar of support throughout my postgraduate studies. Thank you for your love and motivation which pushed me to work and achieve my goals.

Scatec Solar and Ivan Hobbs for investing in my studies. I will be forever grateful for your resources and support which made my research possible.

Dedications

Hierdie tesis word opgedra aan my vrou, Linda Louw.

Contents

List of Figures

List of Tables

Nomenclature

Units

V	Volt
A	Ampere
W	Watt
Ω	Ohm
m	Meter
s	Second
h	Hour
C	Celsius
K	Kelvin
J	Joule

Variables

G	Irradiance	W/m^2
V	Voltage	V
I	Current	A
R	Resistance	Ω
P	Power	W
E	Energy	Wh
T	Temperature	$^{\circ}C$
φ	Bifaciality factor	
BG	Bifacial gain	

Abbreviations

PV	Photovoltaic
GHI	Global Horizontal Irradiance
DNI	Direct Normal Irradiance
DHI	Diffuse Horizontal Irradiance

LCOE	Levelised Cost of Energy
RMSE	Root Mean Square Error
MBE	Mean Bias Error
MPP	Maximum Power Point
EPW	Energy Plus Weather
TMY	Typical Meteorological Year
RGB	Red Green Blue
CAD	Computer Aided Design
GUI	Graphical User Interface
N	North
S	South
E	East
W	West

Chapter 1

Introduction

As an emerging market, South Africa is highly dependent on the development of it's energy sector in order to grow the economy in a highly competitive global environment [1]. South Africa's primary energy producer is ESKOM which heavily relies on coal powered generation to supply the ever growing electricity demands of the country. In 2015, coal generation made up 59% of South Africa's energy supply with crude oil, gas, nuclear and renewables making up the rest of the market [1]. Coal reserves are subject to depletion and greatly contributes to greenhouse gas emissions, which makes renewable energy an attractive solution for South Africa's future in energy production.

In South Africa, the Renewable Energy Independent Power Producer Procurement Programme (REIPPPP) was established in 2003 which allowed for independent power producers (IPPs) to produce 30% of the energy supply [1]. In 2018, a target of 14725 MW was set to be produced by renewable energy sources by 2030, which consisted of solar PV, concentrated solar power (CSP), hydro, wind and gas [1]. The amount of 6225 MW was allocated to solar PV which is 42% of the total target [1]. As Figure 1.1 shows, solar PV contributed 1.9% to the global renewable energy market, which shows that there is large room for solar PV's future growth [2].

Conventionally, solar PV electricity generation was realised by monofacial PV modules. Monofacial modules produce electricity by converting the incident radiation on the front side of a module into electricity by harnessing the photovoltaic effect. By removing the opaque rear electrode and replacing it with a transparent glass sheet, it is possible to expose PV cells to rear side irradiance. This leads to the existence of bifacial PV modules which can potentially increase the power output for the same per unit cell area due to additional rear side irradiance.

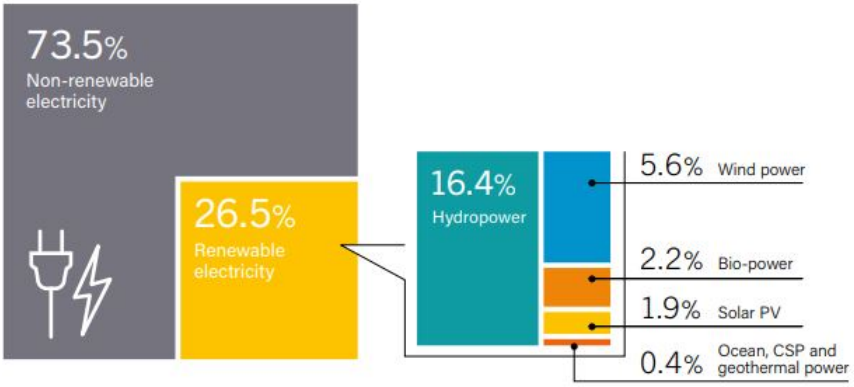

Figure 1.1: Estimated renewable energy contribution in global energy market. [2]

1.1 Bifacial PV

A key role player in solar PV's market expansion is bifacial PV. Historically, bifacial PV costs were significantly greater than that of monofacial PV. Due to numerous advances in the manufacturing process of bifacial modules, the significant difference in price between the two technologies have decreased [3]. This allowed bifacial technology to enter the solar PV market and offer a number of properties from which investors can benefit. By the end of 2017, bifacial PV only contributed 5% to the solar PV market, but this contribution is expected to grow to 40% by 2028 [4]. The main concern for the solar industry is to lower the Levelised Cost of Energy (LCOE) of PV technology as a whole. Bifacial PV can have a great impact on the LCOE of PV plants as it offers the following benefits:

- Up to 30% increase in power output [5].
- Increased power generation for the same area of land. (Increased power density)
- The same amount of PV plant equipment and construction is needed for an increased energy yield.

In a 2017 Saudi Arabia solar bid, the lowest bid came in at 1.79 US cents/kWh [4]. Although this tender was disqualified, it included bifacial technology which leads to positive and negative conclusions. A positive sign of this occurrence is that bifacial PV is at the forefront of lowering the LCOE of large scale PV plants. The negative part shows that solar PV investors are not yet convinced that bifacial technology is the way forward. This is mainly due to a lack of knowledge in some key areas where there is a shortage of field data and experimental evidence to back the technology [6]. To understand these pitfalls, it is important to look into the operation of bifacial PV cells and modules.

1.1.1 The operation of bifacial PV cells

A bifacial PV cell's operation is based on the same principles as for a monofacial PV cell: the combination of a p-n junction and the photovolatic effect. A p-n junction is formed by joining positively doped (p-type) and negatively doped (n-type) semiconductor materials (Si) as shown in Figure 1.2. The p-type material is characterized by having an excess of holes (positive charge) and the contrary being true for the n-type material having an excess of electrons (negative charge) [7].

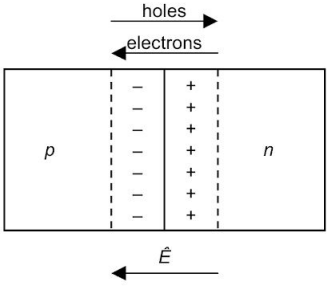

Figure 1.2: P-N junction formation. [7]

The joining of the p- and n-type material causes a flow of electrons and holes between the two materials. The remaining exposed charges causes an electric field ($\hat{E}$) to form between to the p- and n-type material known as the depletion region [7]. Once a voltage with a magnitude large enough to overcome $\hat{E}$ is applied over the junction, electrons and holes will able to flow freely and produce current. In the case of PV cells, the incident solar energy (photon energy) is applied onto the p-n junction to overcome $\hat{E}$, which leads to current flow and in effect an output voltage. This phenomenon is better known as the photovoltaic effect. Apart from the photovoltaic effect, the design and assembly of PV modules are just as important in it being a reliable source of electricity.

A monofacial PV module is formed by combining a number of individual PV cells. In high power output modules, 60 or 72 cells will most commonly be combined to deliver outputs ranging from 150-350 W. Two critical parts of any PV cells are the front and the back electrodes with both being oppositely charged. The front electrode is connected to the n-type material and therefore negatively charged. The back electrode is connected to the p-type material and is positively charged. Hence, current will be able to flow from the back electrode (positive) to the front electrode (negative) through whatever load is connected to the output terminals. As shown in Figure 1.3, the back electrode

is realised by an opaque conductor that covers the entire rear side of the cell. This is where bifacial cells are different in design.

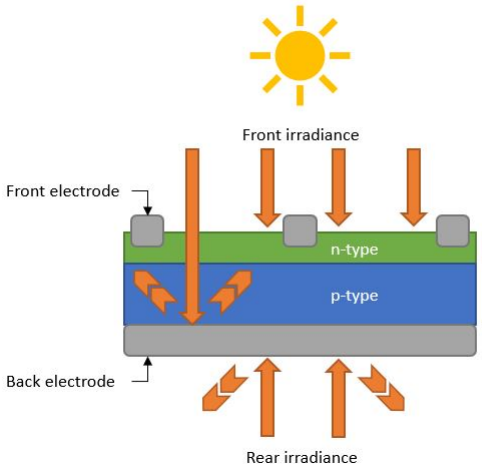

Figure 1.3: Monofacial PV cell.

A bifacial cell's ability to produce electricity is also based on the photovoltaic effect, as described for monofacial cells. The operation of bifacial PV cells are described in it's name. The prefix, 'bi-', is related to the fact that both the front and rear side's irradiance contribute to the total power output of a module. The additional active contribution is achieved by exposing the PV cell to irradiance incident on the rear side. This is made possible by replacing the opaque back electrode with grid-like contacts that are similar to the front electrode as shown in Figure 1.4 [3]. The removal of the opaque back electrode allows radiation to enter and penetrate the PV cell from the front as well as the rear. The increased radiation penetration leads to an increased flow of holes and electrons between the p- and n-type layers which increases current flow and power output. The gain in power output can vary between 5-30% and is mainly dependent on the additional rear side irradiance [5].

1.1.2 Simulation and modelling of bifacial PV

It is given that the rear side irradiance is dependent on a number of influential factors such as ground surface albedo, module elevation above the ground, spacing between adjacent rows and tilt angles [8]. In order to fully evaluate and predict the performance of bifacial PV modules, it is necessary to accurately model the complex rear side irradiance distribution. Some attempts have been made to model the rear side irradiance by means of implementing view factors, but there is evidence that this method underestimates when compared to other modelling techniques such as ray tracing [9, 10]. Ray tracing proves to be a

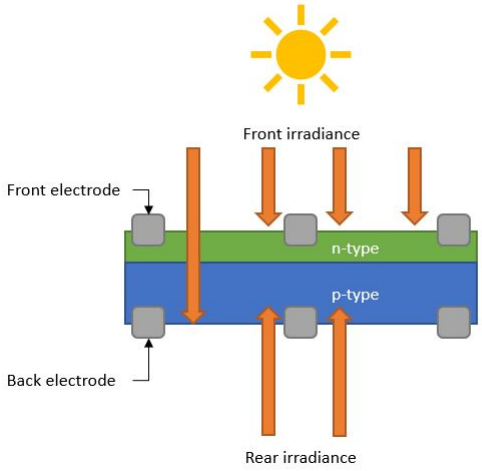

Figure 1.4: Bifacial PV cell.

technique that can model the effects of light and radiation accurately [11]. Although ray tracing is already implemented in PV simulation applications for modelling effects on a microscopic level [12], it may be of interest to implement ray tracing to model irradiance on cell and module level, and more specifically the rear side of bifacial modules [13].

For simulating the electrical behaviour of bifacial modules, the most common implementation is the $R_{sh} - R_s$ one-diode model [3]. Literature shows that this model and the parametrisation method as proposed by [14] delivers satisfying results. However, there is little to no research that shows the effectiveness of alternative methods for the electrical modelling of bifacial modules. The characterisation of bifacial modules have recently been standardised, which leaves the opportunity to investigate a parametrisation method that only requires input values as obtained by the standardised characterisation.

The overall simulation of bifacial PV can greatly help PV designers and investors to understand the technology better. Currently there are only two commercial software tools available that can simulate bifacial PV modules [3]. These tools are not yet able to simulate bifacial technology to a full extent as they are still in development and somewhat unsure if the modelling techniques are the most accurate. There are several ongoing research projects, [9, 13, 15, 16], that aim to find the most effective methods for simulating the distribution of irradiance on bifacial modules in order for PV developers to gain a better understanding of bifacial technology. There is also little research that compares the accuracy of existing simulation tools such as *PVSyst*, with alternative modelling methods and real world data.

1.2 Problem statement

It is clear that there is room for the solar PV market to grow within the global renewable energy market. Bifacial PV is expected to greatly contribute to this projected growth by offering more energy production per unit area. There are numerous uncertainties surrounding bifacial PV with regards to design optimisation, energy production and expected energy gain when compared to monofacial PV. Accurate simulation and modelling of bifacial PV can help clarify many of these uncertainties, but there is currently a shortage in PV modelling software that can accurately model the complexities of rear side irradiance and the electrical behaviour of bifacial PV. Existing software implements modelling techniques that fall short of delivering accurate and trustworthy results.

1.3 Objectives and goals

The goal for this thesis is to investigate and develop modelling software that can accurately simulate the performance and behaviour of bifacial PV modules. In order to accomplish this goal, there are two key areas that will undergo investigation and development namely, irradiance modelling and electrical modelling of bifacial modules.

1.3.1 Irradiance modelling objectives

The key focus of irradiance modelling for bifacial PV is the rear side irradiance distribution. By improving the accuracy of the modelled rear side irradiance, it will be possible to greatly improve the overall accuracy of bifacial PV simulation. The following objectives are provided for the irradiance modelling of bifacial PV:

- Investigate existing irradiance models for monofacial and bifacial PV.
- Determine the key factors that influence the rear side irradiance of PV modules.
- Investigate the possibility of implementing the ray tracing technique to model irradiance for bifacial modules.
- Design and develop a ray tracing irradiance model.
- Verify the accuracy of the developed ray tracing irradiance model by comparing modelled irradiance with measured irradiance.
- Compare the developed ray tracing model with an existing view factor model as implemented by commercial simulation software.

1.3.2 Electrical modelling objectives

In order to study and simulate the performance of bifacial modules on an energy level, it is necessary to set the following objectives with regards to the electrical modelling of bifacial PV:

- Investigate the characterisation standards for bifacial modules.
- Investigate the existing electrical models and parametrisation methods for bifacial PV and how they correspond with existing characterisation standards.
- Develop an electrical model and parametrisation approach for bifacial PV which takes the datasheet characteristics as input.
- Verify the developed electrical model with measured power output.

1.3.3 Project goal

The final objective will be critical in achieving the goal of accurately simulating bifacial PV modules:

- Integrate the developed ray tracing irradiance model with the electrical model in order to simulate the effects of various design parameters on the performance of bifacial modules.

The investigation and development of accurate irradiance and electrical models will aim to simulate and model bifacial modules accurately and solve some of the uncertainties surrounding bifacial technology.

1.4 Thesis layout

The remainder of the thesis will guide the reader through the process of investigating and developing the key parts that are needed for accurate simulation of bifacial PV.

1.4.1 Chapter 2

Chapter 2 gives the reader some background and context with regards to the importance of rear side irradiance in bifacial PV and conventional irradiance modelling techniques. The proposed irradiance modelling technique, ray tracing, is also described in order to test it's viability in bifacial simulation tool.

1.4.2 Chapter 3

In Chapter 3 the electrical behaviour of bifacial PV modules will be investigated in order determine the model that will be implemented in the developed simulation software. The characterisation standards of bifacial modules are also researched in order to determine the critical values that characterises the performance of bifacial modules.

1.4.3 Chapter 4

The methodology of developing the bifacial PV simulation software is given in Chapter 4. First the development of the irradiance model with ray tracing is described after which two versions of a one-diode model is described which will be utilized to model the power output of bifacial modules. The flow and operation of the integrated simulation software is also given in this chapter.

1.4.4 Chapter 5

In Chapter 5 the developed irradiance and electrical models are verified, first separately and then together in their integrated version. Once the models are verified, a set of simulations are done in order to test the effects of various design parameters, such as tilt angles, module height, albedo and row spacing. The analysis of these effects on the energy performance of bifacial modules then leads to a simulation where the energy production of an optimised bifacial PV system is compared with a non-optimised bifacial PV system. Lastly the developed simulation software is compared with existing commercial simulation software named *PVsyst*, which implements the view factor method for modelling rear side irradiance.

1.4.5 Chapter 6

Finally in Chapter 6, some important conclusions are drawn with regards to the development and results that the bifacial PV simulation software delivered. Some recommendations are also given which relates to the bifacial PV design and maximisation of bifacial PV performance.

Chapter 2

Irradiance modelling

For bifacial PV, the rear side irradiance contributes to the power output of the the module. The rear side contribution is therefore critical in the gained energy production when compared to monofacial modules. It is equally important for PV plant designers to model and simulate the full extent of the rear side's effects on the expected energy output of a bifacial PV module. Existing irradiance modelling techniques fall short in some ways when modelling the irradiance on the rear side of a module.

2.1 The importance of rear side irradiance

The operation of a bifacial PV module is not only dependent on the incident irradiance on the front side of the module, but it's also dependent on the diffuse and reflected irradiance received by the rear side. This additional irradiance dependency leads to numerous complexities with regards to designing for a bifacial PV implementation. In the case of bifacial PV modules, extra care needs to be taken to maximise the irradiation of the rear side and in effect make the technology more profitable.

2.1.1 Factors that influence Rear Side Irradiance

The rear side irradiance is influenced by a variety of module design- and environmental parameters as shown in Figure 2.1. Design parameters include the azimuth- and tilt angles, module height above the ground and the size or packing factor of the plant [8]. The geographic location of the plant as well as the albedo of the surrounding ground cover are categorised as environmental parameters. PV plant designers have less influence on the environmental parameters compared to the design parameters.

By optimizing the combination of environmental- and design parameters one can potentially maximize the energy yield produced by the plant. There are many uncertainties regarding the optimal design of a bifacial PV plant,

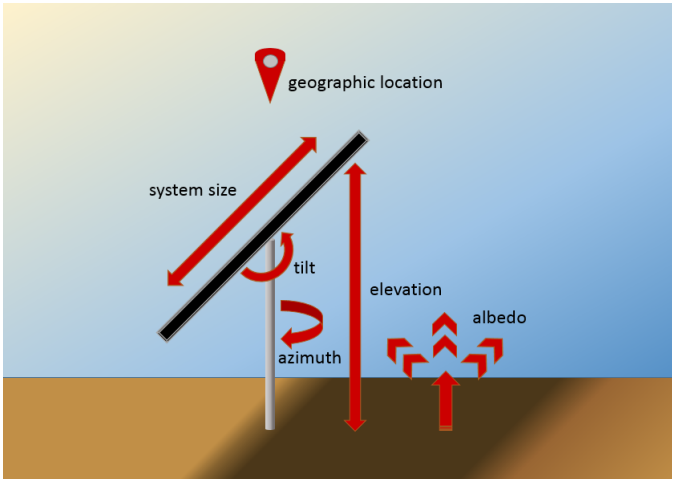

Figure 2.1: Factors that influence the rear side irradiance of bifacial PV modules.

but some design parameters are known to have a large impact on the power output of a plant. These most influential parameters include :

1. **Mounting height** - research done by [8] shows an increase in rear side irradiance with an increase of mounting height between 0-1m.

2. **Albedo** - ground surfaces can reflect a certain amount of the irradiance that it recieves. The ratio between the reflected irradiance and the total recieved irradiance is known as the surface albedo. The rear side irradiance can be significantly increased by enhancing the albedo propeties of the surrounding ground cover as [8] concludes in their study. Table 2.1 shows various ground types and it's albedo characteristics.

3. **Row spacing** - the distance between adjacent rows in a PV plant can greatly influence the amount of ground surface area that receives irradiation. By increasing the row spacing, it is possible for more irradiance to be reflected to the rear side of bifacial modules.

4. **Mounting structure** - the shading effects of the module's mounting structure has a significant impact on the rear side irradiance. A study done by [17] shows a decrease in performance once the rear side is severely shaded by some form of structure.

Although there are many factors and parameters that influence the rear side irradiance, these factors named above are known to mainly effect the rear side and have less effect on the front side of a bifacial module. These factors are more likely to have an effect on the energy yield of the plant while other design parameters become problematic while designing a bifacial PV plant.

Table 2.1: Albedo values of various ground types. [8]

Ground type	Albedo
Concrete	0.25 - 0.70
Grass	0.20 - 0.30
Ice	0.30 - 0.50
Fresh Snow	0.75 - 0.95
Old Snow	0.40 - 0.70
Sand (dry)	0.35 - 0.45
Soil	0.40 - 0.50
Gravel	0.20 - 0.35

2.1.2 Conventional PV Plant Design Flaws

PV plant designers and engineers are more interested in the factors that will determine the successful and seamless operation of PV plants. Some conventional PV plant design implementations as shown in Figure 2.2, become tedious problems when designing bifacial PV plants.

Figure 2.2: Convential PV plant design implementation of wiring and inverter.

Wiring plays a big role in PV plants and can sometimes become quite complex to handle. The wires of module strings are normally bound at the back of modules as form of protection against solar damage. Bifacial PV plants may require new ways of handling wires as they can potentially block the rear sides of modules from optimal exposure to radiation. Inverters and combiner boxes are also usually placed behind fixed tilt PV modules and are designed to handle maximum voltage and current circumstances. Due to a lack of accurate modelling and simulation of bifacial modules, it becomes hard for engineers to design the bifacial PV plants at their true maximum and minimum ratings. By accurately simulating bifacial PV plants beforehand, PV plant designers can

prevent under or over design of various PV plant equipment. The combination of all the above named factors and the lack of extensive characterisation of modules, leads to some uncertainties regarding the operation of bifacial PV.

2.2 Conventional irradiance modelling

With a conventional monofacial PV module, only the front side irradiance needs to be modelled. The techniques used were developed over many years and are used widely in PV modelling [9]. The total incident irradiance on the front side of a module can be described by the following equation.

$$G_{front} = G_{direct} + G_{diffuse} + G_{reflect} \tag{2.1}$$

By giving the global horisontal irradiance (GHI) and the solar position as input to the Perez model, G_{direct} can be calculated which relates to the direct normal irradiance (DNI) [18]. The Perez model can also be implemented to acquire the value of $G_{diffuse}$ [18]. The Perez model is implemented in most solar energy modelling tools which makes it a benchmark in the irradiance modelling industry.

For $G_{reflect}$, an isotropic model is implemented which assumes that the reflected radiation is uniformly distributed over an entire surface [19]. The model as developed by [19] incorporates geometrical parameters of the sun which relates to solar zenith and azimuth. Meteorological parameters such as humidity are also taken into account [19].

The techniques used to calculate the latter three values prove to be accurate for modelling the front side irradiance [9].This is not the case for bifacial modules where the rear side irradiance is mainly dependent on $G_{reflect}$ and the contributions of G_{direct} and $G_{diffuse}$ are far less significant. As researchers in [16] show, the view factor method can be used to provide a more accurate estimation of $G_{reflect}$ when compared to the isotropic model used in [19].

2.3 View factor modelling

The view factor (VF) is a fundamental concept used in heat transfer theory, that describes the amount of radiation reflected by one surface (A_1) and received by a second surface (A_2) as shown in Figure 2.3 [20].

The view factor $VF_{A_1 \to A_2}$ is merely a geometric fraction and can be described by the following equation [20].

$$VF_{A_1 \to A_2} = \frac{1}{A_1} \int_{A_2} \int_{A_1} \frac{cos\theta_1 cos\theta_2}{\pi S^2} dA_1 dA_2 \tag{2.2}$$

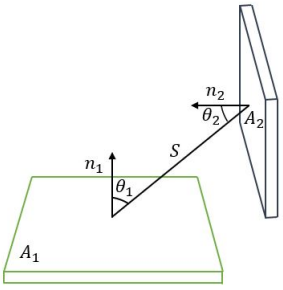

Figure 2.3: Illustration of the view factor parameters of two surfaces.

The implementation of the view factor is demonstrated in Figure 2.4, where a PV module casts a shadow onto a ground surface. In this case the reflecting surface can be broken up into two parts, i.e., the shadowed surface (A_s) and the non-shadowed surface (A_{ns}). The total reflected irradiance ($G_{reflect}$) on the rear side of the module (A_{mod}) can be described as follows [16]:

$$G_{reflect} = \alpha(GHI)(VF_{A_{ns} \to A_{mod}}) + \alpha(DHI)(VF_{A_s \to A_{mod}}) \tag{2.3}$$

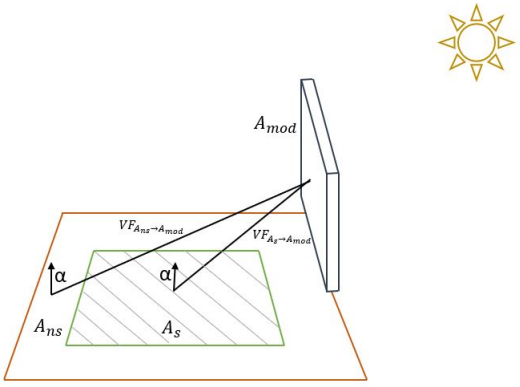

Figure 2.4: Illustration of a view factor implementation to estimate the rear side irradiance of a PV module.

In equation 2.3, α describes the ground surface albedo coefficient and is multiplied with both GHI and DHI respectively. The non-shadowed surface is primarily radiated by the GHI (Global Horizontal Irradiance) component whereas the shadowed surface is only radiated with the DHI (Diffuse Horizontal Irradiance) component. It is clear that view factor modelling is an analytical approach that may become tedious if the complexity of surfaces intensifies. Another approach would be to solve the problem by means of an optical technique such as ray tracing.

2.4 Ray tracing

The concept of ray tracing was realised in computer graphics to synthesise a 2D image of a 3D environment [11]. In basic terms, ray tracing operates in the same way a camera would when snapping a picture of a scene. To further understand ray tracing, a brief explanation regarding the two methods of ray tracing, forward- and backward tracing, will be given.

2.4.1 Forward ray tracing

Forward ray tracing is the most intuitive method to use for an explanation as to how ray tracing works. The operation of forward ray tracing is illustrated in Figure 2.5.

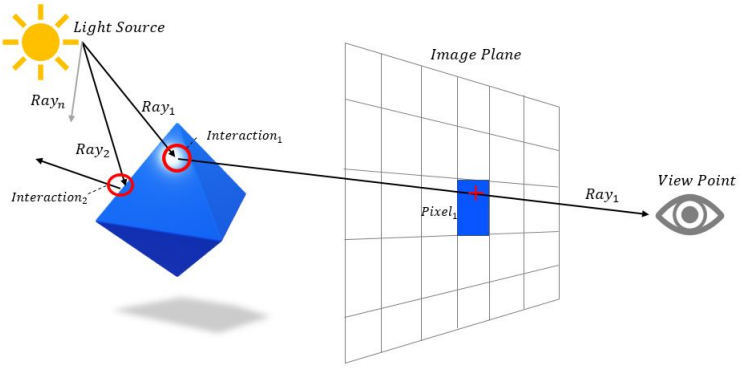

Figure 2.5: Forward Ray Tracing.

The process starts by following the path of a photon (Ray_1) from it's origin which can be any form of light source. As Ray_1 hits the surface of the object, an interaction ($Interaction_1$) takes place. The pre-defined material characteristics and geometry of the object, together with a set of mathematical equations will determine the outcome of $Interaction_1$. In this case $Interaction_1$ reflects Ray_1 toward the $ViewPoint$. The intersection between Ray_1 and the $ImagePlane$ results in $Pixel_1$ to be displayed.

If the same steps are followed for Ray_2, it is clear that the outcome of $Interaction_2$ will lead to a reflection away from the $ImagePlane$. This results in no pixel being displayed in the $ImagePlane$ for Ray_2. This process can be repeated for n number of rays. The amount of calculations needed to successfully render the scene would therefore range from $(1, 2...n)$.

With forward ray tracing it is possible for n to approach infinity and none of the rays reached the *ImagePlane* [11]. Backward ray tracing solves this problem.

2.4.2 Backward ray tracing

For scene rendering purposes one will only be interested in the result shown in the *ImagePlane* with the least amount of computational power required.

This is realised by reversing the process of forward ray tracing which follows a general direction from a light source, toward an object and hopefully toward the *ImagePlane*. Backward ray tracing, as illustrated in Figure 2.6, follows the paths of rays from the *ViewPoint* through the *ImagePlane* until a object is intersected. The outcome of the interaction with the object then determines whether the ray path can be traced toward a light source. If the path to a light source is blocked by another object, as with Ray_2 in Figure 2.6, the specific path will be identified as a shadow ray. The outcome of the traced path determines the value of the pixel of origin.

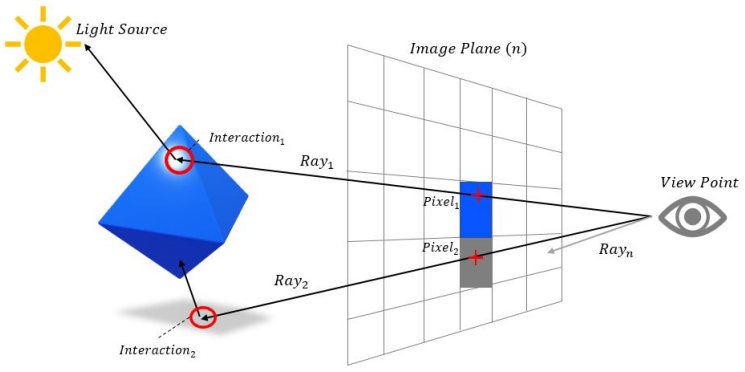

Figure 2.6: Backward Ray Tracing.

With this process, the number of rays (n) are limited to the number of pixels required to successfully render a scene, hence a reduction in computation time. Backward tracing is therefore the most common implementation of ray tracing [11] and can be extensively utilized for irradiance modelling of PV applications.

2.5 Ray tracing in PV applications

Although ray tracing is already an established technique used in the PV industry, these applications are focused on cell properties such as light entrapment,

optical concentration and more [12]. It could be of great interest to further utilize ray tracing for modelling the rear side irradiance of bifacial modules as [13] has shown. Figure 2.7 shows how backward ray tracing can be implemented to model the rear side irradiance of bifacial modules.

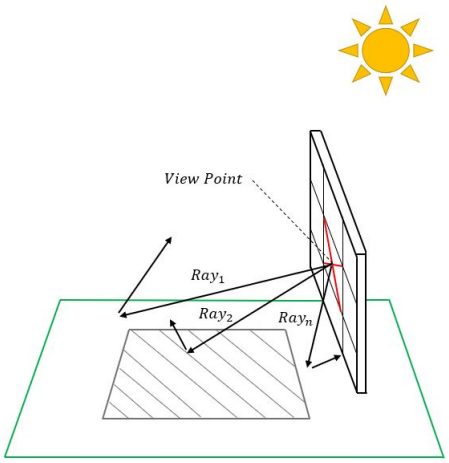

Figure 2.7: Backward Ray Tracing in a PV application.

To model the rear side irradiance of a bifacial module, the $ViewPoint$ can be set to a point on the rear side of the module. The incident irradiance at the $ViewPoint$ may then be measured by tracing n number of rays by means of backward ray tracing. This method seems intuitive as it is a virtual representation of measuring irradiance in the real world by means of a pyranometer.

2.6 Summary

It is evident that the rear side irradiance plays an important role in the operation of bifacial PV modules. It is therefore important to accurately model the rear side irradiance when it comes to simulating bifacial modules. Conventional means of irradiance modelling mostly implements the theory of view factors [9]. This method may fall short when modelling the rear side irradiance due to it's robustness when handling complex geometries [3]. Ray tracing and more specifically backward ray tracing may serve as a viable solution as it is widely used in accurate light rendering software such as *Radiance*. Although ray tracing is implemented in modelling cell-level effects [12], there exists only a few implementations for irradiance modelling [13].

Chapter 3

Electrical modelling

3.1 Electrical characterisation

Electrical characterisation plays an important role when modelling the electrical behaviour of PV modules. Unfortunately there are many uncertainties regarding the characterisation of bifacial PV modules [6].

To better understand the shortcomings of bifacial module characterisation, some background will be given with regards to electrical characterisation of monofacial modules.

3.1.1 Characterisation of monofacial modules

PV modules are primarily characterised by the relationship between the current and voltage output of a single module. This current-voltage relationship is known as the I-V characteristics of a PV module and is a function of output current and voltage with a load varying between open-circuit and short-circuit [21]. A typical I-V characteristic curve is shown in Figure 3.1.

In Figure 3.1, a few important points are marked and are typically the most valuable measured specifications of a PV module where:

- Isc is the short-circuit current,
- Voc is the open-circuit voltage,
- $Pmax$ is the maximum power point,
- $Impp$ is the current at maximum power point and
- $Vmpp$ is the voltage at maximum power point.

The characteristics named above allow PV designers and engineers to accurately design PV plants within the designated constraints and limitations.

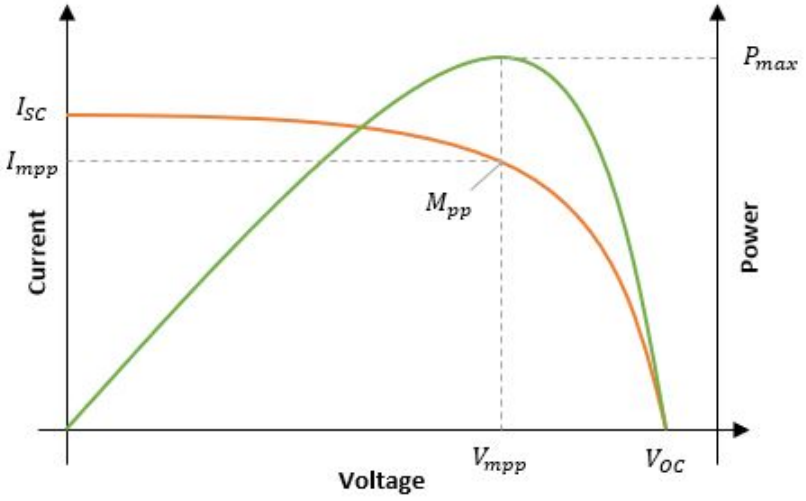

Figure 3.1: Typical I-V characteristics curve of a PV module.

These key characteristics are measured and given in the module data-sheets by their respective manufacturers. The process of measuring the I-V characteristics of a PV module has to comply with Standard Test Conditions (STC) as stated in the $IEC60904-1$ regulation [22]. The most important STC values are given in Table 3.1.

Table 3.1: Standard Test Conditions (STC) for characterising monofacial PV modules.

Variable	STC value
Irradiance (G)	1000 W/m^2
Temperature (T)	25 $^{\circ}C$
Air Mass (AM)	1.5

Characterisation of monofacial modules must strictly comply with IEC standards. This makes the process of comparing various PV modules easier as it is known that the given power rating of a module from one manufacturer, was acquired by means of the same process as a module from a different manufacturer [23]. This however, is not yet the case for bifacial modules as standardised characterisation was just recently published.

3.1.2 Characterisation of bifacial modules

The characterisation of bifacial modules has been studied thoroughly and a number of methods were proposed [14]. However, a standardised characterisa-

tion procedure for bifacial PV devices was released under $IEC60904-1-2$ in January 2019 [24]. This procedure can be described by the following steps [25]:

Step 1: Determine Bifaciality The bifaciality coefficient (φ) describes the relationship between the output contribution of the rear side versus the front side under the same illumination conditions and is given as a percentage. The bifaciality is taken as the minimum of three bifaciality coefficients ($\varphi_{Isc}, \varphi_{Voc}, \varphi_{Pmax}$) and these are presented in Equations (3.1)-(3.4).

$$\varphi_{Isc} = \frac{I_{sc-r}}{I_{sc-f}} \tag{3.1}$$

$$\varphi_{Voc} = \frac{V_{oc-r}}{V_{oc-f}} \tag{3.2}$$

$$\varphi_{Pmax} = \frac{P_{max-r}}{P_{max-f}} \tag{3.3}$$

$$\varphi = min(\varphi_{Isc}, \varphi_{Pmax}) \tag{3.4}$$

The bifaciality coefficients are determined by taking measurements whilst illuminating the front and rear side separately at STC (Table 3.1) as shown in Figure 3.2.

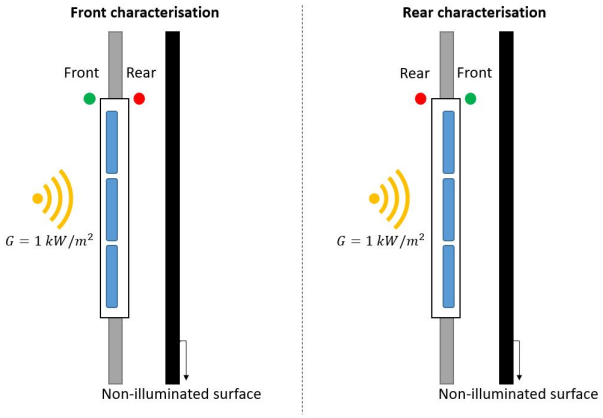

Figure 3.2: Procedure to determine the bifaciality coefficients.

Step 2: Determine bifacial Gain bifacial gain is the nett power produced by a module as a result of the additional contribution from the rear side. The $IEC60904-1-2$ allows two methods to determine the bifacial gain of a module [25].

Double-sided illumination requires that both the front and the rear sides are illuminated simultaneously as shown in Figure 3.3a. The front side is illuminated at 1 sun intensity ($1kW/m^2$) while the rear side receives at least 3 respective intensity levels of illumination (G_{R_i}). The maximum power output (P_{max}) for each rear side illumination (G_{R_i}) is then measured and plotted. This procedure may be executed indoors or outdoors.

Equivalent one-sided illumination must be performed indoors and requires no additional equipment to perform when compared to the bifaciality test. The test procedure is illustrated in Figure 3.3b. Only the front side is illuminated with at least 3 irradiance intensities (G_{E_i}), where G_{E_i} is described by [25]

$$G_{E_i} = 1000W/m^2 + \varphi(G_{R_i}) \tag{3.5}$$

where

$$i = 1, 2, 3, ...$$

and φ relates to the bifaciality coefficient as given in Equations (3.1)-(3.4). From Equation (3.5) it is clear that the chosen rear side irradiance intensities (G_{R_i}) are scaled down with φ and added to the reference front side irradiance of 1000 W/m^2 to form an equivalent irradiance G_{E_i}. This procedure aims to overexpose the cells with the same amount of effective irradiance that would reach the front and rear surfaces of the module.

(a) Double-sided illumination. (b) Equivalent one-sided illumination.

Figure 3.3: Two methods to determine bifacial gain.

Step 3: Report Key Data It is not only important to standardise the characterisation procedure, but also the data that needs to be reported by module manufacturers. This allows PV investors to make equal comparisons

between various modules. The $IEC60904-1-2$ requires the following data to be reported for bifacial PV devices [24]:

1. STC data as characterised for monofacial modules ($IEC60904-1$)
   - Short-Circuit Current (Isc)
   - Open-Circuit Voltage (Voc)
   - Maximum Power Point ($Pmax$)
2. Bifaciality (φ)
3. Maximum Power Points with rear side contributions
   - $Pmax_{BiFi100}$ ($G_{R_i} = 100W/m^2$)
   - $Pmax_{BiFi200}$ ($G_{R_i} = 200W/m^2$)

With sufficient characterisation data it is now possible to find an optimal solution to model the electrical behaviour of bifacial modules.

3.2 One-diode model for mono-facial PV

Like many other facets of bi-facial technology, there are uncertainties regarding the electrical modelling of modules. In order to progress toward an electrical model for bi-facial PV modules, the one-diode model of mono-facial modules will be used as a base. Many researchers extensively study the electrical behaviour of mono-facial PV cells. There are a number of possible methods to electrically model mono-facial modules. The best-known models are [26]:

- One-diode model
  - Ideal one-diode model
  - Series-resistance (R_s) one-diode model
  - Shunt- and series-resistance (R_{sh}-R_s) one-diode model
- Two-diode model

The complexity and accuracy of each model varies, but it is known that the R_{sh}-R_s one-diode model sufficiently simulates the electrical behaviour of a PV cell [3]. The equivalent circuit is shown in Figure 3.4 and yields the following equation for the output current (I) [26]:

$$I = I_{ph} - I_0\left[\exp\left(\frac{q(V+IR_s)}{nkT}\right) - 1\right] - \frac{V+IR_s}{R_{sh}} \tag{3.6}$$

In Equation 3.6, k is known as the Boltzmann's constant ($k = -1.380653 \times 10^{-23}\ J/K$) and q is the value of an electron charge ($q = 1.60217646 \times 10^{-19}$

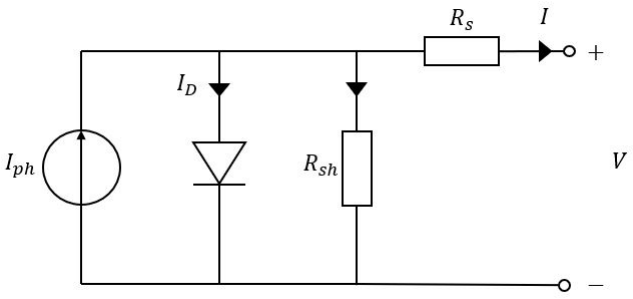

Figure 3.4: R_{sh}-R_s one-diode model for monofacial PV cells.

C) [26]. T is the module temperature at a given time and apart from the dependent values of I and V, Equation (3.6) leaves five unknown parameters: photon-current (I_{ph}), saturation current (I_0), ideality factor (n), shunt-resistance (R_{sh}) and series-resistance (R_s). I_{ph} can easily be solved with Equation (3.7).

$$I_{ph} = \frac{G}{G_{ref}}\left(I_{sc} + \alpha\Delta T\right) \tag{3.7}$$

From Equation (3.7) it is clear that the photon-current I_{ph} is dependent on the incident irradiance (G) with relation to the reference irradiance ($G_{ref} = 1000\ W/m^2$), the short-circuit current (I_{sc}), the temperature effects as described by the module's short-circuit current temperature coefficient (α) and the temperature difference (ΔT), where

$$\Delta T = T - T_{STC}. \tag{3.8}$$

T_{STC} is the reference temperature of 25 $°C$. The $R_{sh} - R_s$ one-diode model can be further developed to model bifacial PV cells [3].

3.3 One-diode model for bi-facial PV

The $R_{sh} - R_s$ one-diode model as given for mono-facial PV cells can be modified for bifacial PV cells by adding an additional current source I_{ph-r} [3], as shown in Figure 3.5. In this equivalent circuit, the current sources I_{ph-f} and I_{ph-r} represent the photovoltaic contribution of the front and rear side, due to incident irradiance, respectively [3].

The one-diode model as shown in Figure 3.5, yields Equation (3.9) for the output current (I) and Equations (3.10)-(3.11) for the front and rear photon currents (I_{ph-f} and I_{ph-r}). In Equations (3.10)-(3.11), G_f and G_r represent the values of the incident irradiance on the front and rear surface of the bifacial cell respectively. The photon currents can therefore be calculated with measured or simulated front and rear side irradiance values. In order to further model a

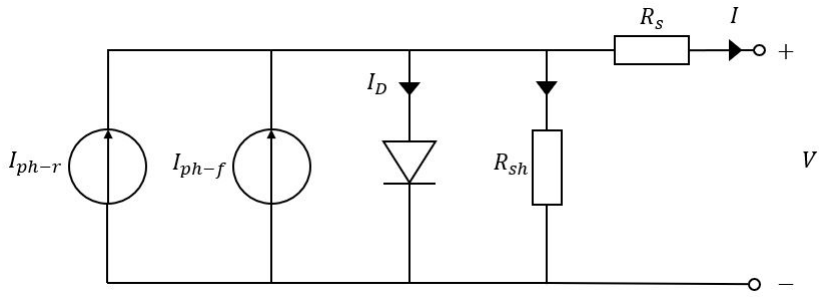

Figure 3.5: R_{sh}-R_s one-diode model for bifacial PV cells.

specific bifacial PV module, the four unknown parameters, I_0, n, R_{sh} and R_s, needs to be solved on module-level.

$$I = I_{ph-r} + I_{ph-f} - I_0\left[\exp\left(\frac{q(V+IR_s)}{nkT}\right) - 1\right] - \frac{V+IR_s}{R_{sh}} \tag{3.9}$$

$$I_{ph-f} = \frac{G_f}{G_{ref}}\left(I_{sc-f} + \alpha\Delta T\right) \tag{3.10}$$

$$I_{ph-r} = \frac{G_r}{G_{ref}}\left(I_{sc-r} + \alpha\Delta T\right) \tag{3.11}$$

3.4 Parameter solving for the one-diode model

A method for solving the unknown parameters of the designated one-diode model for bifacial cells is given by [14]. This proposed method relies strongly on measurement points that are not standardised parameters for bifacial modules that needs to be reported according to [24] and the $IEC60904-1-2$. With regards to monofacial modules, there are a number of methods for solving the unknown parameters of the one-diode model [26], with the most common being the method presented by *De Soto et al.* [27], where the equivalent circuit equation at module-level is described by:

$$I = I_{ph} - I_0\left[\exp\left(\frac{q(V+IR_s)}{nkTN_s}\right) - 1\right] - \frac{V+IR_s}{R_{sh}} \tag{3.12}$$

where N_s is the number of cells that are connected in series to form a PV module. From Equation (3.12), the following unknown parameters are left I_0, n, R_{sh} and R_s. In [27], a parameter extraction method is presented that only relies on value points that are made available by PV module manufacturers and most commonly found in module data-sheets. These values are determined at STC and include: short-circuit current (I_{sc-ref}), open-circuit voltage (V_{oc-ref}), voltage and current at maximum power point ($V_{mpp-ref}$ and $I_{mpp-ref}$) and open-circuit voltage temperature coefficient ($\beta_{V_{oc}}$). The value points are substituted into Equation (3.12) and yield Equations (3.13)-(3.17) [27].

At short-circuit current, $I = I_{sc-Ref}$ and $V = 0$.

$$I_{sc-ref} = I_{ph} - I_0\left[\exp\left(\frac{q(I_{sc-ref}R_s)}{nkTN_s}\right) - 1\right] - \frac{I_{sc-ref}R_s}{R_{sh}} \tag{3.13}$$

At open-circuit voltage, $I = 0$ and $V = V_{oc-ref}$.

$$0 = I_{ph} - I_0\left[\exp\left(\frac{q(V_{oc-ref})}{nkTN_s}\right) - 1\right] - \frac{V_{oc-ref}}{R_{sh}} \tag{3.14}$$

At maximum power point, $I = I_{mpp-ref}$ and $V = V_{mpp-ref}$.

$$I_{mpp-ref} = I_{ph} - I_0\left[\exp\left(\frac{q(V_{mpp-ref} + I_{mpp-ref}R_s)}{nkTN_s}\right) - 1\right] - \frac{V_{mpp-ref} + I_{mpp-ref}R_s}{R_{sh}} \tag{3.15}$$

Finally, from Figure 3.1 in section 3.1.2, it is known that the derivative of the output power (IV) at maximum power point ($\frac{d(IV)}{dV}\big|_{mpp}$) is equal to zero.

$$\left.\frac{d(IV)}{dV}\right|_{mpp} = I_{mpp} - V_{mpp}\left.\frac{d(I)}{dV}\right|_{mpp} = 0 \tag{3.16}$$

where

$$\left.\frac{d(I)}{dV}\right|_{mpp} = \frac{\frac{-qI_0}{nkTN_S}e^{\frac{q(V_{mpp}+I_{mpp}R_s)}{nkTN_s}} - \frac{1}{R_{sh}}}{1 + \frac{qI_0R_s}{nkTN_s}e^{\frac{q(V_{mpp}+I_{mpp}R_s}{nkTN_s} + \frac{R_s}{R_{sh}}}} \tag{3.17}$$

Equations 3.13-3.17 must then be iteratively solved to yield values for I_0, n, R_{sh} and R_s. The complete one-diode model together with incident irradiance values may then be implemented to calculate the current, voltage and power output of a PV module at any given time.

3.5 Summary

3.5.1 Electrical characterisation

Up until now, the task of comparing bifacial modules from various manufacturers was tedious [23]. This was due to the lack of standardised characterisation for bifacial PV modules. A standardised characterisation methodology was recently published under $IEC60904-1-2$ [24]. This will force bifacial PV manufacturers to report specified data, which includes the bifaciality coefficient, that have been acquired by standardised tests. PV investors may now make easier comparisons between various bifacial technologies.

3.5.2 Electrical modelling

The most common model used to simulate the electrical behaviour of bifacial PV cells is an adjusted $R_{sh} - R_s$ one-diode model [3]. This one-diode model is similar to that of monofacial PV cells but it consists of an additional current source, I_{ph-r}, that separately models the photovoltaic effect of incident irradiance on the rear side of the cell [3]. Although a parameter extraction method specifically for bifacial modules is proposed by [14], this method makes use of some data that is not required by $IEC60904-1-2$ to be reported. Therefore a parameter extraction method as proposed by [27] may be investigated.

Chapter 4

Simulation software for bifacial PV

As described in Chapter 1, the objective is to develop accurate simulation software for bifacial PV in order to optimise bifacial plant designs and configurations. As shown in Figure 4.1, there are three integral parts i.e. irradiance model, electrical model and miscellaneous features, that needs to be implemented in order to simulate bifacial modules extensively. This chapter will first look at existing bifacial simulation software and thereafter work through the methodology of developing a novel implementation of simulating bifacial PV modules.

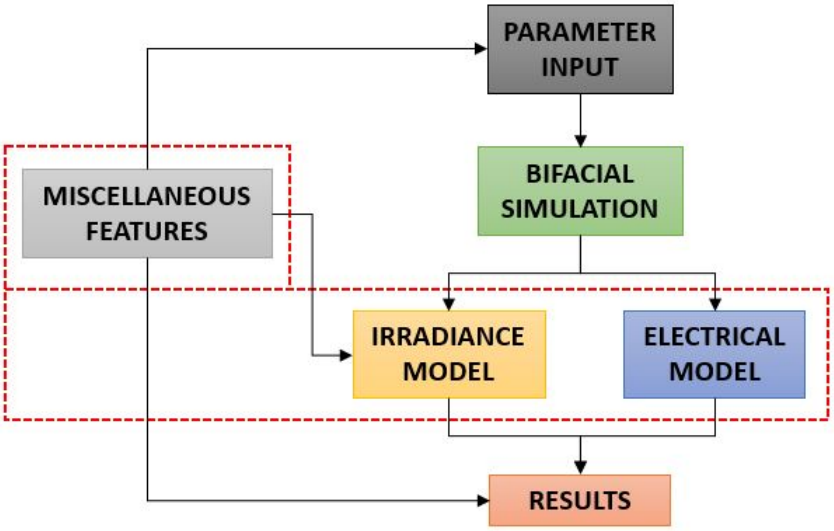

Figure 4.1: The integrated parts that make up the bifacial simulation software.

4.1 Existing bifacial PV modelling and simulation software

Estimating the power gain of bifacial PV plays an important role in determining the levelised cost of electricity (LCOE) of the technology [3]. In order to successfully make such estimations, a seamless integration of accurate irradiance- and electrical modelling is needed. The added complexity of rear side irradiance and lack of field data to support existing electrical models, leads to a scarcity of simulation software tools that can model bifacial modules accurately [3].

4.1.1 Commercial software

There are two commercial software tools available that have bifacial modelling capabilities [3]. The first is the well known *PVSyst* that is widely used in commercial yield predictions etc. Bifacial modelling was added to the software in March 2017 with version 6.6.1 and received further development and upgrades with later updates [28]. At first the bifacial modelling capabilities were only available for *PVSyst*'s shed-like 2D PV systems with no 3D features such as tracking and vertical installations [28]. A single-axis tracking feature was added in version 6.7.0 [28]. *PVSyst* implements view factors, as described in section 2.3, for modelling the rear side irradiance and the one-diode model for bifacial modules, as given in section 3.3, is utilised for estimating power output [29].

The second commercial software tool with bifacial modelling capabilities is *Polysun* [3]. The calculation used in *Polysun* results in a *energy boost* value that is acquired by multiplying the albedo and bifaciality coefficients with the effective geometry of the bifacial plant [30].

4.1.2 Software in development

Due to the scarcity of bifacial simulation software, the academic and research communities are motivated to find viable solutions that can accurately model bifacial systems. Most of the contributions [9,13,15,16] make use of view factor and ray tracing implementations to model irradiance [3].

The National Renewable Energy Laboratory (NREL) developed open-source view factor [31] and ray tracing [32] models that are easily accessible and free to use. These models are each implemented to show the effects of various design parameters, such as albedo and mounting height, on the rear side irradiance and power gain of bifacial modules [3]. In [15] it is shown that there is a significant difference in accuracy when comparing various modelling techniques.

Simulation results vary up to 10% between models that implement view factors and ray tracing respectively [15]. There clearly is a need for accurate simulation software for bifacial technology.

4.2 Irradiance modelling

After evaluating the work done by [13], it was determined that there is interest to implement ray tracing as an irradiance modelling tool for bifacial PV. By implementing ray tracing, which is known to model the behaviour of light accurately [11], it is expected to model the incident irradiance, more specifically the rear side irradiance, very effectively. As with the research done in [13], a ray tracing tool named *Radiance* was chosen as an effective implementation for modelling the irradiance of bifacial modules.

4.2.1 Implementing the *Radiance* software tool

Radiance is an open-source ray tracing tool that was originally developed for architectural lighting analysis [33]. The software was developed in *UNIX* and operates by means of running text commands which calls a series of executable programs (.exe files). The executable programs operate by taking defined parameters as input and returning the desired results. The software therefore has no user interface that can control commands or design virtual environments.

As the diagram in Figure 4.2 shows, there are three parts that need to be modelled in order to take irradiance measurements on the front and rear side of modules by means of ray tracing. These three parts are the sky model, ground model and the geometric description of bifacial modules. Together, the three parts form the virtual environment in which a PV plant can be simulated.

4.2.2 Sky model

The sky model will play the most important role in the irradiance modelling process, as it will form the source of radiation in the virtual environment. The modelled sky will consist of two parts i.e. the sun which is the primary light source and the sky itself which radiates reflected energy throughout the virtual environment. The sun is represented by direct normal irradiance (DNI) where the sky's reflected energy consists of diffuse horizontal irradiance (DHI). The combination of DNI and DHI is the global horizontal irradiance (GHI) and can be mathematically described by Equation (4.1).

$$GHI = DNI \times \cos(\theta) + DHI \tag{4.1}$$

In equation 4.1, θ represents the solar zenith angle and is defined as the sun's angular position (0°- 90°), measured from the the vertical z-axis. Another

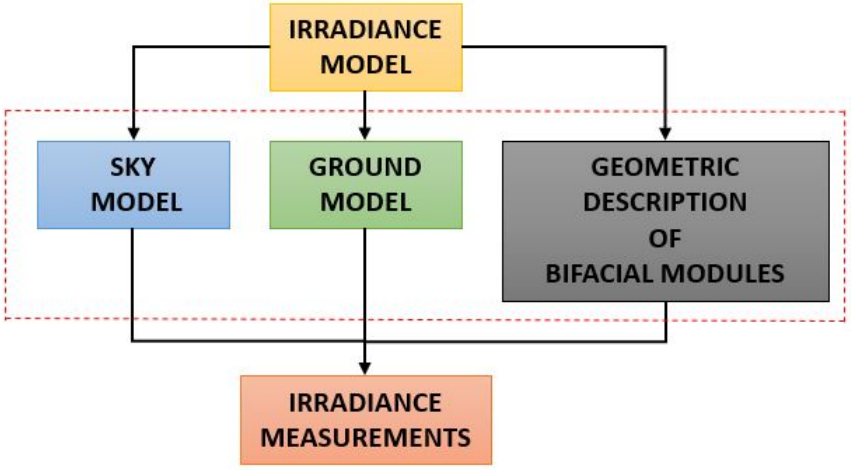

Figure 4.2: The three parts that make up the virtual environment for modelling irradiance.

angular value known as the azimuth angle (γ), describes the sun's position in the horizontal plane (0°- 360°) and is measured clockwise from the axis facing directly north. The definitions of the zenith- and azimuth angles are illustrated in Figure 4.3.

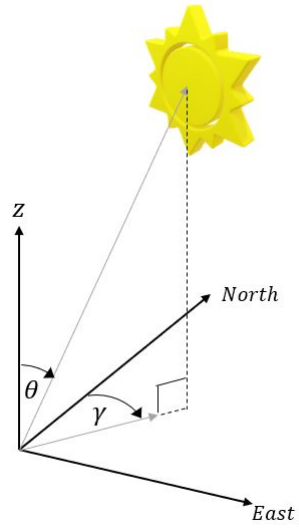

Figure 4.3: Illustration of solar zenith and azimuth angles.

If the GHI, DNI, DHI, zenith and azimuth values are known for any given time, it is possible to model the total radiation as produced by the sun and the sky for that specific time. With *Radiance* it is possible to build a sky model with one of three functions:

- *gensky* - a sky description is defined by implementing a CIE standard sky for a given day, month and time of day at a chosen location. This function does not take GHI, DNI or DHI values as input.
- *gendaylit* - the sky is realised by implementing Perez models [18]. In order to model the direct and diffuse components, the DNI and DHI values are given as input. The solar position can either be given directly with zenith and azimuth values or it can be calculated by giving the location, day, month and time of day.
- *gencumulativesky* - this function is ideal for modelling extended periods as with seasonal or annual simulations. The result of this function is the cumulative radiation of a sky definition over a designated period.

In order to have better control over the input parameters such as DNI, DHI and solar angles, it was chosen to implement the *gendaylit* function to model the sky.

4.2.2.1 Implementation of *gendaylit*

The *gendaylit* function was implemented to build a sky model for a designated time. The function takes the DNI, DHI and corresponding solar zenith and azimuth angles to produce two light sources i.e. the sky and the sun. The zenith and azimuth angles are acquired by calling the *pvlib.location.getsolarposition()* function. The corresponding DNI and DHI values are produced by utilising the *pvlib.irradiance.erbs()* function which takes the GHI and zenith angle as input. The GHI values can be acquired by means of historic weather data (EPW or TMY files) or it can be measured on site for model verification purposes. The flowchart in Figure 4.4 shows the process of implementing *gendaylit* to create a sky definition file (*sky.rad*) for a designated time.

4.2.3 Ground model

Accurate modelling of the ground plane is as important as modelling the sky, especially with regards to accurate modelling of the rear side irradiance of bifacial modules. As shown in Figure 4.5, the ground plane is divided into two parts: an infinite ground plane and a finite ground plane. The infinite ground plane is also defined by implementing the *gendaylit* function, as it has the ability to model two hemispheres, each representing the sky and the ground respectively. The only input required is the average reflectance of the ground surface which relates to albedo. As this ground plane is defined to be infinitely large, it is not able to account for shadows on it's surface. Therefore the additional finite ground plane is created.

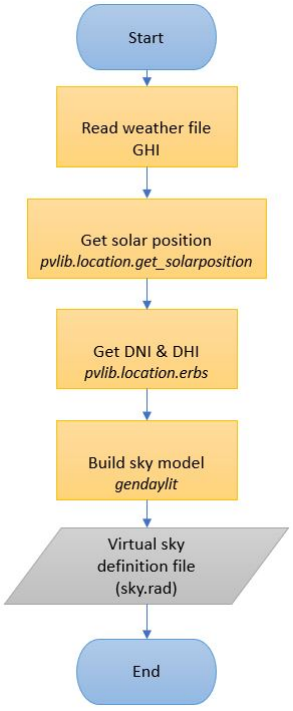

Figure 4.4: Flow chart for modelling the sky with *gendaylit*.

The finite ground plane is built with a finite geometry that spans the area of the virtual PV plant. For this implementation, the normalised reflectance of each colour component of the ground surface i.e. red, green and blue (RGB), has to be given as input. The RGB values that describe the finite ground surface are normalised and given as described by Equations (4.2)-(4.3), where α describes the albedo value of the ground surface [33].

$$RGB_{norm} = (\alpha \times 0.216) + (\alpha \times 0.7152) + (\alpha \times 0.0722) \tag{4.2}$$

$$R = G = B = \frac{\alpha}{RGB_{norm}} \tag{4.3}$$

By giving the R, G and B values and the designated area as input, a finite ground surface can be created in the form of a ground description file (*ground.rad*).

4.2.4 Geometric description of bifacial modules

After building the virtual environment with a sky and ground model, the next step is to represent the PV modules that make up a plant. With *Radiance* there are two ways in doing this. One way is to import a geometric CAD file that was designed with a third party CAD software tool. The second option is to define the modules geometrically in the form of text (*.rad* file), as was done for this project.

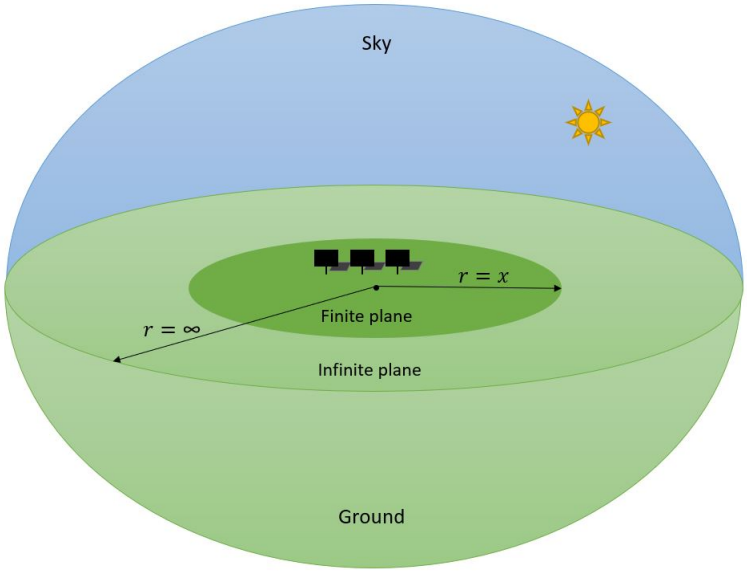

Figure 4.5: Illustration of modelled sky and two ground planes.

Each module is described by a predefined material and coordinates that are dependent on the module's geometry i.e. length, width and thickness. The *Radiance* function named *genbox* is implemented to build each module with the material and geometry given as inputs. The *xform* function is then called to transform each module for the designated plant set-up i.e. tilt and azimuth angles, elevation above ground and spacing between modules. The results of this process is a text file (*modules.rad*) that contains the geometric coordinates of each module in the virtual PV plant as shown in Figure 4.6.

4.2.5 Rendering the scene with an octree file

With the modelled sky, ground and modules in the form of text files, *sky.rad, ground.rad, modules.rad*, it is first necessary to create an octree file that describes the entire virtual scene. Octree files are commonly used in three-dimensional graphic rendering where a scene is recursively subdivided into partitions of eight. This allows for a more efficient way of describing a entire three-dimensional scene with one single file. In *Radiance*, the *oconv* function can be called with the scene text files as input, which results in an octree file named *pv-plant.oct*. This octree file may then be used as input to one of *Radiance*'s ray tracing functions such as *rtrace, rpict* or *rvu*.

4.2.6 Determining incident irradiance on module surfaces

Now that the virtual environment is built with a modelled sky, ground and bifacial PV modules, it is possible to determine the incident irradiance on the

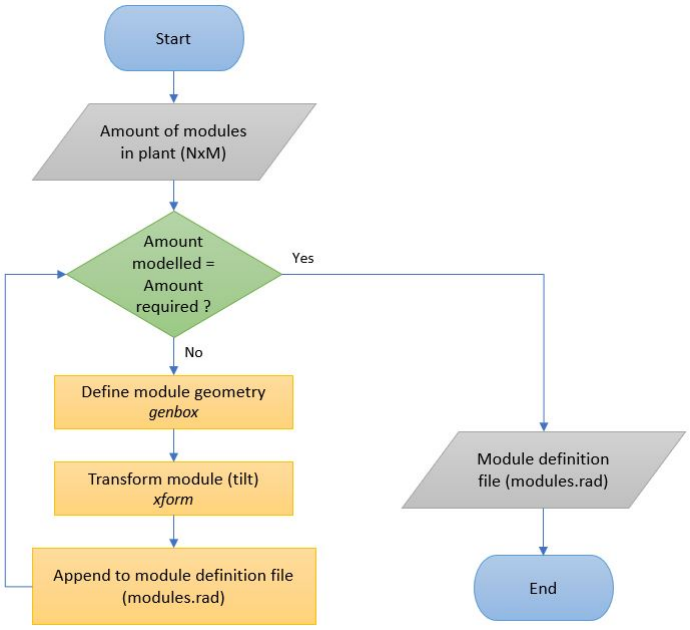

Figure 4.6: Flowchart that illustrates the process of describing bifacial modules geometrically in a *Radiance* scene.

front and rear sides of each module that requires simulation. In the real world, irradiance is measured with a pyranometer. A pyranometer is a device that can be placed at any given point and be faced in any direction to take a irradiance measurement with high accuracy. The implementation of a pyranometer is shown in Figure 4.7.

Figure 4.7: Implementation of a pyranometer to measure incident irradiance.

In the case of measuring the irradiance that is incident on the front or rear surface of a module, the pyranometer must be installed in the same plane and

have a direction normal to the surface of the module. This is known as the plane of array (POA) irradiance. In order to take irradiance measurements in the virtual scene, it is necessary to determine the point on each virtual module at which the measurements must be made.

4.2.6.1 Determining virtual irradiance measurement points

The module description file, *modules.rad*, contains the coordinates of each module's front and rear surface. By extracting the coordinates of each module's front and rear surface, it is possible to perform vector calculations that will result in in-plane coordinates and direction vectors that are normal to each surface. Equations (4.4)-(4.7) show the vector calculations used to determine an irradiance measurement point and direction vector for a module surface defined by coordinate points $\boldsymbol{P}$, $\boldsymbol{Q}$, $\boldsymbol{R}$ and $\boldsymbol{S}$, as illustrated in Figure 4.8.

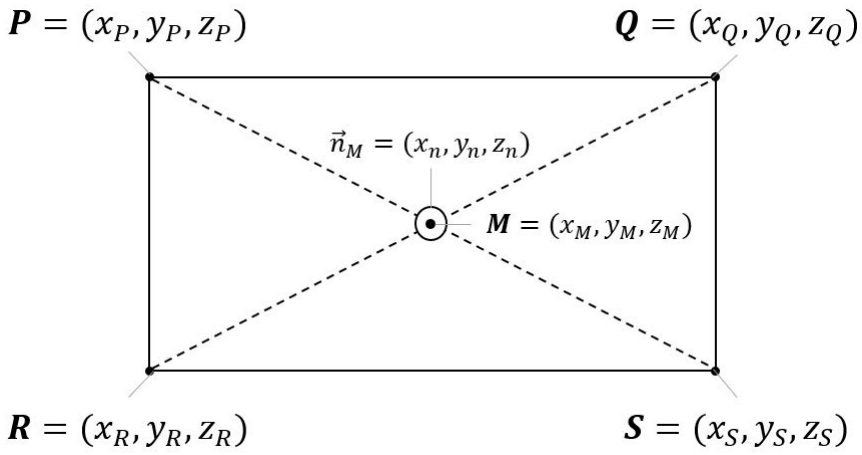

Figure 4.8: Illustration of a surface with coordinates P, Q, R and S.

First the midpoint, $\boldsymbol{M}$, of the surface is determined with a simple calculation that adds the x, y and z coordinates of two opposite corners of the surface, in this case $\boldsymbol{P}$ and $\boldsymbol{S}$.

$$\mathbf{M} = \frac{\mathbf{P} + \mathbf{S}}{2} \tag{4.4}$$

Next, the directional vector, $\vec{n}_M$, that is normal to the surface, $\boldsymbol{PQRS}$, must be determined. This is done by taking the cross product of two vectors that exist in the same plane as $\boldsymbol{PQRS}$. In this case the two vectors were chosen to be $\vec{PQ}$ and $\vec{PR}$.

$$\vec{PQ} = \mathbf{Q} - \mathbf{P} \tag{4.5}$$

$$\vec{PR} = \mathbf{R} - \mathbf{P} \tag{4.6}$$

$$\vec{n}_M = \vec{PQ} \times \vec{PR} \tag{4.7}$$

With the midpoint, $\boldsymbol{M}$, and the corresponding normal directional vector, $\vec{n}_M$, it is possible to take an irradiance measurement that is known to be on the surface and in plane of the desired module. This process is followed for both the front and rear surfaces, the rear surface normal directional vector, $\vec{n}_M$, is just inverted by multiplying with -1.

4.2.6.2 Irradiance analysis with ray tracing

The *Radiance* function named *rtrace* was chosen to analyse and determine the incident irradiance on the front and rear sides of the virtual bifacial modules. The *rtrace* function implements backward ray tracing to find the incident irradiance at a chosen location in the virtual scene. There are two possible methods of measuring irradiance with *rtrace*. The chosen method imitates the process of measuring irradiance in the real world with a pyranometer by giving the coordinates of the measurement point and the directional vector which corresponds to the plane of array.

As illustrated in Figure 4.9a, the front irradiance is measured by implementing *rtrace* at midpoint M_{front} where ray tracing takes place along the path described by the directional vector $\vec{n}_{front}$. As a result *rtrace* returns the irradiance value at the point M_{front}. The same process is followed for the rear the rear side, as shown in Figure 4.9b. To better analyse the rear irradiance distribution, it was decided to take measurements at two points, M_{rear1} and M_{rear2}, together with their corresponding directional vectors, $\vec{n}_{rear1}$ and $\vec{n}_{rear2}$. The midpoints (M_{front}, M_{rear1}, M_{rear2}) and directional vectors ($\vec{n}_{front}$, $\vec{n}_{rear1}$, $\vec{n}_{rear2}$) are given as input to *rtrace* and calculated as shown in Equations (4.4)-(4.7). The irradiance at three points, as returned by the *rtrace* function, are now known which can be used as input to the electrical model in order to determine the power output of specific modules under certain conditions.

4.2.7 Summary of irradiance modelling methodology

The modelling functions of the open-source software, *Radiance*, was implemented to model the irradiance distribution of bifacial modules. The process of modelling an entire bifacial PV plant and it's immediate surroundings is illustrated in the flowchart given in Figure 4.10.

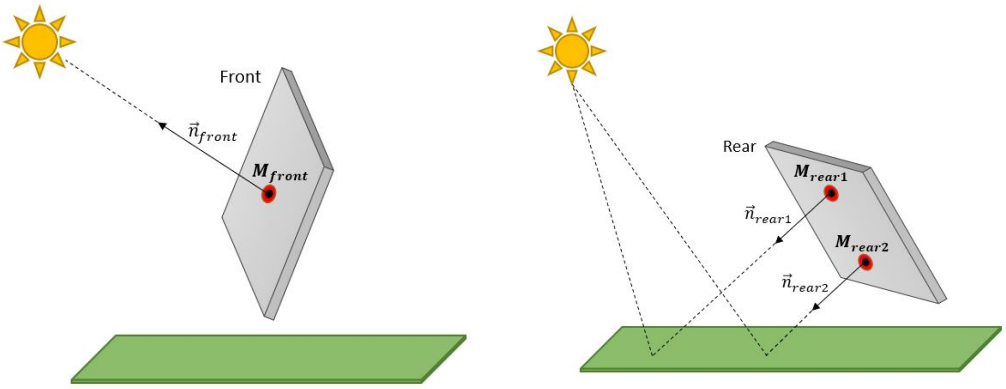

(a) Front surface irradiance measurement. (b) Rear surface irradiance measurement.

Figure 4.9: Measuring modelled irradiance with ray tracing.

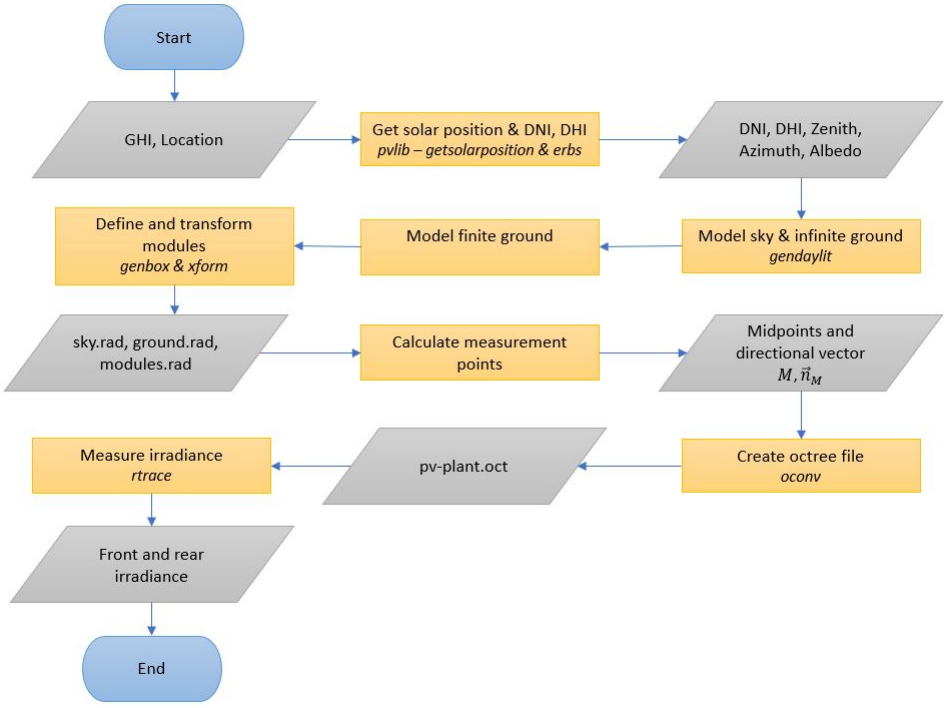

Figure 4.10: Flowchart of the irradiance modelling methodology.

First the sky is modelled with the *Radiance* function, *gendaylit*, by providing the DNI, DHI, zenith- and azimuth angles as input. These input values are modelled and calculated with *pvlib*'s *getsolarposition* and *erbs* functions which takes inputs of location coordinates and GHI respectively. The *gendaylit* function is also used to model one of two ground planes in the virual environment i.e. the infinite ground plane which takes the desired albedo value as input. In order to take shadows into account, a second finite ground plane

must be implemented by defining a ground surface with designated area and normalised RGB values that correspond to the specified albedo of the surface. The bifacial modules with specified length, width and thickness are then modelled with the *genbox* function and transformed with *xform* to take on the specified tilt, elevation and spacing between modules. Three scene description files, *sky.rad*, *ground.rad* and *modules.rad*, are then converted using the *oconv* function which produces an octree file named *pv-plant.oct*. The points at which irradiance measurements must be taken is determined with vector mathematics as given by Equations (4.4)-(4.7). Ray tracing is then implemented with *rtrace* to determine the irradiance on the front and rear side of any given module.

With the irradiance values as measured on the front and the rear side of a bifacial module in a simulated environment, it is possible to calculate the electrical power output of the bifacial module at that given time. The following section will provide the methodology of modelling the electrical behaviour of bifacial modules.

4.3 Electrical modelling

Although many research has been done on bifacial PV [13,15,31,32], the work is mainly focused on modelling the rear side irradiance [3]. The implementation of an electrical model together with accurate irradiance modelling therefore plays a critical role in the research done for this thesis.

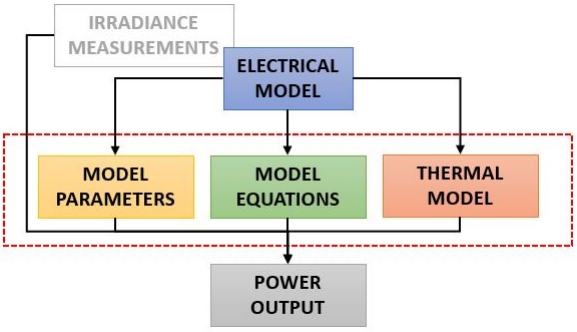

Figure 4.11: Illustration of the parts that make up the electrical model.

As shown in Figure 4.11, there are three parts that need to be solved in order to produce power output data that is dependent on the modelled irradiance data. The implemented electrical model will determine the parameters to be solved as well as the equations that can be derived in order to calculate power for a bifacial module.

4.3.1 Implementation of two electrical models

As shown in [3], the electrical model for bifacial PV is somewhat established, but there is a lack of comparison between various implementations of electrical models. It was therefore decided to implement two variations of electrical models that may later be compared and verified for accuracy. The first variation is a $R_{sh} - R_s$ one-diode model for bifacial PV as described in chapter 3 where the rear sides contribution is modelled with an irradiance dependent current source. The second variation is realised by placing two $R_{sh} - R_s$ one-diode models in parallel with each representing the front and the rear contributions respectively.

4.3.1.1 Effective $R_{sh} - R_s$ one-diode model

The $R_{sh} - R_s$ one-diode model for bifacial PV cells as described in chapter 3, section 3.3, can be reduced from two current sources (I_{ph-f} and I_{ph-r}) to one effective current source (I_{ph-eff}). The circuit of the implemented effective $R_{sh} - R_s$ one-diode model is given in Figure 4.12.

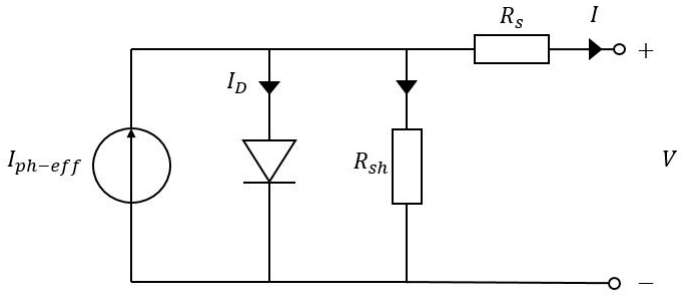

Figure 4.12: Circuit diagram of the effective $R_{sh} - R_s$ one-diode model for bifacial PV cells.

The current source noted as I_{ph-eff}, produces current that is dependent on the effective irradiance of the bifacial module i.e. the sum of the front irradiance and the weighted rear irradiance with regards to the bifaciality factor (φ). I_{ph-eff} can be described by Equation (4.8) and table 4.1 clarifies the variables used in the equation.

$$I_{ph-eff} = \frac{G_{front} + \varphi G_{rear}}{G_{ref}} \left(I_{sc-bi} + \alpha(T - T_{ref}) \right) \tag{4.8}$$

The circuit for the effective $R_{sh} - R_s$ one-diode model yields Equation (4.9) with regards to the output current (I) and output voltage (V) for a bifacial module. Table 4.2 describes the variables and constants found in Equation (4.9) and identifies the unknown parameters that needs solving.

Table 4.1: Description of variables in effective photon current (I_{ph-eff}) equation 4.8.

Variable	Description
I_{ph-eff}	Effective photon current
G_{front}	Front irradiance
G_{rear}	Rear irradiance
G_{ref}	Reference irradiance at STC (1000 W/m^2)
I_{sc-bi}	Short-circuit current as characterised for specific bifacial module
α	Short-circuit temperature coefficient
T	Instantaneous module temperature
T_{ref}	Reference temperature at STC (25 $°C$)

$$I = I_{ph-eff} - I_0\left[\exp\left(\frac{q(V+IR_s)}{nkTN_s}\right) - 1\right] - \frac{V+IR_s}{R_{sh}} \tag{4.9}$$

Table 4.2: Description of variables, constants and unknowns in output current (I) equation 4.9.

Variable	Description
I	Output current
V	Output voltage
T	Instantaneous module temperature
Constants	**Description**
q	Electron charge ($1.60217646 \times 10^{-19}$ C)
k	Boltzmann's constant ($-1.380652 \times 10^{-23}$ J/K)
N_s	Number of cells in specific bifacial module
Unknown parameter	**Description**
I_0	Diode saturation current
R_s	Series resistance
R_{sh}	Shunt resistance
n	Ideality factor

The process of solving the unknown parameters for the output current equation is explained in section 4.3.2. Once the parameters are solved, it will be possible to determine the output power of a bifacial module at a given time for corresponding irradiance values.

4.3.1.2 Parallel $R_{sh} - R_s$ one-diode model

The parallel $R_{sh} - R_s$ one-diode model is implemented as an alternative model when compared to the models commonly found in literature. The model is

realised by placing two independent one-diode circuits in parallel as shown in Figure 4.13. Each independent one diode circuit's output current contributes to the total output current (I) of the model and represents the front (I_f) and rear (I_r) sides of a bifacial module respectively.

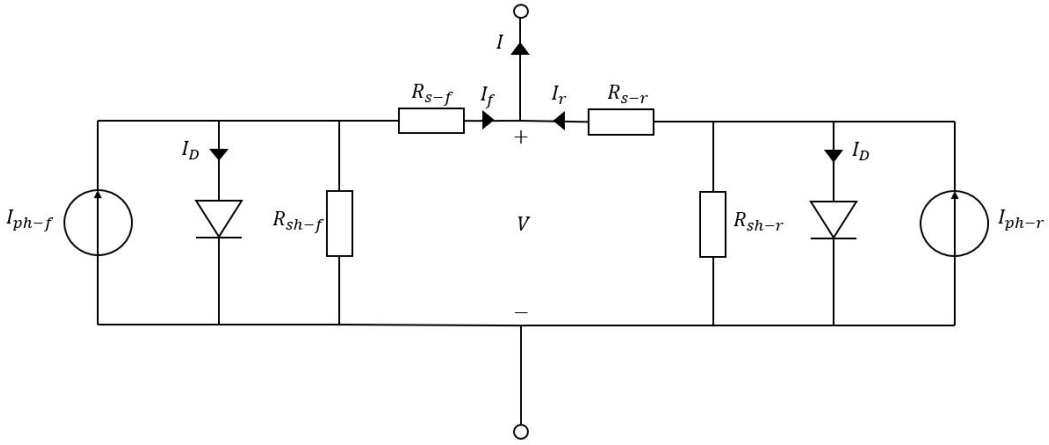

Figure 4.13: Circuit diagram of the parallel $R_{sh} - R_s$ one-diode model for bifacial PV cells.

The parallel $R_{sh} - R_s$ one-diode model yields Equations (4.10)-(4.12) where table 4.4 describes the variables that are not found in previous equations.

$$I = I_f + I_r \tag{4.10}$$

$$I_f = I_{ph-f} - I_{0-f}\left[\exp\left(\frac{q(V + I_f R_{s-f})}{n_f k T N_s}\right) - 1\right] - \frac{V + I_f R_{s-f}}{R_{sh-f}} \tag{4.11}$$

$$I_r = I_{ph-r} - I_{0-r}\left[\exp\left(\frac{q(V + I_r R_{s-r})}{n_r k T N_s}\right) - 1\right] - \frac{V + I_r R_{s-r}}{R_{sh-r}} \tag{4.12}$$

where

$$I_{ph-f} = \frac{G_{front}}{G_{ref}}\left(I_{sc-f} + \alpha(T - T_{ref})\right) \tag{4.13}$$

$$I_{ph-r} = \frac{G_{rear}}{G_{ref}}\left(I_{sc-r} + \alpha(T - T_{ref})\right) \tag{4.14}$$

From table 4.4 it is clear that double the amount of unknown parameters need to be solved for the parallel $R_s - R_{sh}$ one-diode model. The following section described the methodology for solving the unknown parameters for both electrical model implementations.

Table 4.3: Description of variables, constants and unknowns in output current (I_f and I_r) equations (4.10)-(4.12).

Variable	**Description**
I_f, I_r	Front and rear side current contribution
I_{ph-f}, I_{ph-r}	Front and rear side photon current
Unknown parameter	**Description**
I_{0-f}, I_{0-r}	Front and rear side diode saturation current
R_{s-f}, R_{s-r}	Front and rear side series resistance
R_{sh-f}, R_{sh-r}	Front and rear side shunt resistance
n_f, n_r	Front and rear side ideality factor

4.3.2 Solving unknown model parameters

From section 4.3.1 it can be seen that the implementation of an electrical model yields a set of equations that allows one to simulate the electrical behaviour of bifacial PV modules. The sets of equations that are derived from the two varying implementations of the $R_{sh} - R_s$ one-diode model, consist of some unknown parameters that are unique to each PV module and are identified in tables 4.2 and 4.4. In order to obtain accurate results for the output current and voltage, it is necessary to solve the unknown parameters for each individual module. The parameter solving methodology for bifacial modules, as proposed in [3], requires a range of input values that are obtained from extensive characterisation tests. It was not possible to perform these extensive characterisation tests at the facilities where the research for this thesis was done, therefore generic monofacial parameter solving methodologies were investigated and implemented.

4.3.2.1 Effective one-diode model parameter estimation

From table 4.2 it is clear that there are essentially four unknown parameters that need solving, namely: I_0, R_{sh}, R_s and n. In order to solve these four parameters, it is necessary to derive equations that can be utilised in the solving process. A combination of the methodology as proposed by *De Soto et al.* and *Mahmoud et al.* was chosen as it only requires input values that are obtainable from a module's data-sheet i.e. I_{sc}, V_{oc}, I_{mpp} and V_{mpp} [27] [34]. The illustrated IV-curve in Figure 4.14 shows the relationship of the input points. These input values are standardised for all PV modules at STC and are required by the $IEC60904-1-2$ as part of the standardised characterisation for bifacial modules (section 3.1) [24]. By inserting these known values into equation 4.9, the following intermediate equations are obtained [27]:

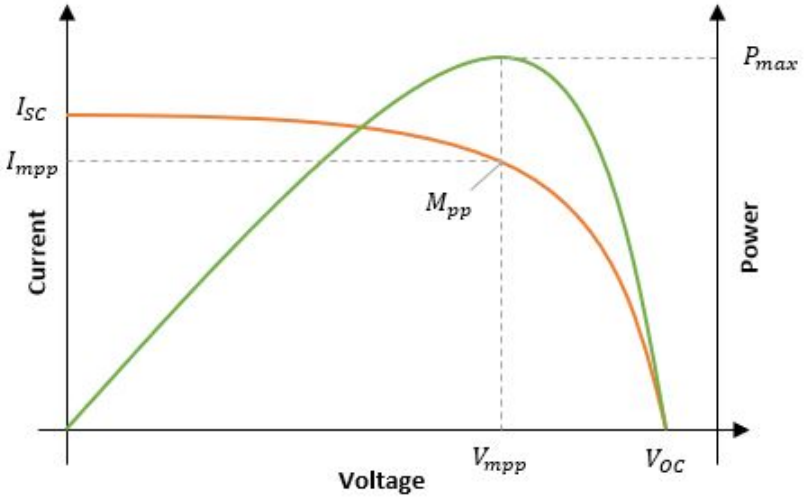

Figure 4.14: Input values obtained from PV module IV-characteristic curve .

For short-circuit current: $I = I_{sc}$ and $V = 0$.

$$I_{sc} = I_{ph} - I_0\left[\exp\left(\frac{q(I_{sc}R_s)}{nkTN_s}\right) - 1\right] - \frac{I_{sc}R_s}{R_{sh}} \tag{4.15}$$

For equation (4.15), the second and third terms are negligible which results in the following approximation.

$$I_{ph} \cong I_{sc} \tag{4.16}$$

Open-circuit voltage: $I = 0$ and $V = V_{oc}$.

$$0 = I_{ph} - I_0\left[\exp\left(\frac{q(V_{oc})}{nkTN_s}\right) - 1\right] - \frac{V_{oc}}{R_{sh}} \tag{4.17}$$

Maximum power point: $I = I_{mpp}$ and $V = V_{mpp}$.

$$I_{mpp} = I_{ph} - I_0\left[\exp\left(\frac{q(V_{mpp} + I_{mpp}R_s)}{nkTN_s}\right) - 1\right] - \frac{V_{mpp} + I_{mpp}R_s}{R_{sh}} \tag{4.18}$$

From Figure 4.14, it is clear that the derivative of the output power (IV) at maximum power point $(\frac{d(IV)}{dV}\big|_{mpp})$ is equal to zero. Therefore,

$$\frac{d(IV)}{dV}\bigg|_{mpp} = I_{mpp} - V_{mpp}\frac{d(I)}{dV}\bigg|_{mpp} = 0 \tag{4.19}$$

where

$$\left.\frac{d(I)}{dV}\right|_{mpp} = \frac{\frac{-qI_0}{nkTN_S}e^{\frac{q(V_{mpp}+I_{mpp}R_s)}{nkTN_s}} - \frac{1}{R_{sh}}}{1+\frac{qI_0R_s}{nkTN_s}e^{\frac{q(V_{mpp}+I_{mpp}R_s}{nkTN_s}+\frac{R_s}{R_{sh}}}} \tag{4.20}$$

Now there are four equations (4.16)-(4.19) and five unknown parameters $(I_{ph}, I_0, n, R_{sh}, R_s)$. It is therefore necessary to estimate one parameter in order to obtain the other four parameters. Here, the estimation process as described by [34] is implemented. First the value of R_{sh} is set to infinity (10^7) and substituted into equations (4.18) and (4.19) in order to solve R_s and n. If the result for R_s and n is a viable solution i.e. R_s is positive and n is not significantly greater than 1.5, it is possible to estimate I_0 with equation (4.17). If a viable solution for R_s and n is not found after the first step, R_s can be set to zero in order to estimate R_{sh} and n from equations (4.18) and (4.19), after which I_0 can be estimated with equation (4.17). This process is illustrated in the flowchart that is given in Figure 4.15.

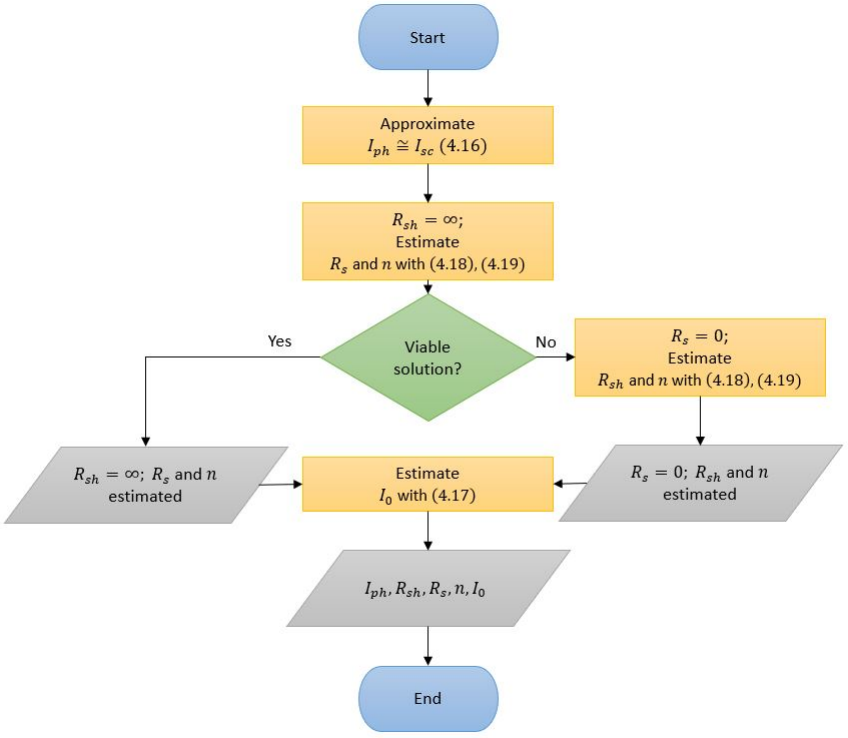

Figure 4.15: Flowchart illustration of the unknown parameter solving methodology.

The simultaneous solving of equations is done by utilising the *root* function in *python*'s *scipy.optimize* package. The function takes the equations to be solved and rough estimate values for the unknowns as input and returns the solutions for the given equations.

4.3.2.2 Parallel one-diode model parameter estimation

The same process as described above is followed in solving the unknown parameters for the parallel one-diode model as given in table 4.4. The only difference is that the process is followed twice in order to solve the unknown parameters of the front and the rear side. While the unknown parameters of one side is being estimated, the assumption is made that the opposite side is virtually blocked out and delivers no contribution to the current output. Therefore, in equation (4.10), $I_r = 0$ while estimating the front side parameters and $I_f = 0$ while estimating the rear side parameters.

This parallel one-diode model implementation and it's accompanying parameter solving method is only possible if the data-sheet of the specific bifacial module contains the rated values of the front and rear side as they were characterised separately. Some manufacturers [35] do provide the separate rated values as seen in the cut-out given in Figure 4.16. Once the model parameters are solved, it is necessary to implement a thermal model in order to accurately simulate the electrical behaviour of bifacial modules.

Testing Condition	Front	Back
Maximum Power (Pmax/W)	350	263
Open Circuit Voltage (Voc/V)	47.2	46.8
Short Circuit Current (Isc/A)	9.39	7.19
Voltage at Maximum Power (Vmp/V)	39.2	40.2
Current at Maximum Power (Imp/A)	8.93	6.54

Figure 4.16: Cut-out of a bifacial module data-sheet that contains separately rated values for both the front and the rear sides [35].

4.3.3 Thermal model

It is known that the operation and output of PV modules are highly dependent on the effects of temperature. Some solar cells are rated to have a negative temperature coefficient of 0.4% which will lead to a 1% decrease in output power for every 2.5 K that the module temperature is over 25 $^{\circ}C$ [3]. The thermal behaviour of monofacial modules is extensively researched and studied, but the work done for bifacial modules is rather scarce [3]. Although the thermal behaviour of bifacial modules can vary significantly due to transparent rear covering and higher power output, it was decided to implement a thermal model as proposed for monofacial modules. The goal is to model the module temperature with the ambient temperature as input and then utilise the characterised temperature coefficients to model the effects of the module

temperature. The following equation is implemented to estimate the module temperature given the ambient temperature and wind velocity [36].

$$T = T_a + \left(\frac{9.5}{5.7 + 3.8V_w}\right)\left(\frac{G}{G_{nom}}\right)\left(T_{nom} - T_{ref}\right)\left[1 - \frac{\eta_c}{\tau\alpha}\right] \tag{4.21}$$

Table 4.4: Description of variables, constants and unknowns in output current (I_f and I_r) equations 4.10-4.12.

Constants	**Description**
$\tau\alpha$	*Nusselt-Jurgess* correlation for convection ($\tau\alpha = 0.9$)
Variable	**Description**
T	Module temperature (K)
T_a	Ambient temperature (K)
V_w	Wind velocity (m/s)
G	Incident irradiance (W/m^2)
G_{nom}	Irradiance at nominal operating conditions (W/m^2)
T_{nom}	Temperature at nominal operating conditions (K)
T_{ref}	Temperature at STC (K)
η_c	Module efficiency

The estimated module temperature, T, is then used in equations (4.8) and (4.9) for the implementation of the effective one-diode model and in equations (4.11), (4.12), (4.13) and (4.14) for the parallel one-diode model implementation.

4.3.4 Determining bifacial module power output at maximum power point

With all the necessary parameters and independent values now obtained, it is possible to calculate the output power of a specific bifacial module by applying the modelled irradiance conditions to the chosen electrical model equations as given by (4.22)-(4.24).

$$I = I_{ph-eff} - I_0\left[\exp\left(\frac{q(V + IR_s)}{nkTN_s}\right) - 1\right] - \frac{V + IR_s}{R_{sh}} \tag{4.22}$$

$$I_f = I_{ph-f} - I_{0-f}\left[\exp\left(\frac{q(V + I_fR_{s-f})}{n_fkTN_s}\right) - 1\right] - \frac{V + I_fR_{s-f}}{R_{sh-f}} \tag{4.23}$$

$$I_r = I_{ph-r} - I_{0-r}\left[\exp\left(\frac{q(V + I_rR_{s-r})}{n_rkTN_s}\right) - 1\right] - \frac{V + I_rR_{s-r}}{R_{sh-r}} \tag{4.24}$$

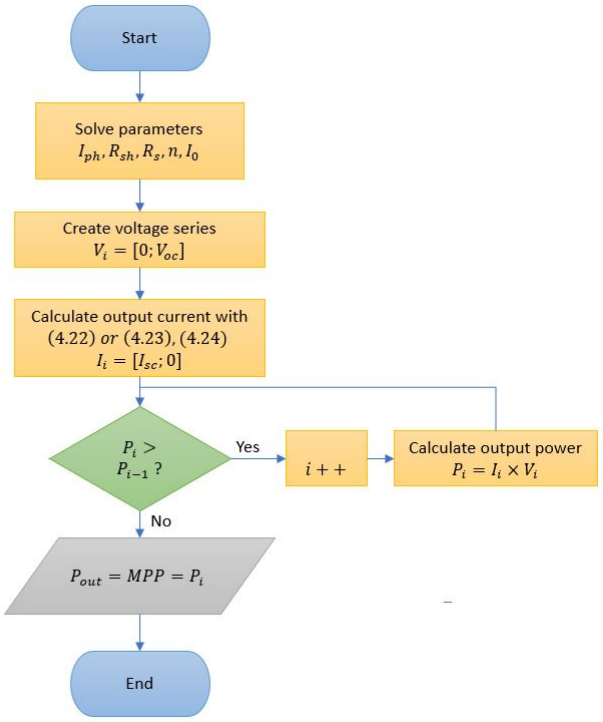

Figure 4.17: Flowchart illustrating the process of determining the power output at MPP for a bifacial module.

The output power is determined by modelling the IV-curve of the module at a designated irradiance value and then determining the maximum power point (MPP) as illustrated in Figure 4.17. The IV-curve is modelled by creating a voltage series with n equally spaced values ranging from short-circuit- to open-circuit voltage. The voltage series can be described as:

$$V_i = [0; V_{oc}] \tag{4.25}$$

where $i = 0, 1, 2...n$

Each voltage value in V_i, irradiance measurement (G_{front} and G_{rear}) and module temperature value (T) is then applied to equation (4.22) or (4.23) and (4.24) to calculate the corresponding current value. A current series is then created which corresponds to the voltage series and can be described as:

$$I_i = [I_{sc}; 0] \tag{4.26}$$

From this a power series can be created by sequentially multiplying the voltage- and current series with one another. It is then possible to determine the MPP by identifying the maximum value in the power series. The MPP is then chosen to be the output power value of the bifacial module at that given time. The power series, MPP and output power can be given as:

$$P_i = I_i \times V_i \tag{4.27}$$

$$P_{out} = MPP = max(P_i) \tag{4.28}$$

Although the output power at a given time can be calculated, some software functions are required to help the process of integrating the irradiance and electrical models, as well as provide some features that will allow simulation of bifacial modules.

4.4 Miscellaneous features

The two most important parts, the irradiance and electrical models, of the bifacial simulation software are successfully implemented in order to produce power output values for corresponding modelled irradiance measurements. There are a number of miscellaneous features that need to be implemented to allow some flexibility when it comes to data handling, verification tests and running simulations. These features include data-file handling, tracking algorithms and a graphical user interface.

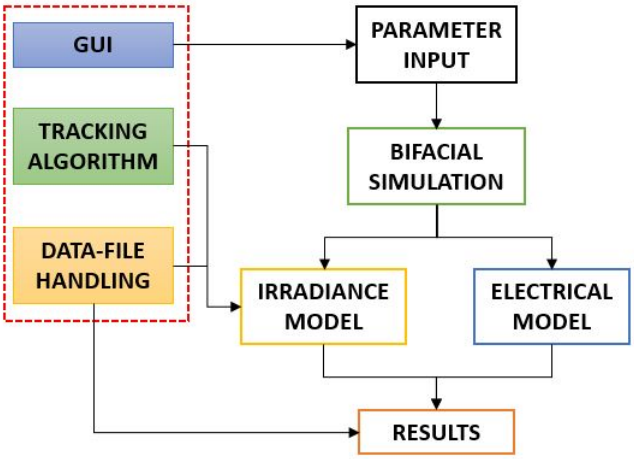

Figure 4.18: Illustration of the interaction between the miscellaneous features and the simulation process.

4.4.1 Graphical user interface

A graphical user interface (GUI) is implemented to allow a user to input various parameters that are specific to the simulation requirements. The GUI adds some flexibility to the simulation software without the need to alter the source code of the software for each variation in simulation requirements. The GUI

focusses on four areas of user input as the illustration in Figure 4.19 shows. Each area focusses on a category of input parameters that are required to obtain the required simulation results.

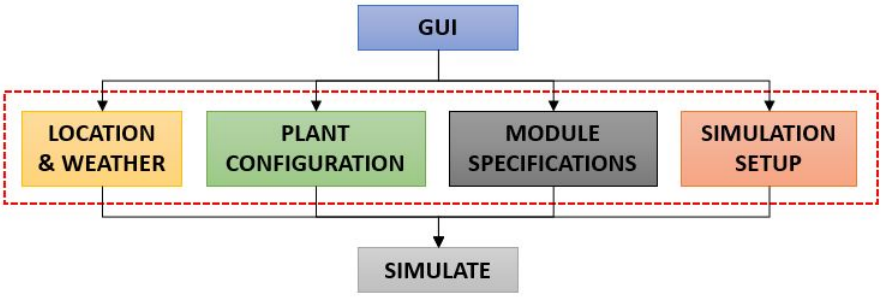

Figure 4.19: Illustration of the four areas on which the GUI focusses.

4.4.1.1 Location and weather

The location and weather tab takes input parameters that correspond with the environment at which a bifacial installation will be simulated. Figure 4.20 shows a copy of the location and weather tab. There are three main parameters that are obtained from this tab i.e. ground albedo, latitude and longitude coordinates and the time zone. A weather file must be specified that holds the data needed to build the irradiance model. The option between manual or weather file entry is also given which allows the site information to be extracted from the specified weather file.

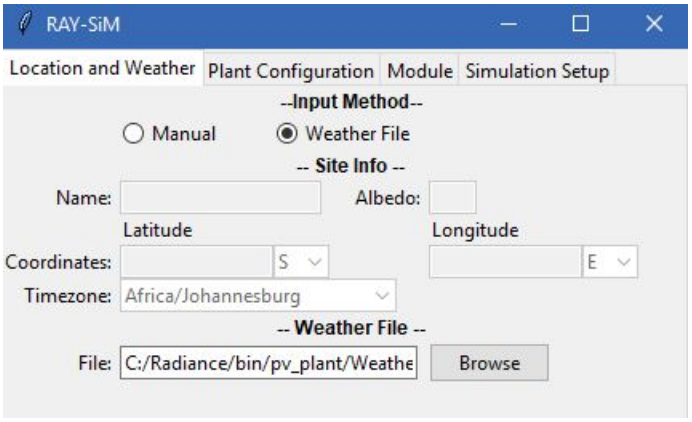

Figure 4.20: Location and weather tab in the GUI.

4.4.1.2 Plant configuration

The plant configuration tab allows users to input data that is relevant to the design and layout of the bifacial PV installation that requires simulation. The input fields of the plant configuration tab is shown in Figure 4.21. The plant configuration tab takes the amount of rows and columns in the plant as well as the spacing between adjacent rows and columns. The module mounting elevation can also be specified as it plays an important role in the rear side's exposure to irradiance. An option is given for the modules to follow a tracking algorithm or the specified fixed tilt and azimuth angles can be input. This input data allows the modelling of the virtual environment for a bifacial simulation.

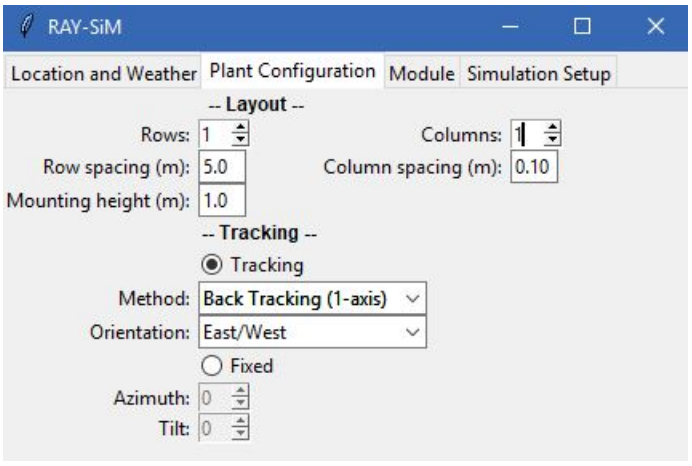

Figure 4.21: Plant configuration tab in the GUI.

4.4.1.3 Module specifications

The module specifications tab requires input that corresponds to the design and characteristics of the bifacial module that is implemented for the required simulation. Figure 4.22 shows the fields that a user can input in order to specify the designated bifacial module. The required input data corresponds to the electrical characteristics of a given bifacial module and can be obtained from the module's datasheet. The module geometry is also required in order to define the modules virtually. All the fields can be input manually or by means of a module file which can be pre-defined and contains all the data as mentioned. The data acquired from the module specifications tab is critical in setting up the electrical model of the bifacial simulation.

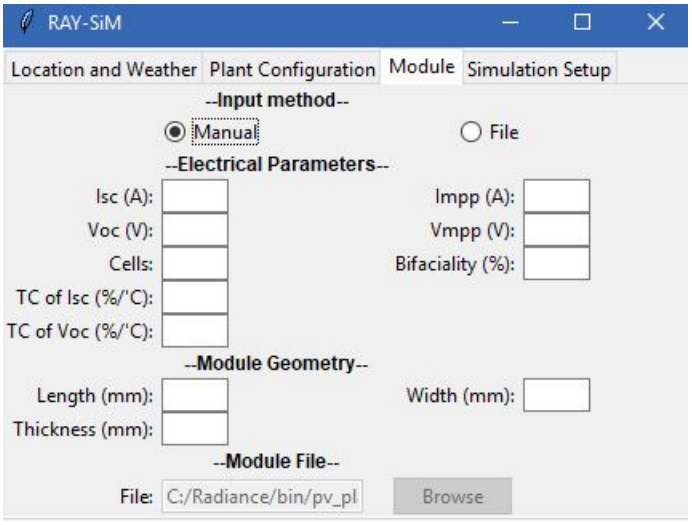

Figure 4.22: Module specification tab in the GUI.

4.4.1.4 Simulation setup

The simulation setup tab relates to the period of the required simulation as well as the data with which the simulation results can be compared. Figure 4.23 shows the simulation setup tab with it's input fields. The simulation period is determined by defining a start date together with the required period i.e. one day, one month or one year (annual). A custom start and end date can also be set by the user for a custom simulation period. The option is given to specify a file which contains data with which the simulation output can be compared by means of line plots and output files. The simulation setup tab receives user input that is essential to the simulation period and how the output compares with measured data.

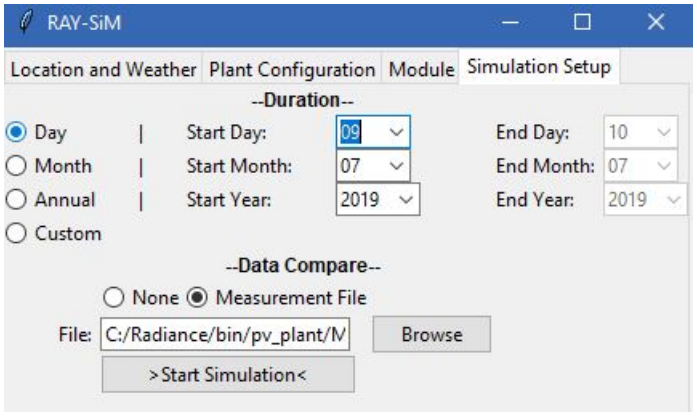

Figure 4.23: Simulation setup tab in the GUI.

4.4.2 Data-file handling

In order to verify and compare the irradiance and electrical models, it will be necessary to receive controlled real world input data as well as in-field measurement data. The real world input data may be used to build and compare the irradiance and electrical models and may include GHI, ambient temperature, wind velocity and plane of array angles. In-field measurements will be useful when verifying the output of irradiance and electrical models with real world data. Data-file handling is also necessary for presenting the simulation output data in an organised and interpretable manor. In table 4.5, the data-files that are used and produced in the simulation process are presented.

Input	
File	**Data contained**
Weather file	GHI Ambient temperature Wind velocity
Measurement file	Plane of array front irradiance Plane of array rear irradiance Plane of array angle Output voltage Output current
Output	
Simulation results	Output voltage Output current Output power Module temperature Plane of array front irradiance Plane of array rear irradiance

Table 4.5: Input and output files that are used and produced by the simulation software.

It is required that the data of the input files are accompanied with time stamps that relates to the date and time of the corresponding data fields. It is therefore possible to extract the given data for a specific time of the year and period and present it in the form of *python dataframes* for ease of access throughout the simulation process. From the weather and measurement input files, two *dataframes* are created. The weather *dataframe* is used in the process of modelling the irradiance with modelled DNI and DHI data with GHI as input. The ambient temperature and wind velocity fields in the weather *dataframe* are used to implement the thermal model and in effect calculate the

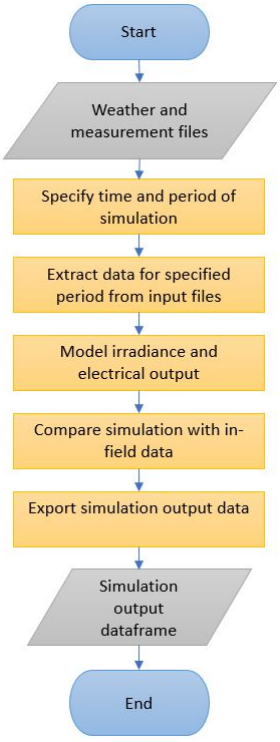

Figure 4.24: Flowchart illustrating the process of extracting and handling data throughout the simulation.

output power. Modelled output verification and comparison can be done by applying the measurement *dataframe* after which a simulation output data-file is produced. The data handling process is illustrated in the flowchart given in Figure 4.24.

4.4.3 Tracking algorithm

Tracking plays an important role in the maximisation of solar PV power output. A tracking implementation allows a single PV module or an array of modules to track the path of the sun which results in more direct irradiance exposure of PV cells, hence an increase in power output as opposed to fixed tilt applications. Solar PV tracking has taken on many forms from which single- and dual-axis trackers are the most common examples of trackers [37].

As illustrated in Figure 4.25a, single-axis tracking is limited to the movement of PV modules around one axis. Commonly, the chosen axis will be in the horizontal plane and a north-south orientation which allows the PV modules to track the sun's path in a hemispherical manner from sun rise to sun set. Dual-axis trackers have the ability to move along two axis as shown in Figure 4.25b. This form of tracking leads to more flexibility when it comes to accurate

(a) Single-axis tracking. (b) Dual-axis tracking.

Figure 4.25: Two variations of PV tracking.

tracking of the sun's varying path between seasons. Dual-axis trackers tend to be more expensive as they require more hardware to operate when compared to single-axis trackers. When focussing on single-axis tracking, the back tracking algorithm is the most commonly used which not only mimics the sun's path, but also focusses on reducing shading between rows of PV modules.

4.4.3.1 Single-axis back tracking algorithm

As single-axis tracking only allows rotation around one axis, it is impossible to constantly keep a PV module's front surface orthogonal to the incident irradiance. With basic tracking, the tracking angle is therefore calculated to orientate the front surface of a PV module as close as possible to the sun's position with regards to the solar zenith and azimuth angle. The optimal alignment of a PV array with single-axis tracking is in an east-west orientation as shown in Figure 4.26a. The corresponding cross-section of the PV array in Figure 4.26b indicates how the ground plane (β) and the tracking angles (α) are defined.

The tracking angle can be calculated if the solar elevation (θ_e), azimuth (ϕ) and ground slope (β) angles are known. Solar elevation is the sun's elevation angle with respect to the ground plane and therefore given as:

$$\theta_e = 90 - \theta \tag{4.29}$$

where θ is defined as the solar zenith angle.

The solar coordinates (x_s, y_s, z_s) can be obtained from the elevation and azimuth angles as described in equations (4.30)-(4.32). The solar coordinates together with the ground plane angle can then be used in equation (4.33) to calculate the tracking angle [37].

$$x_s = r \cos\phi \cdot \sin\theta_e \tag{4.30}$$

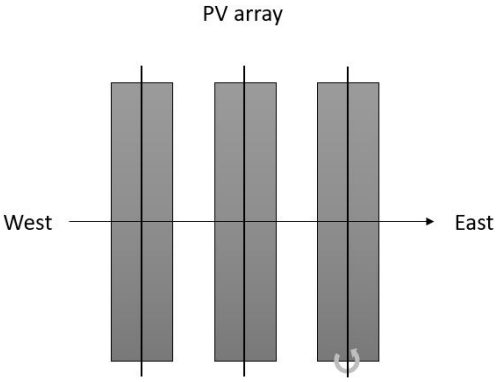

(a) Optimal PV array alignment for single-axis tracking.

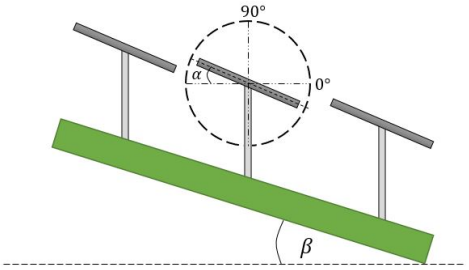

(b) Cross-section of PV array with definition of tracking angle (α) and ground plane slope (β).

Figure 4.26: Top view and cross-section of a single-axis tracking PV array.

$$y_s = r \sin\phi \cdot \cos\theta_e \tag{4.31}$$

$$z_s = r \cos\theta_e \tag{4.32}$$

$$\alpha = \arctan\left(-\frac{y_s}{z_s}\right) - \beta \tag{4.33}$$

Although this tracking angle (α) attempts to maintain orthogonality between the PV modules and incident irradiance, it is possible for the PV array rows to cause shading on adjacent rows, especially with solar elevation angles that are associated with sunrise and sunset. This occurrence of shading is illustrated in Figure 4.27. The implementation of a back tracking algorithm aims to solve this shading problem between adjacent rows with spacing (D) and width (H). The first step is to determine if shading actually occurs between adjacent rows. This is done by defining a vector $\vec{\mathbf{S}}$ that originates at the sun's position ($\mathbf{s}$) and passes through point $\mathbf{p}$. Point $\mathbf{B}$ is the point at which $\vec{\mathbf{S}}$ intersects the plane in which the adjacent row is located. The vector $\vec{\mathbf{S}}$ and intersection $\mathbf{B}$ can be determined as described in equations (4.34)-(4.36) [37].

$$\vec{\mathbf{S}} : \mathbf{p} + \lambda \mathbf{s} \tag{4.34}$$

$$\lambda = -\frac{D \sin\alpha}{z_s \cos\alpha - y_s \sin\alpha} \tag{4.35}$$

By substituting (4.35) into (4.34) it is possible to determine the Cartesian coordinates of the intersection point $\mathbf{B}$:

$$\mathbf{B} = \mathbf{p} - \frac{D \sin \alpha}{z_s \cos \alpha - y_s \sin \alpha} \mathbf{s} \tag{4.36}$$

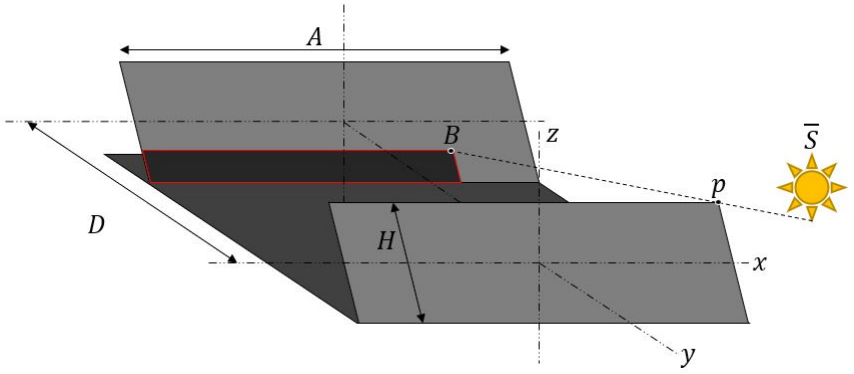

Figure 4.27: Illustration of a shading occurance between adjacent rows in a PV array.

As $\mathbf{B}$ can lie anywhere in the plane of the adjacent row, a boundary check is executed in order to determine if shading does indeed occur. Once it is known that shading is caused between adjacent rows due to the original tracking angle α, a new back-tracking angle α_{BT} can be calculated with equations (4.37)-(4.40) [37].

$$\alpha_{BT} = \arccos \frac{a - \sqrt{b}}{c} - \beta \tag{4.37}$$

where

$$a = H \cdot D \cdot z_s^2 \tag{4.38}$$

$$b = H^4 y_s^4 + H^4 y_s^2 z_s^2 - H^2 D^2 y_s^2 z_s^2 \tag{4.39}$$

$$c = H^2 y_s^2 + H^2 z_s^2 \tag{4.40}$$

With the back-tracking algorithm as described above, it is possible to mimic the tracking implementation of most monofacial PV installations. With the integration of the irradiance and electrical models together with the miscellaneous features, it will be possible to determine if this form of tracking and other implementations are applicable to bifacial technology.

4.5 Integration of irradiance and electrical models

In order to accurately simulate bifacial PV applications it is necessary to integrate the independent irradiance and electrical models together with the miscellaneous features. Although both the irradiance and electrical models are able to function independently, it is essential to combine their functionality which will enable simulations to evaluate a variety of design parameters for bifacial PV. The integration was realised by using the *python* development language. *Python* offers the functionality that is required to complete the following tasks:

- Receive input from a user by means of a GUI.
- Run the necessary *Radiance* commands in order to model irradiance.
- Execute scientific calculations which models the electrical behaviour of bifacial modules.
- Handle input and output data and create and read data files.
- Plot output data for comparison and verification.

A summarised flowchart of the simulation process is given in Figure 4.28. Upon initiation, the user is able to provide essential input data by means of a GUI. The simulation period is determined and a corresponding timestamp series is created. The applicable files are read and the necessary data is then extracted for the designated time period. The simulation process then starts by building the virtual environment given the weather input with a series of text files. After converting the applicable files to an octree file, the irradiance measurement points for the front and rear surfaces are determined after which the *rtrace* command returns the irradiance values at these points. This process is followed for each timestamp in the series which relates to the simulation period. The irradiance at each timestamp is stored in a *dataframe* which will be utilised later on.

Now the electrical model is built by extracting the module parameters as given by the user. The unknown parameters are solved and given to the model equations. The software then steps through the modelled irradiance values which serves as input to the electrical model equations. First the module temperature is calculated after which the output current-voltage characteristic series (*IV-series*) is calculated. From the *IV-series* the MPP is determined and defined as the output power which corresponds to the given instantaneous

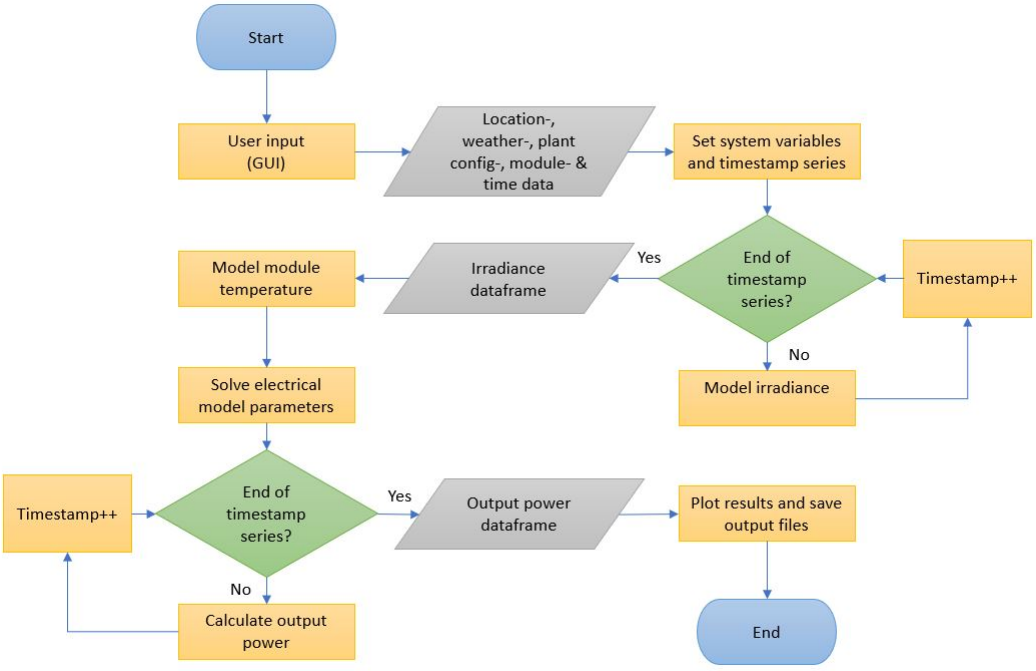

Figure 4.28: Summarised flowchart illustration of the integrated bifacial simulation software.

irradiance and module temperature. This process is followed for each irradiance value in the modelled irradiance *dataframe*. The modelled output power for each time step is stored in a *dataframe*.

The modelled irradiance and output power are then plotted against the data with which it was chosen to be compared. For irradiance, the front and rear irradiance are plotted seperately in order to evaluate the rear side irradiance individually. The output data is also saved in the form of a simulation output file (*.csv*) which can be used for third party analysis.

Chapter 5

Practical verification and results

The simulation software for bifacial PV is developed by integrating independent models for the irradiance and the electrical behaviour. The goal is to design a simulation tool that can be used to model and optimise the design for bifacial PV installations. To achieve this goal it is important to verify the accuracy functionality of the irradiance and electrical models separately before evaluating the outcome and results of the bifacial simulation software as a whole.

Firstly the irradiance and electrical models will be verified with independent experiments which compares the modelled outputs with real-world measurements. Upon verifying that the models are accurate and functional in modelling the essential factors such as rear side irradiance and electrical output, it is possible to validate the effectiveness of the simulation software after integrating the two models. Successful integration of the irradiance and electrical models will allow a range of simulations to be run in order to gain some insight into bifacial technology and make some recommendations with regards to optimisation of bifacial plants etc.

5.1 Comparison metrics used for verification

This section will give context with regards to the error calculations that are used to verify the irradiance and electrical models. The respective models will be verified by comparing the modelled irradiance and power output with data as measured at a designated bifacial PV test site. The accuracy of the models will be determined by calculating the root mean square error (RMSE) and mean bias error (MBE).

The RMSE is used to quantify the accuracy of a predicted dataset with a corresponding observed or measured dataset. For the verification process, the modelled and measured datasets consist of data points for 24-hour day with

10 minute intervals. To calculate the RMSE, the mean of the summed squared deviations between modelled (p_i) and measured (o_i) values in the dataset with size N is obtained. The RMSE value is then determined by taking the square root of the calculated mean as shown by Equation (5.1) [38].

$$RMSE = \sqrt{\frac{\sum_{i=1}^{N}(p_i - o_i)^2}{N}} \tag{5.1}$$

The second metric used for comparison is the MBE which relates to a value that indicates whether a prediction model under- or overestimates when compared to measured data. The MBE is calculated as the mean of the summed deviations between modelled and measured datasets. A negative MBE would mean that the model underestimates and a positive MBE relates to an overestimation. The MBE value relates to the margin by which the model under- or overestimates. Equation (5.2) shows the formula for calculating MBE [38].

$$MBE = \frac{\sum_{i=1}^{N}(p_i - o_i)}{N} \tag{5.2}$$

Other comparison metrics such as mean absolute error (MAE) and mean absolute percentage error (MAPE) will not be used for verification purposes as the RMSE and MBE will give sufficient insight with regards to model accuracy.

5.2 Experimental bifacial PV installation

For the sake of verifying the irradiance and electrical models, it is necessary to compare the modelled results with measurements taken on an actual bifacial PV installation. The chosen bifacial PV installation is the Stellenbosch University PV test site at Mariendahl. The bifacial installation consists of two adjacent rows of twenty-eight modules that form part of a six row installation. The layout of the PV installation at Mariendahl is given in Figure 5.1 where the two bifacial rows are also identified. The two 28-module bifacial rows are connected to a central single-axis tracking controller that allows single-axis backtracking for all the rows in the plant.

5.2.1 Weather station

For verification purposes it is necessary to acquire the GHI as measured at the PV test site.The irradiance and other weather measurements are taken by a on-site weather station. The weather station consists of a control unit, a thermometer for ambient temperature readings and a pyranometer for GHI readings. It must be mentioned that the GHI pyranometer has a measurement uncertainty of 2% which must be taken into consideration for analysing the verification results. Readings are automatically taken in one-minute intervals

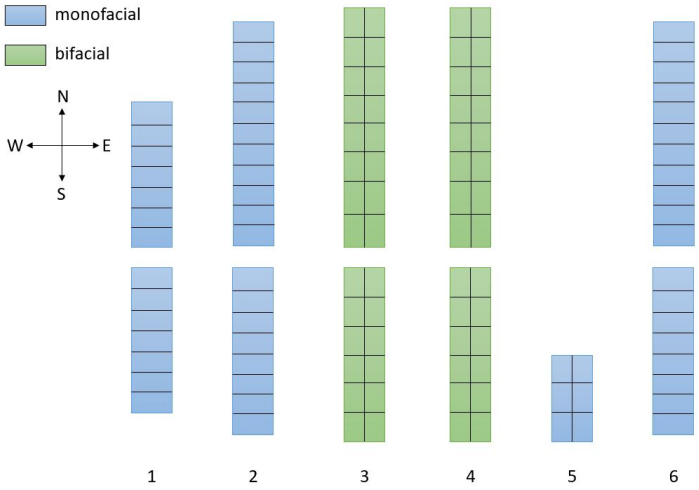

Figure 5.1: Plant layout at Mariendahl test site.

Figure 5.2: Weather station at Mariendahl test site.

from where the data is stored for later access. The weather station unit is shown in Figure 5.2.

5.3 Verification of irradiance model

The irradiance model plays a critical role in simulating bifacial PV modules as it is proven in [15] that there are some complexities with regards to modelling of the rear side irradiance. It was therefore decided to implement the ray tracing algorithm as an irradiance modelling technique as described in chapter 4, section 4.2. It is now essential to verify the accuracy and functionality of the ray tracing irradiance model by comparing the modelled irradiance with real-world irradiance measurements.

5.3.1 Experiment methodology

In order to verify the irradiance model, it is necessary to compare the modelled irradiance results with irradiance measurements taken on an actual PV installation. It is essential that irradiance measurements are taken on the front and rear sides of bifacial modules as the accuracy of both sides' irradiance is of high importance. The real-world irradiance measurements of the front and rear sides are obtained with the installed pyranometers as described in section 5.3.2. The real-world environment is modelled by providing the GHI data, as measured by the on-site weather station, for the same time the irradiance measurements were taken. The modelled and measured irradiance are then compared and the accuracy of the model is determined.

5.3.2 Experiment input

In order to compare the modelled irradiance with measured irradiance, it is necessary to provide input data that models the bifacial installation and PV test site as close as possible. The irradiance model input data for the irradiance verification experiment is given in Table 5.1.

Table 5.1: Input data for irradiance model verification.

Site specifications	
Location	33.85 °S 18.86 °E
Modules	LR6-72BP-350
Rows	4
Row spacing	5 m
Module height	1 m
Tilt & tracking	Single-axis backtracking
Albedo	0.2
Model specifications	
Start date	09-07-2019
Period	2 days
Weather input	GHI (on-site)
Measured input	Front and rear irradiance

A set of three pyranometers are mounted onto the bifacial installation for in plane irradiance measurements and are located on the south side of the fourth row as Figure 5.3 illustrates. A plane of array front facing pyranometer is installed as shown in Figure 5.4a and two plane of array rear facing pyranometers are installed as shown in Figure 5.4b. The pyranometers used for the verification measurements have a uncertainty of 2% which might influence

the verification process. The irradiance measurements are taken and logged by the weather station for later access.

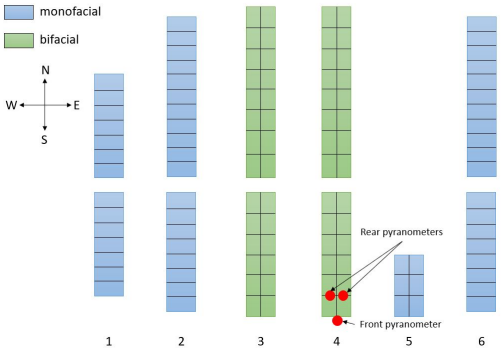

Figure 5.3: Illustration of the pyranometer locations within the PV test site.

(a) Front facing pyranometer. (b) Rear facing pyranometers.

Figure 5.4: Plane of array pyranometers at Mariendahl test site.

5.3.3 Verification results

The irradiance model is verified by comparing the modelled irradiance with pyranometer irradiance measurements for two days. It was decided to verify the irradiance model for a clear sky day as well as an intermittent day. The GHI as measured by the on-site weather station of a clear sky and intermittent day is given in Figures 5.5 and 5.6. The measured GHI is given as input to the irradiance model in order to ensure the validity of the verification. The modelled and measured results for the clear sky and intermittent days are compared in Figures 5.7-5.8 and 5.9-5.10 respectively. Table 5.2 gives the RMSE and MBE for the comparison between modelled and measured front and rear side irradiance for clear sky and intermittent days.

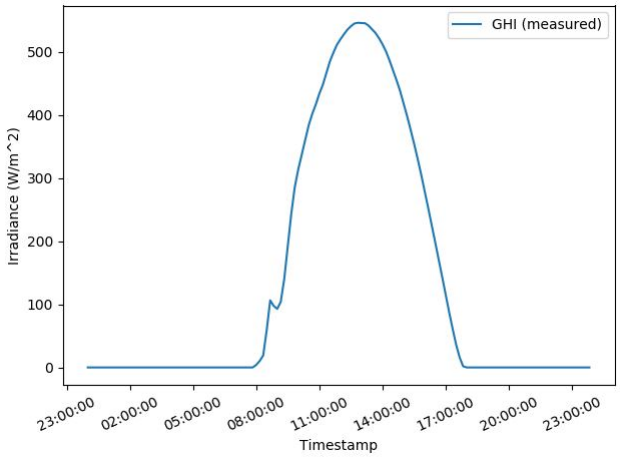

Figure 5.5: On-site measured GHI for a clear sky winter day.

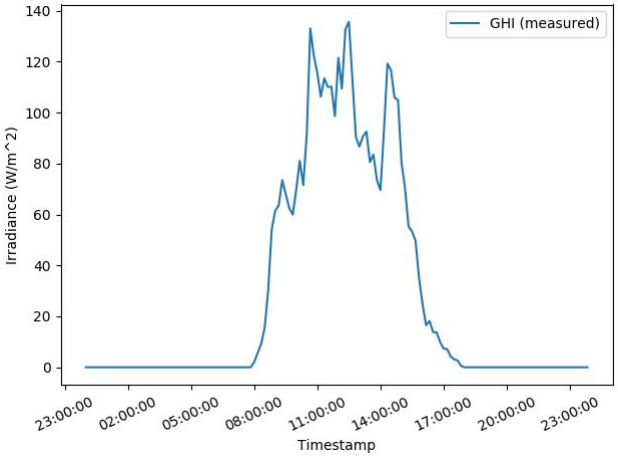

Figure 5.6: On-site measured GHI for a intermittent winter day.

The results of the clear sky verification as shown in Figures 5.7 and 5.8 are satisfying. The front side irradiance RMSE of 46.32 W/m^2 is substantial but when compared to a peak front irradiance of around 680 W/m^2, it becomes somewhat more acceptable. The MBE shows that the irradiance model underestimates the front irradiance by 20 W/m^2. The rear side irradiance errors are very satisfying with a mean RMSE of 3.8 W/m^2 and a mean MBE of 0.935 W/m^2 for the two rear measurement locations. This indicates that the irradiance model overestimates the rear side irradiance slightly when compared with measured data for a clear sky day.

A comparison between modelled and measured irradiance was also done for an intermittent day. The modelled and measured front and rear side irradiance are given in Figures 5.9 and 5.10. The RMSE for the front and two rear side irradiance measurements are 1.71 W/m^2, 1.56 W/m^2 and 1.54 W/m^2

Table 5.2: Statistical errors for the irradiance model verification.

Variable	**RMSE** (W/m^2)	**MBE** (W/m^2)
Clear sky day (Daily total irradiation: 3.25 kWh/m^2**)**		
Front irradiance	46.32	-20.19
Rear irradiance 1	3.57	1.09
Rear irradiance 2	4.04	0.78
Intermittent day (Daily total irradiation: 0.67 kWh/m^2**)**		
Front irradiance	1.71	0.54
Rear irradiance 1	1.56	0.29
Rear irradiance 2	1.54	0.41

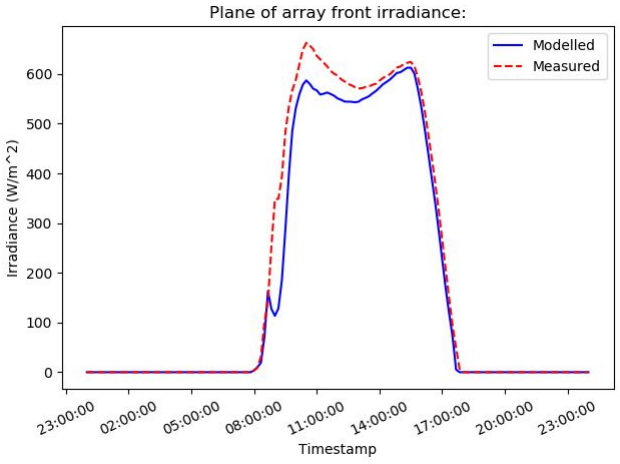

Figure 5.7: Comparison between modelled and measured plane of array front irradiance for a clear sky day.

respectively, which is satisfactory. The MBE values show that the irradiance model overestimates the front and rear irradiance slightly with an average MBE of 0.413 W/m^2 for an intermittent day.

When the assumption is made that the irradiance distribution is equally divided between clear sky and intermittent days over a long period, it is possible to determine that the ray tracing technique will model irradiance with an average RMSE of 24.01 W/m^2 for the front side and 2.68 W/m^2 for the rear side. The front irradiance is underestimated with a MBE of -9.825 W/m^2 where the rear side irradiance is overestimated with a MBE of 0.64 W/m^2. It must be noted that the verification was done in the winter season which may influence the results.

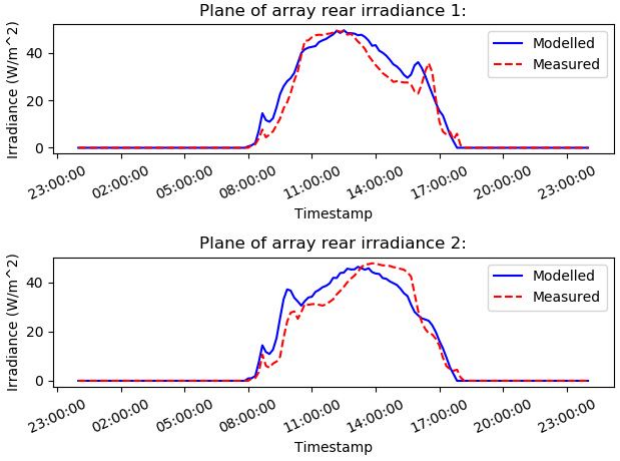

Figure 5.8: Comparison between modelled and measured plane of array rear irradiance for a clear sky day.

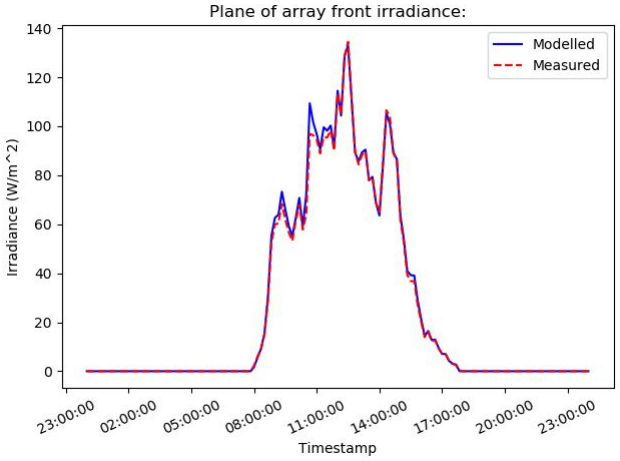

Figure 5.9: Comparison between modelled and measured plane of array front irradiance for an intermittent day.

5.4 Verification of electrical model

The simulation software for bifacial PV will rely on the accuracy of both the irradiance and electrical models. Now that the irradiance model is verified, it is necessary to verify the accuracy of the electrical model by comparing the modelled power output with measured power output of the bifacial installation at the PV test site. It will also be of interest to determine which of the two electrical models are more accurate.

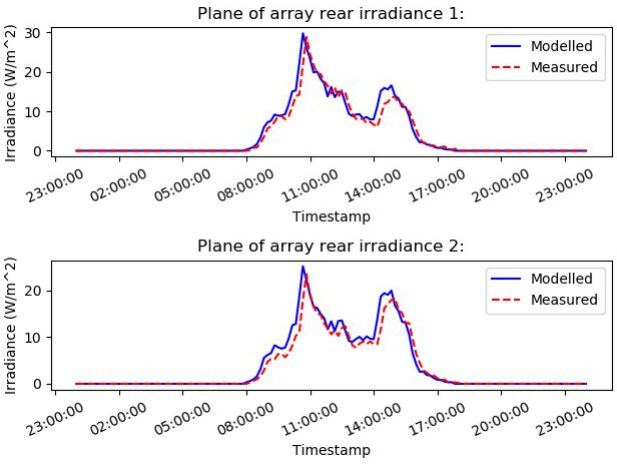

Figure 5.10: Comparison between modelled and measured plane of array rear irradiance for an intermittent day.

5.4.1 Experiment methodology

In order to verify the electrical model, the model results must be compared with measured power data. The output power is measured with a power logger that is connected in series with an installed *LONGI Solar* bifacial module at the PV test site. The front and rear irradiance as measured at the location of the designated bifacial module is given as input to the electrical model of which the result is modelled power output. The output of the two respective models, the effective and parallel $R_{sh} - R_s$ one-diode models, can then be compared with the measured output as the input irradiance is identical for both datasets.

5.4.2 Experiment input

The electrical power output is measured by a current and voltage logger that is connected in series with the designated bifacial module. The designated bifacial module is at the south side of the fourth row as illustrated in Figure 5.11. This location is chosen as it is exactly where the rear pyranometers are located which will measure the irradiance input to the electrical model. The power logger digitally takes voltage and current measurements in one-minute intervals. The measured data is then sent to a database via a central *Lora* network. The power logger is installed in a way that it does not significantly obstruct any cells from rear irradiance as shown in Figure 5.12. The performance and verification of the power logger can be observed in [39].

As the electrical model verification is reliant on the variation in irradiance and temperature it requires no input parameters with regards to the PV test site specifications. The bifacial module characteristics is however needed to

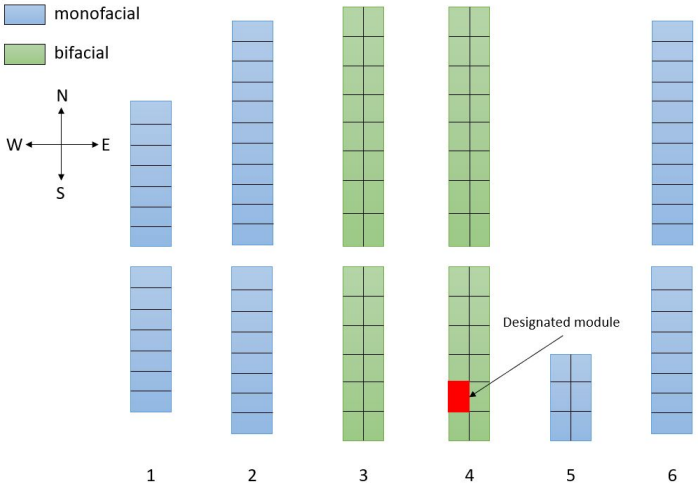

Figure 5.11: Illustration of the designated bifacial module's location at which the power logger is installed.

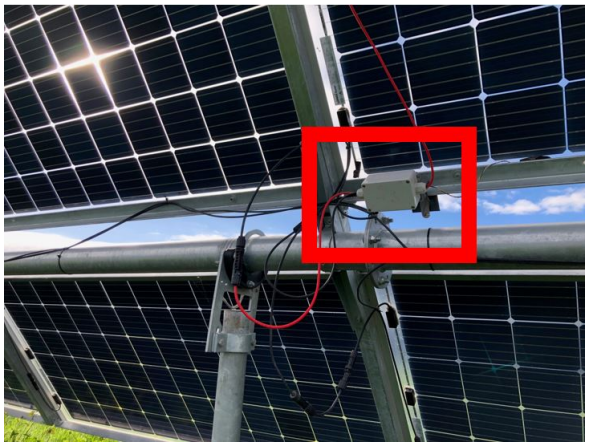

Figure 5.12: Installation of the power logger at the PV test site.

model the power output. The module input data is given and described in Table 5.3. It must be noted that the specific bifacial modules were characterised before the standard of $IEC-6094-1-2$ as described in 3.1, has been accepted as a standard. The modules are therefore separately characterised by the front and rear sides at STC of 1000 W/m^2 and 25 $^{\circ}C$.

5.4.3 Verification results

With all the input data available, it is now possible to model the electrical behaviour of the designated bifacial module by implementing two respective models namely the parallel and effective irradiance $R_{sh}-R_s$ one-diode models, as described in section 4.3.1. Both models are verified for intermittent and clear sky days for which the power output results are shown in Figures 5.13 and 5.15

Table 5.3: Characteristics of *LongiSolar* bifacial modules as installed at bifacial test site.

Model Code			LR6-72BP-350M
Characteristic	**Front**	**Rear**	**Unit**
Maximum power (P_{max})	350	263	W
Open-circuit voltage (V_{oc})	47.2	46.8	V
Short-circuit current (I_{sc})	9.39	7.19	A
Voltage at MPP (V_{mpp})	39.2	40.2	V
Current at MPP (I_{mpp})	8.93	6.54	A
Module efficiency (η_c)	17.8	13.3	%
Bifaciality (φ)	75		%
Temperature coefficient of I_{sc} (α)	+0.06		%/°C
Temperature coefficient of V_{oc} (β)	-0.30		%/°C

respectively. The modelled and measured energy output is also plotted and given in Figures 5.14 and 5.16 for both the intermittent and clear sky days. Table 5.4 gives the calculated RMSE and MBE for the two electrical models and the measured data.

Table 5.4: Statistical errors for the electrical model verification.

Variable	**RMSE**	**MBE**	**Unit**
Clear sky day (Daily measured energy: 9.93 kWh)			
Power (effective)	11.74	4.60	W
Power (parallel)	10.15	-2.16	W
Energy (effective)	0.393	0.243	kWh
Energy (parallel)	0.265	-0.209	kWh
Intermittent day (Daily measured energy: 1.5 kWh)			
Power (effective)	3.86	-1.42	W
Power (parallel)	7.34	-3.88	W
Energy (effective)	0.137	-0.103	kWh
Energy (parallel)	0.369	-0.273	kWh

First an analysis is done for the comparison between the parallel model and measured energy output. The intermittent and clear sky days yield respective RMSE values of 0.369 kWh and 0.265 kWh on the modelled and measured energy output. When observing the MBE for the two days, it is clear that the parallel model underestimates with an average MBE of -0.241 kWh.

After analysing the results of the effective model, it can be determined that this form of electrical modelling is the most accurate for bifacial modules.

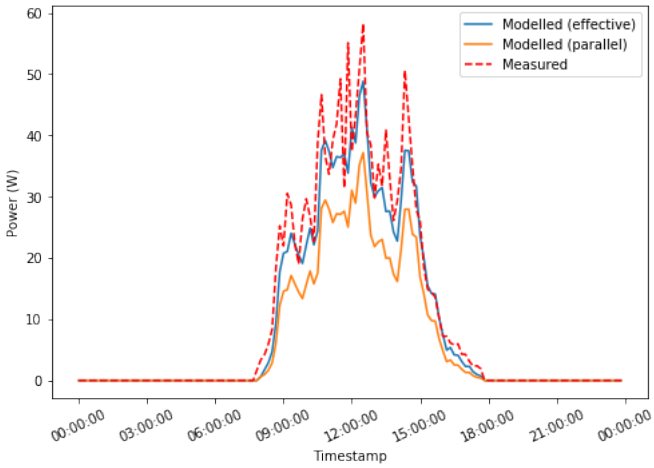

Figure 5.13: Comparison between two modelled (parallel and effective) and measured power output for an intermittent day.

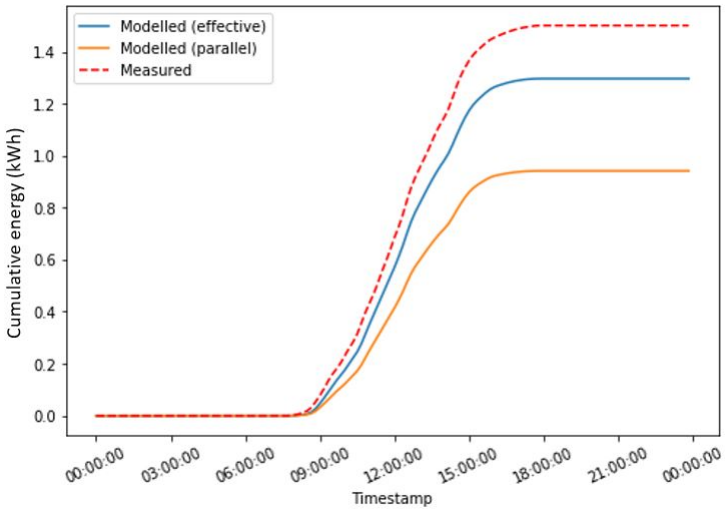

Figure 5.14: Comparison between two modelled (parallel and effective) and measured energy output for an intermittent day.

Although the effective model shows an overestimation on the energy output with a RMSE and MBE for a clear sky day of 0.393 kWh and 0.243 kWh respectively, this model yields an underestimation for an intermittent day with a RMSE and MBE of 0.137 kWh and -0.103 kWh. These values result in an overall energy output RMSE of 0.265 kWh and a MBE of 0.07 kWh which relates to a slight overall overestimation.

By comparing the average errors of the parallel and effective models, it is intuitive to prefer the results of the effective model, as it is 19.62% more accurate relative to the parallel model when comparing the average RMSE's.

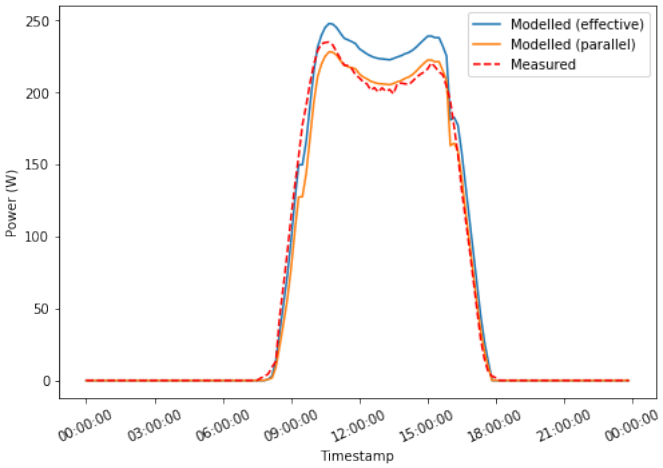

Figure 5.15: Comparison between two modelled (parallel and effective) and measured power output for a clear sky day.

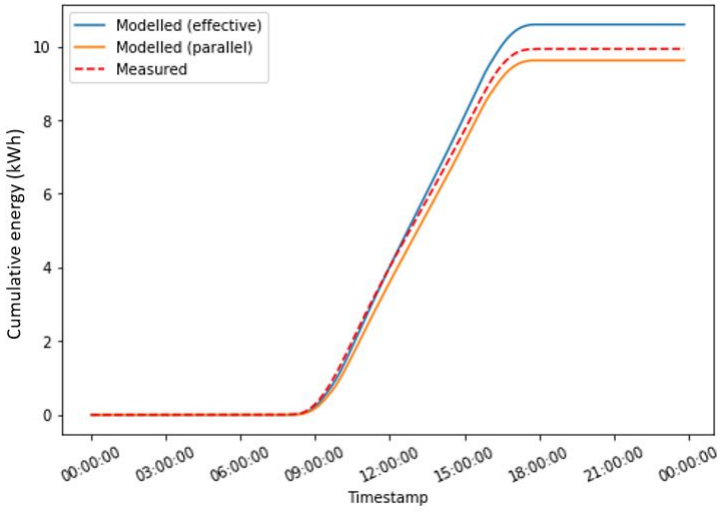

Figure 5.16: Comparison between two modelled (parallel and effective) and measured energy output for a clear sky day.

As the electrical and irradiance models are verified separately, it is of great interest to verify the results of the integrated model.

5.5 Verification of bifacial PV simulation software

Now that the irradiance and electrical models are verified, it is possible to integrate the two models to perform simulations that are more independent from real-world data. The successful integration of the irradiance and electrical

models will lead to the possibility of performing a range of simulations that may shed some light on the intricacies of bifacial technology.

5.5.1 Experiment methodology

The goal of this experiment is to verify the integration of the irradiance and electrical models. This is done by first modelling the front and rear irradiance with the measured GHI as reference input. The modelled irradiance is then fed to the electrical model for each time step. The power output is then modelled for both the parallel and effective irradiance models. The total modelled power output of a single bifacial module may then be compared with measured data in order to verify the integrated bifacial model. This process can be followed for both clear sky and intermittent days.

5.5.2 Experiment input

The experiment will require two forms of input namely modelling dependent and comparison dependent input. The modelling dependent input relates to the parameters that describes the physical environment for irradiance modelling and electrical characteristics for electrical modelling. The modelling dependent input data is the same as for the irradiance and electrical model verification experiments and are given in Tables 5.1 and 5.3.

The input data used for comparison and analysis relates to the data as measured on the bifacial PV test site. The measured input required for this experiment is the power output of the designated bifacial model. The exact same process is followed as for the electrical model verification, except the modelled irradiance is now given as input to the electrical model. No measured front and rear irradiance data is required for comparison as it will yield the same results as for the irradiance model verification.

5.5.3 Verification results

The integrated irradiance and electrical models are separately verified by modelling an intermittent and clear sky day. The modelled and measured results for the intermittent and clear sky days are given in Figures 5.17-5.18 and 5.19-5.20 respectively. The calculated errors that will be used for comparison is given in Table 5.5.

The comparison between the integrated parallel model and the measured energy output for clear sky and intermittent days lead to an average RMSE of 0.545 kWh which is quite substantial when compared to the effective model average RMSE of 0.155 kWh for the two days. Both integrated models shows

Table 5.5: Statistical errors for the integrated irradiance and electrical model verification.

Variable	RMSE	MBE	Unit
Clear sky day (Daily measured energy: 9.93 kWh)			
Power (effective)	12.9	-0.88	W
Power (parallel)	17.47	-7.35	W
Energy (effective)	0.201	-0.141	kWh
Energy (parallel)	0.741	-0.572	kWh
Intermittent day (Daily measured energy: 1.5 kWh)			
Power (effective)	3.57	-1.16	W
Power (parallel)	7.0	-3.68	W
Energy (effective)	0.11	-0.083	kWh
Energy (parallel)	0.349	-0.258	kWh

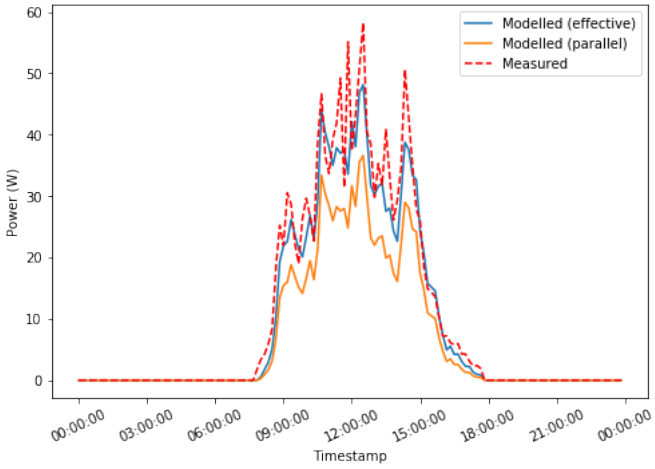

Figure 5.17: Comparison of the integrated irradiance and electrical model and measured power output for an intermittent day.

an underestimation with average MBE values of -0.415 kWh and -0.112 kWh for the parallel and effective integrated models respectively.

The integration of the irradiance model with the effective irradiance electrical model leads to more accurate results when compared to the RMSE and MBE of the parallel electrical model. This makes the effective irradiance $R_{sh} - R_s$ one-diode model the model of choice when moving towards further simulation of bifacial PV.

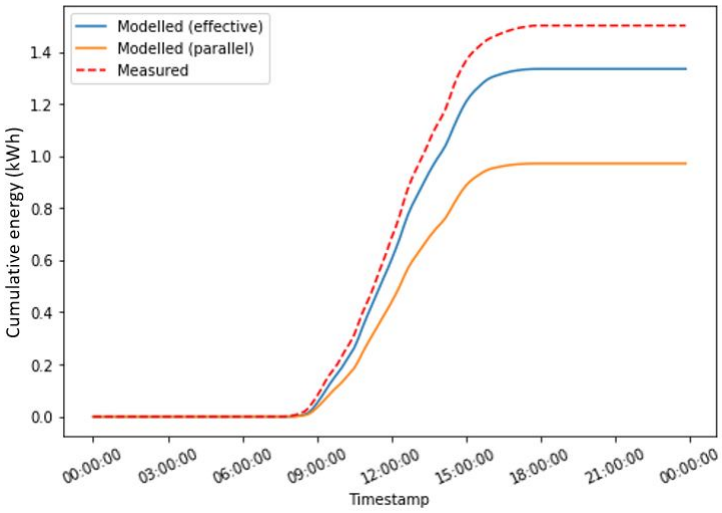

Figure 5.18: Comparison of the integrated irradiance and electrical model and measured energy output for an intermittent day.

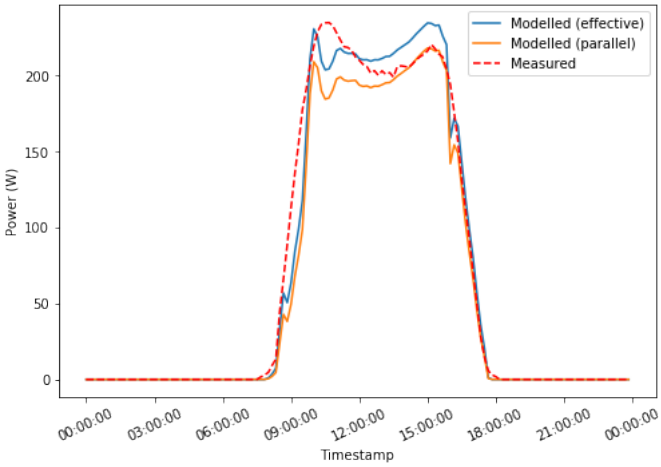

Figure 5.19: Comparison of the integrated irradiance and electrical model and measured power output for a clear sky day.

5.6 Bifacial PV simulations

With the verified integrated irradiance and electrical models, it is possible to simulate and compare results of bifacial PV for a variety of design parameters. The following areas will be investigated with regards to variation in PV design and capabilities:

- Tracking versus fixed tilt
- Effects of module height
- Effects of albedo

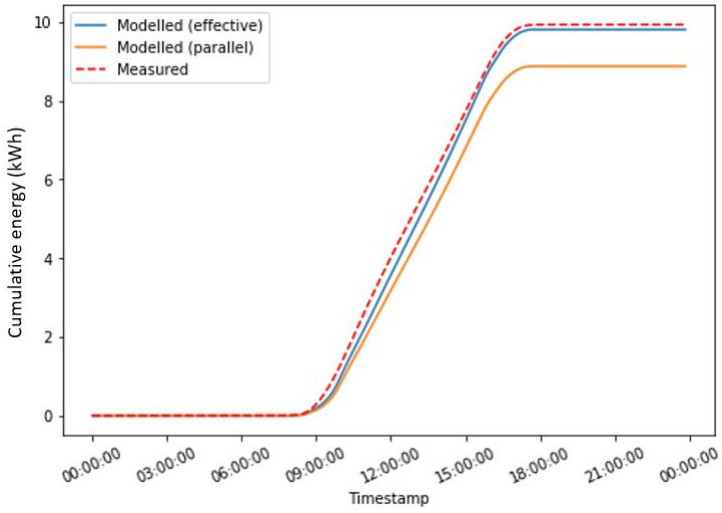

Figure 5.20: Comparison of the integrated irradiance and electrical model and measured energy output for a clear sky day.

- Effects of row spacing (pitch)

The results of the simulations will be analysed in order to quantify the effects of the various parameters. The simulation results will be given in two forms namely the bifacial energy and bifacial gain for the varying parameter values. Bifacial gain is a percentage that relates to the energy gain of a bifacial module relative to a monofacial module with a front irradiance only contribution. The bifacial gain therefore quantifies the effects of rear side irradiance contributions. Bifacial gain (BG)can be calculated by the following Equation (5.3) where E_{bi} and E_{mono} relates to the bifacial and monofacial energy respectively.

$$BG = \frac{E_{bi} - E_{mono}}{E_{mono}} \times 100 \tag{5.3}$$

By simulating a designated bifacial PV module for the variations as named above, it will be possible to draw some conclusions with regards to the optimal design of a bifacial PV plant.

5.6.1 Specifications of bifacial system under investigation

The bifacial system under investigation consists of 3 rows with 12 modules in a 2-in-portrait configuration. The bifacial system is illustrated in Figure 5.21 and identifies the designated bifacial module. It must be noted that the designated module under investigation remains constant throughout the simulations in order to compare results diligently. The parameters of the system are given in

Table 5.6. All the simulations will be performed for the same clear sky days as noted in Table 5.6.

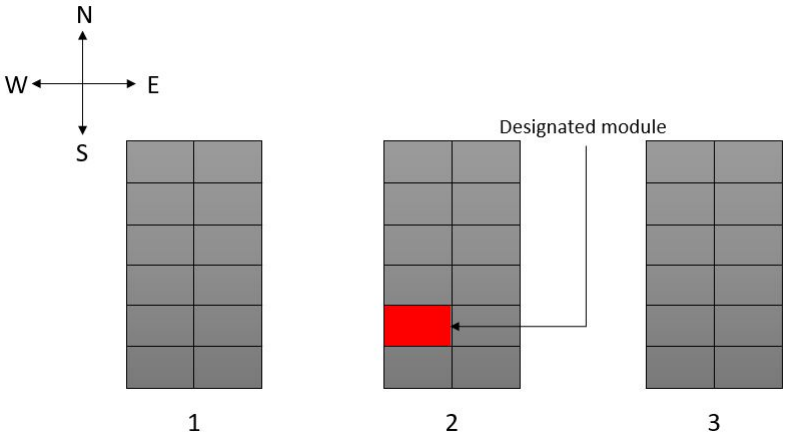

Figure 5.21: Illustration of the bifacial system layout for simulation purposes.

Table 5.6: Input parameters for simulating various effects on bifacial power output.

Fixed parameters	
Location	33.85 °S 18.86 °E
Module	LR6-72BP-350
Rows	3
Row spacing	5 m
Measured module	Middle row
Module height	1.5 m
Albedo	0.2
Simulation dates	05/07/2019 and 03/01/2019
Simulation period	1 day
Sky conditions	Clear sky

5.6.2 Tracking versus fixed tilt

In order to compare fixed tilt systems with single axis tracking systems, it is necessary to determine the optimal tilt angle for bifacial modules. Thus, simulations were done for clear sky winter and summer days in order to obtain the optimal tilt angle.

5.6.2.1 Determining optimal tilt angle for bifacial PV

The modelled bifacial energy for various tilt angles on clear sky winter and summer days are given in Figure 5.22. It can be seen that the energy declines with an increase in tilt angle in summer where the inverse is true for winter. The dashed line plot shows the average energy between winter and summer for each tilt angle, from where it is visible that the a tilt angle of 33° yields the largest energy output for winter and summer.

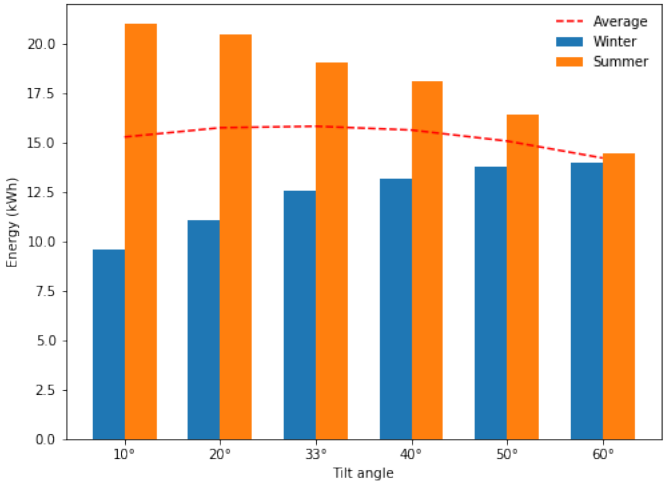

Figure 5.22: Simulated bifacial energy output for variation in tilt angles for clear sky winter and summer days.

The bifacial gain for varying tilt angles can be observed in Figure 5.23. For summer, the bifacial gain increases with a increase in tilt angle where the bifacial gain declines with an increase in tilt angle for winter. The plot for average bifacial gain between winter and summer shows that 60° yields the greatest bifacial gain. However, when determining the optimal tilt angle, it is of more interest to choose the tilt angle that results in the greatest energy yield. Therefore a tilt angle of 33° is chosen to move forward with fixed tilt simulations.

5.6.2.2 Comparison between backtracking and fixed tilt systems for bifacial PV

The first simulation compares the impact of tracking versus fixed tilt systems on bifacial power output. The simulations are done by implementing a east-west backtracking algorithm for a clear sky day in winter and summer while all other parameters remain constant. The same process is followed for a north facing fixed tilt system at an optimal angle close to the latitude of the site location i.e. 33°.

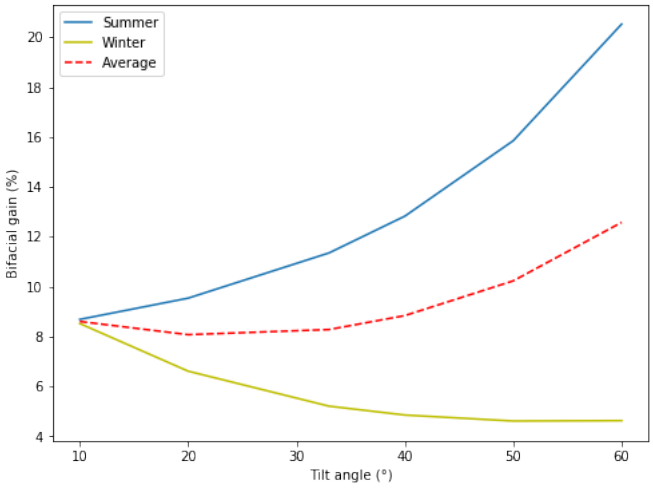

Figure 5.23: Simulated bifacial gain for variation in tilt angles for clear sky winter and summer days.

The simulated bifacial energy output for winter and summer clear sky days are given in Figure 5.24. For winter, it is evident that the fixed tilt system yields an increased energy production when compared to a backtracking system. This is due to the lower zenith angle of the sun during winter. The same can not be said for the summer where a backtracking system shows an energy increase of 40.3% relative to a fixed tilt system. With respective average energy output values of 17.9 kWh and 15.4 kWh for backtracking and fixed tilt systems, it is clear that the bifacial backtracking system outperforms the bifacial fixed tilt system.

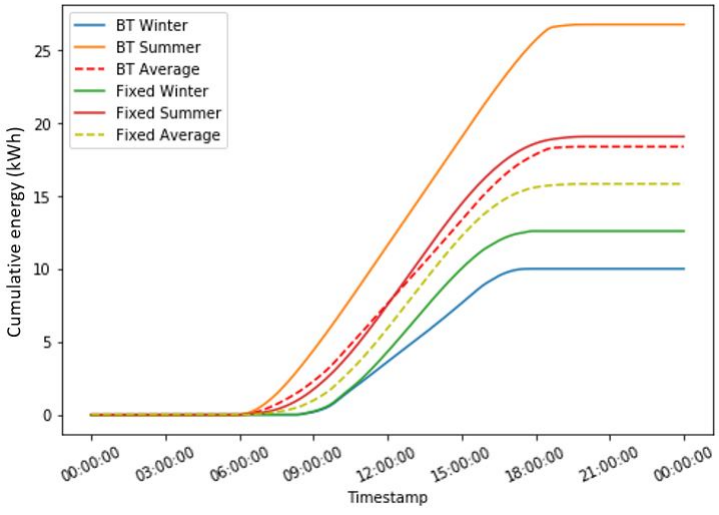

Figure 5.24: Simulated bifacial energy output for fixed and backtracking systems in winter and summer.

By analysing bifacial gain for backtracking and fixed tilt systems, as Table 5.7 shows, some interesting results are obtained. The summer fixed tilt system produces the highest bifacial gain of 11.35%. The average gain of the fixed tilt system for the summer and winter days is 8.3% where the backtracking system yields an average gain of 6.6%. A higher energy production is however more favourable, therefore the backtracking system will be the optimal solution.

Table 5.7: Simulated bifacial gain for fixed and backtracking systems in winter and summer.

	Bifacial Gain		
System	**Winter**	**Summer**	**Average**
Fixed Tilt	5.21%	11.35%	8.3%
Backtracking	7.52%	5.76%	6.6%

5.6.3 Effects of module height

It is predicted that the height of bifacial modules above the ground will greatly affect the irradiance exposure of the rear side, due to an increased reflective ground surface area [3]. The simulations done for this experiment aims to show the effects of variation in module height with regards to bifacial energy output. The simulations are done for clear sky winter and summer days by varying the module height from 1-3 meters and following a backtracking algorithm while keeping all other parameters constant.

The simulated daily energy for clear sky winter and summer days with variation in module height are given in Table 5.8. It is clear that an increase in power output correlates with an increase in module height. This is due to more rear irradiance exposure from ground reflectivity as the increased module height creates a greater reflective surface area. A 4.6% and 3.6% increase in energy output is observed for winter and summer days respectively, which yields an average of 4.1% energy increase between seasons for module heights between 1 and 3 meters.

Table 5.8: Simulated bifacial energy output for varying module height.

	Energy (kWh)		
Module height	**Winter**	**Summer**	**Average**
1.0 m	9.81	26.37	18.09
1.5 m	10.01	26.78	18.40
2.0 m	10.15	27.06	18.61
2.5 m	10.22	27.23	18.73
3.0 m	10.26	27.34	18.80

The effects of varying module height on bifacial gain is shown in Figure 5.25. Bifacial gains of 9.9% and 7.6% are observed for the respective winter and summer day simulations. The average bifacial gain for the two days increases from 4.7% to 8.8% with an increase of module height from 1-3 meters. This is a substantial increase in energy production when compared to monofacial PV modules. The significant increase in bifacial gain is due to the increase in rear side irradiance while the front side irradiance remains unaffected with module height increase. It is also evident that the average bifacial gain reaches a threshold of 8.8% from where insignificant increases will be observed beyond a module height of 3 meters.

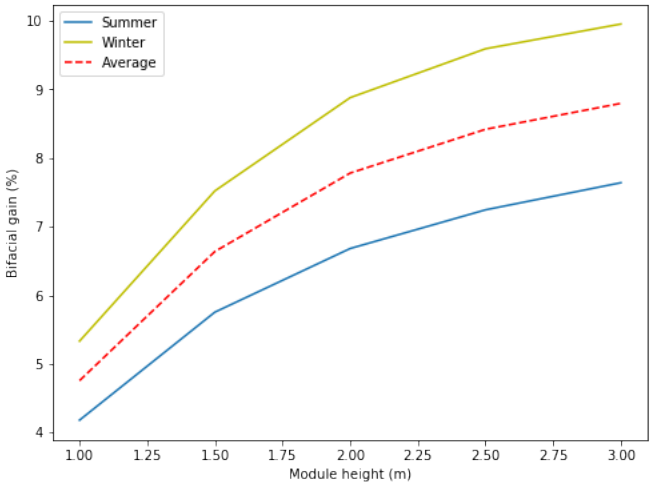

Figure 5.25: Simulated bifacial gain for varying module height.

5.6.4 Effects of albedo

It is evident that the reflective ground surface area significantly increases the power output and gain of bifacial systems [3]. It is therefore necessary to investigate the effects of ground surface albedo on bifacial power output and gain. Albedo relates to the reflective capabilities of the ground with respect to the incident irradiance. The simulations are done for clear sky winter and summer days by varying the albedo of the ground surface from 0.2-0.6 and following a backtracking algorithm while all other parameters remain constant.

The simulated energy output for varying albedo is given in Table 5.9. It can be seen that the bifacial energy output increases significantly with an increase in ground surface albedo. A 13.9% increase in energy output is obtained for winter where a 10.2% increase is observed for summer with variation in albedo values from 0.2-0.6. The average increase of 12.05% in energy output is a result of increased rear irradiance due to higher reflectivity of the ground surface.

Table 5.9: Simulated bifacial energy output for varying ground surface albedo.

	Energy (kWh)		
Albedo	**Winter**	**Summer**	**Average**
0.2	10.02	26.68	18.40
0.3	10.37	27.52	18.94
0.4	10.72	28.24	19.48
0.5	11.06	28.96	20.01
0.6	11.42	29.68	20.55

Figure 5.26 shows the impact of varying albedo on bifacial gain. An average bifacial gain of 17.8% is achievable for an albedo value of 0.6. That is a 11.2% increase in bifacial gain for enhancing the ground surface albedo from 0.2 to 0.6. The winter day yields bifacial gains of 7.5-20.4% which is significantly higher than the 5.8-15.3% gains for summer. Figure 5.26 shows that bifacial gain increases linearly with increased albedo. The combination of increased module height and albedo should yield promising results.

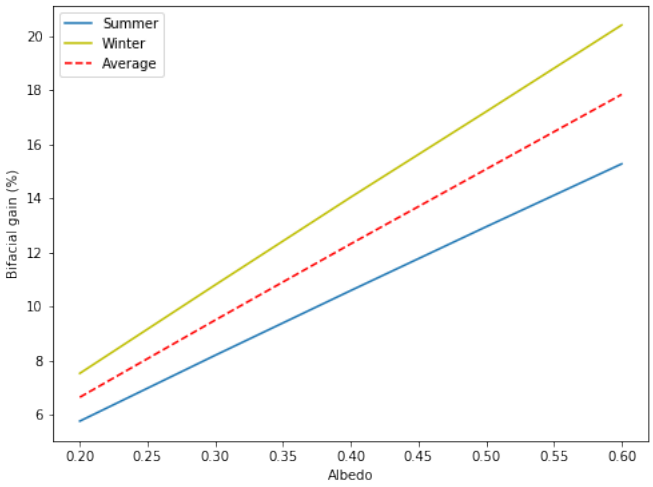

Figure 5.26: Simulated bifacial gain for varying ground surface albedo.

5.6.5 Effects of row spacing

Row spacing (pitch) relates to the distance between adjacent rows. In order to expose the rear sides of bifacial modules to increased irradiance, it is necessary to increase the reflective surface of the ground surface behind or beneath the modules [6]. The effects of module height and albedo clearly shows positive results for maximising the reflective ground surface area for bifacial systems. For this test the row spacing is varied from 5-9 meters while following a back-tracking algorithm and all other parameters are kept constant.

The simulated energy output for variation in row spacing is shown in Table 5.10. From the results it is clear that an increase in row spacing leads to an increase in bifacial energy production. An average increase of 3.8% in energy output between winter and summer, leads to row spacing having the smallest effect on bifacial energy production when compared to module height and albedo. There is also little variation on energy output increase for winter and summer with respective increases of 3.5% and 3.9%.

Table 5.10: Simulated bifacial energy output for varying row spacing (pitch).

	Energy (kWh)		
Row spacing	**Winter**	**Summer**	**Average**
5 m	10.77	26.78	18.77
6 m	11.08	27.24	19.16
7 m	11.13	27.50	19.31
8 m	11.16	27.76	19.46
10 m	11.18	27.82	19.50

The effects of row spacing on bifacial gain is shown in Figure 5.27. It can be seen that the bifacial gain initially decreases with variation in row spacing from 5-6 meters. By looking at the energy output graph in Figure 5.8, it is clear that no energy loss occurs between 5 and 6 meters. The decrease in bifacial gain can therefore be attributed to the fact that the front side, together with the rear side, is receiving more irradiance from the additional reflective surface area that is created by the increased row spacing. Thus, the front side irradiance initially increases with rear side irradiance and therefore minimises the effect on bifacial gain.

As with module height, the average bifacial gain reaches a threshold of around 6.8% at a row spacing of 9 meters. The average bifacial gain experiences an increase of only 0.3% with a row spacing variation between 5-9 meters. Although row spacing increases bifacial power output and gain, it is important to note that most PV implementations are restricted with regards to surface area. An increase in row spacing may lead to the installation of less PV modules per unit area, which will have a large negative impact on overall PV plant performance.

5.7 Simulation of an optimised bifacial system

After analysing the results of simulations that show the effects of various design parameters, it is possible to simulate an optimized bifacial system. This

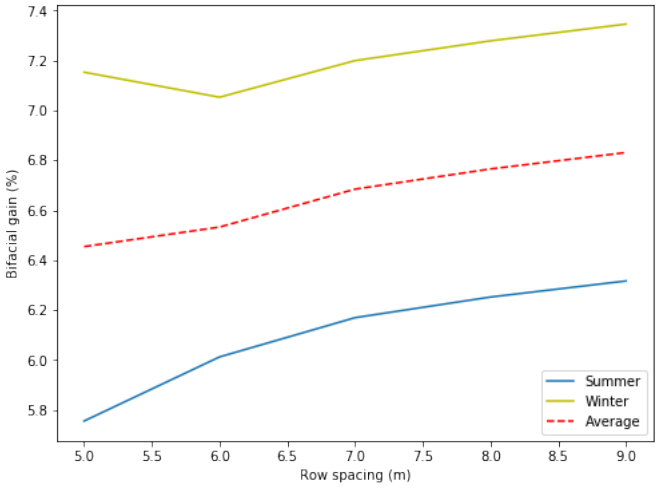

Figure 5.27: Simulated bifacial gain for varying row spacing (pitch).

simulation will show the energy production and bifacial gains that are achievable by optimising the environment and design parameters of a bifacial PV plant. The optimised bifacial system simulation will be done on module level for one clear sky day per month over the course of a full year in order to gain clear perspective of a optimised bifacial PV plant's performance and capabilities. The simulation results will also be compared with a simulation of a non-optimised bifacial system which inherits conventional design parameters i.e. no albedo enhancement and a module height of less than 2 meters. The input parameters for the optimised and non-optimised simulations are given in Table 5.11.

Table 5.11: Input parameters for simulating an optimised and non-optimised bifacial PV plant.

Parameter	**Optimised**	**Non-Optimised**
Row spacing	9 m	5 m
Module height	3 m	1.5 m
Albedo	0.6	0.2
Fixed parameters		
Location	33.85 °S 18.86 °E	
Module	LR6-72BP-350	
Tracking	Backtracking	
Rows	3	
Measured module	Middle row	
Simulation dates	01-2018 to 12-2018	
Simulation period	1 clear sky day per month	

The chosen parameters were obtained after analysing their effects by means of simulation and as given in section 5.6. The parameters were limited to dimensions that are realistic and able to be implemented in a real world situation. It was decided to implement a 3 row tracking system which follows a backtracking algorithm as it showed promising performance when compared to fixed tilt systems. The row spacing is 9 meters with a module height of 3 meters. The albedo is set to a value of 0.6 which is the maximum possible albedo without taking snow as a ground surface type.

The simulated daily energy output over the course of a year for the optimised and non-optimised bifacial module is given in Figure 5.28. It is evident that the optimised module outperforms the non-optimised module in terms of daily energy output. The optimised module produces 0.867 kWh more average daily energy for a full year on clear sky days. This shows that by increasing albedo, module height and row spacing, it is possible to increase average energy production by 29.82%.

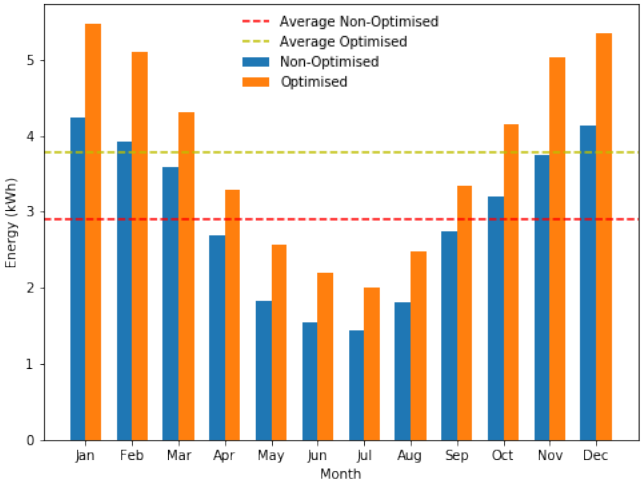

Figure 5.28: Simulated bifacial energy output for optimised and non-optimised bifacial systems on one clear sky day per month.

The simulated bifacial gain for the optimised and non-optimised module is given in Figure 5.29. It can be seen that the optimised module yields an average bifacial gain of 24.15% which is 17.4% higher than the non-optimised module. This shows that optimisation of bifacial PV design parameters plays a critical role in the performance when compared to monofacial PV. It is also evident that the bifacial gain increases for winter months. This additional bifacial gain over winter months may play a role in satisfying the higher energy demands for those months.

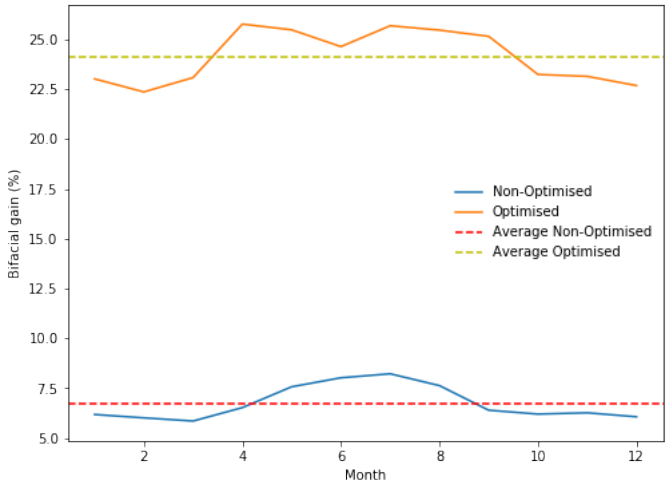

Figure 5.29: Simulated bifacial gain for optimised and non-optimised bifacial systems on one clear sky day per month.

5.8 Comparison with commercial software

As the irradiance and electrical models are verified, it is of high interest to compare the ray tracing method and effective one-diode model with the commercially implemented view factor method and one-diode model. The chosen commercial software for comparison is *PVsyst* version 6.84 which has bifacial modelling capabilities. It was decided to compare the simulated irradiance and electrical output for both software models with measured data in order to gain perspective of their modelling accuracy.

The simulations were done by modelling an identical bifacial system for both software versions. The simulated bifacial system mimics the bifacial installation at the Mariendahl PV test site as described in section 5.2. The rows are spaced by 5 meters and follows a single-axis backtracking algorithm in an east-west orientation. The modelled modules are the *LongiSolar* LR6-72BP-355 and are mounted at a height of 1 meters above the ground. The ground surface is modelled with an albedo of 0.2. Table 5.12 gives the input parameters for both simulation tools. The *PVsyst* report for the simulation is given in Appendix A.

The modelled front and rear irradiance of both simulation tools are compared with measured irradiance. The measured irradiance is obtained with commercial grade pyranometers as described in section 5.3.2 for the irradiance model verification. The measured energy output is obtained by means of a power logger that is connected in series with a bifacial module as described in section 5.4.2 as for the electrical model verification. The energy output of the single module is then multiplied by the amount of modules in the array.

Table 5.12: Input parameters for comparing the developed simulation software with a commercial tool.

Simulation parameters	
Location	33.85 °S 18.86 °E
Module	LR6-72BP-355
Tracking	Backtracking (east-west)
Rows	4
Row spacing	5 m
Module height	1 m
Albedo	0.2
Simulation dates	09-07-2019
Simulation period	1 day

It must be noted that no mismatch or other losses were applied for this comparison. Table 5.13 provides the statistical errors for both modelled irradiance results with the measured data.

Table 5.13: Statistical errors for the comparison between ray tracing, *PVsyst*, measured irradiance and measured energy output.

Variable	**RMSE**	**MBE**	**Unit**
***PVSyst* version 6.84**			
Front irradiance	46.98	-10.81	W/m^2
Rear irradiance	7.67	-2.94	W/m^2
Energy	1.62	-1.08	kWh
Ray Tracing			
Front irradiance	64.29	-25.06	W/m^2
Rear irradiance	3.23	1.37	W/m^2
Energy	1.32	-1.03	kWh

The modelled front side irradiance comparison is given in Figure 5.30. It is observed that *PVsyst* models the front side irradiance with better accuracy. This can be seen when comparing the RMSE of both models with value of 46.98 W/m^2 and 64.29 W/m^2 for *PVsyst* and the ray tracing model respectively. The MBE shows that both models underestimate the front side irradiance with respective values of -10.81 W/m^2 and -25.06 W/m^2 for *PVsyst* and the ray tracing model.

The two modelled rear side irradiances is shown in Figure 5.31, from where it is visible that the ray tracing technique models the rear side irradiance with better accuracy. This can also be observed when analysing the RMSE and

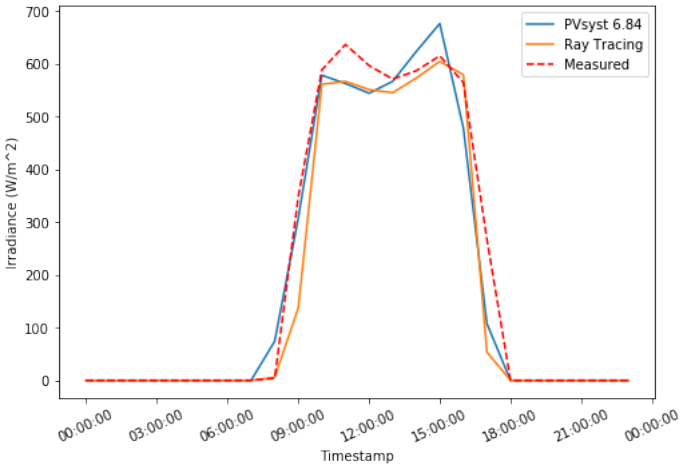

Figure 5.30: Simulated and measured front side irradiance comparison between *PVsyst* and ray tracing model.

MBE values. The ray tracing model yielded RMSE and MBE values of 3.23 W/m^2 and 1.37 W/m^2 where *PVsyst* lead to a RMSE and MBE of 7.67 W/m^2 and -2.94 W/m^2. This shows that the ray tracing model slightly overestimates with better accuracy when compared to the underestimation of *PVsyst*.

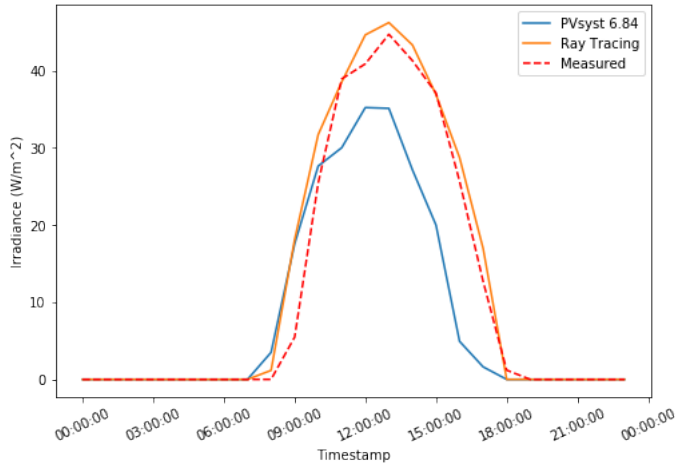

Figure 5.31: Simulated and measured rear side irradiance comparison between *PVsyst* and the ray tracing model.

The two modelled and measured power output is shown and compared in Figure 5.32. It can be seen that *PVsyst* underestimates the energy output with a MBE of -1.08 kWh. The ray tracing model in combination with the effective one-diode model underestimates the energy output with a MBE of -1.03 kWh. The ray tracing and effective one-diode model is slightly more

accurate when compared to *PVsyst* with a RMSE values of 1.32 kWh and 1.62 kWh respectively.

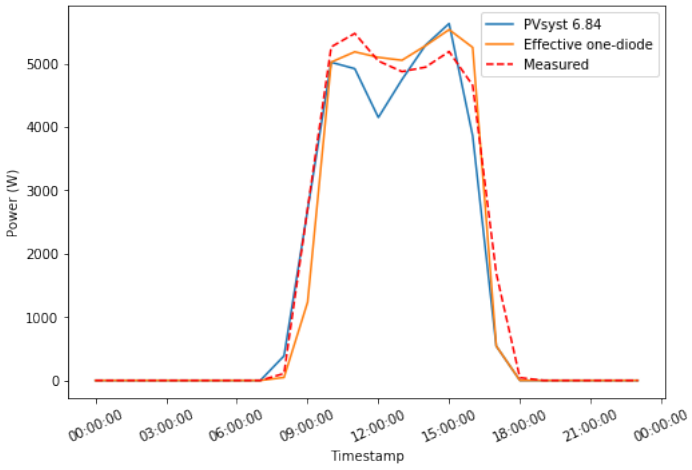

Figure 5.32: Simulated and measured power output comparison between *PVsyst* and ray tracing model.

The comparison with *PVSyst* shows that the view factor modelling of the front side irradiance is more accurate when compared to ray tracing. It is clear that ray tracing can better simulate the rear side irradiance. Therefore, it might be favourable to implement a combination of view factor and ray tracing techniques to model the front and rear side irradiance respectively. The combination of ray tracing and effective one-diode model proves to be slightly more accurate than *PVsyst*'s combination of the view factor and one-diode model. It was not possible to evaluate the electrical models independently as *PVsyst* can't take measured irradiance as an input to it's electrical model.

5.9 Summary

Upon implementing the ray tracing algorithm as well as the effective and parallel $R_{sh} - R_s$ one-diode models, it was necessary to verify the accuracy of the modelled irradiance and electrical output. It was also necessary to verify the integrated irradiance and electrical models which forms the bifacial simulation software that was ultimately utilised to simulate the effects of various bifacial design parameters such as module height, ground surface albedo, row spacing and tracking versus fixed tilt systems. The simulation results lead to the opportunity to simulate and compare an optimised bifacial set-up with a non-optimised set-up by analysing the energy performance and bifacial gain of the two respective systems. Finally a comparison was made between the ray

tracing irradiance model and the view factor irradiance model as implemented in the commercial software, *PVsyst* version 6.86.

5.9.1 Irradiance model verification

The irradiance model and more specifically the ray tracing algorithm was verified by comparing the modelled irradiance with measured irradiance of the front and rear sides on clear sky and intermittent days. The measured front and rear side irradiance was obtained with commercial standard pyranometers that were fitted in the same plane as the bifacial modules. The on-site weather station provided GHI data that was used as input to the irradiance model.

The modelled front side irradiance for a clear sky and intermittent day yielded an average RMSE and MBE of 24.01 W/m^2 and -9.825 W/m^2 which shows an underestimation when compared with measured front irradiance. The modelled rear side irradiance deviated from the measured rear side irradiance with an average RMSE of 2.68 W/m^2 and slightly overestimated with an average MBE of 0.64 W/m^2 for a clear sky and intermittent day.

5.9.2 Electrical model verification

The electrical model was realised with two various methods namely, the parallel $R_{sh} - R_s$ one-diode model and the effective $R_{sh} - R_s$ one-diode model as described in chapter 4, section 4.3.1. Both models were verified by comparing the modelled power and energy output with measured output of an actual bifacial module. The measured power output was obtained with a power logger which was connected in series with the designated bifacial module. The corresponding front and rear irradiance measurements for a clear sky and intermittent day were given as input to the two electrical models from where they were compared in order to determine which model was more accurate.

The parallel $R_{sh} - R_s$ one-diode model was the least accurate of the two with average RMSE and MBE values of 0.317 kWh and -0.241 kWh for the clear sky and intermittent days. The effective $R_{sh} - R_s$ one-diode model proved to be more accurate with an average RMSE of 0.265 kWh and an average MBE of 0.07 kWh, which relates to a slight overestimation on the energy output for clear sky and intermittent days. The two $R_{sh} - R_s$ one-diode models were now integrated with the irradiance model to verify the accuracy of the bifacial PV simulation software.

5.9.3 Bifacial PV simulation software verification

After separately verifying the irradiance and electrical models, it was necessary to verify the integration of the two models which forms the bifacial PV

simulation software. The integrated software was verified by comparing the modelled energy output with measured output of a clear sky and intermittent day. The input given to the software was the corresponding GHI as measured by the on-site weather station. The modelled irradiance was therefore given as input to the two electrical models in order to obtain the modelled energy output.

The results showed that the effective $R_{sh} - R_s$ one-diode model was more accurate with average RMSE and MBE values of 0.155 kWh and -0.112 kWh when compared with the average RMSE of 0.545 kWh and an average MBE of -0.415 kWh. The effective $R_{sh} - R_s$ one-diode model, which slightly underestimates the energy output when compared to measured energy output, was therefore chosen as the electrical model that will be integrated with the irradiance model for further simulations.

5.9.4 Bifacial PV simulations

The fact that the bifacial PV simulation software was successfully verified meant that simulations could be done in order to determine the effects of certain design parameters on the energy yield and bifacial gain of bifacial PV modules. These design parameters included: tracking versus fixed tilt systems, module height, ground surface albedo and row spacing.

5.9.4.1 Tracking versus fixed tilt systems

In order to determine which of tracking or fixed tilt systems are the most effective in maximising the energy output and bifacial gain of bifacial modules, it was necessary to first determine the optimal fixed tilt angle for bifacial modules. The simulation results between winter and summer showed that the average bifacial gain increases non-linearly with a increase in tilt angle. A tilt angle of 60° resulted in the maximum average bifacial gain of around 12.2%. However, when analysing the energy output for various tilt angles, it was clear that a tilt angle of 33° was the most effective angle for maximum energy output.

It was now possible to compare a 33° fixed tilt bifacial system with a single-axis tracking bifacial system which follows a backtracking algorithm for a winter and summer clear sky day. The results showed that a fixed tilt system leads to the highest average bifacial gain of 8.3%. However, when analysing the energy output for the two scenarios, the single-axis backtracking system produced the highest energy output with an average of 17.9 kWh when compared with the fixed tilt's average energy output of 15.4 kWh. It was therefore determined that the single-axis backtracking system outperforms the fixed tilt system with regards to bifacial energy output, and is thus the optimal solution.

5.9.4.2 Effects of module height

The goal of this simulation was to show that an increased reflective surface area would lead to increased rear irradiance exposure and result in higher bifacial energy output and bifacial gain [3]. Simulations were done by plotting the energy output and bifacial gain with an increase of module height from 1-3 meters for clear sky winter and summer days. The results showed that an average energy output increase of 4.1% is achievable by increasing the module height from 1-3 meters. An average bifacial gain of 8.8% is observed between winter and summer at a module height of 3 meters, where the bifacial gain also reaches a threshold and will have less significant effects with a further increase in module height.

5.9.4.3 Effects of albedo

Albedo relates to the reflective capabilities of the ground surface that surrounds the bifacial PV plant. By increasing the ground surface albedo, it is expected that the energy production and bifacial gain will also increase. The simulations were done by increasing the albedo from 0.2-0.6. The results showed that significant linear increases in energy and bifacial gain are achievable by optimising the albedo. The average increase of 12.05% in energy output between winter and summer shows that the increased reflectivity of the ground has a great effect on the rear side irradiance and hence, the bifacial energy output. The increased albedo from 0.2-0.6 significantly increased the average bifacial gain from 6.6-17.8%. This shows that an optimisation of the reflective ground surface area greatly affects the performance of a bifacial PV system.

5.9.4.4 Effects of row spacing

Another way of increasing the reflective surface area is to increase the spacing between adjacent rows in a PV plant. For this experiment, the row spacing (pitch) was increased from 5-9 meters. The average energy output increased by 3.8% with an increase of row spacing from 5-9 meters. The bifacial gain for summer initially decreased with an increase in row spacing. This is due to the fact that the front side irradiance also increases together with the rear side irradiance, which increases the monofacial energy output, hence a decreased bifacial gain. The average bifacial gain increased by only 0.3% with the increase in row spacing which shows that row spacing has the least effect on energy output and bifacial gain when compared with module height and albedo.

5.9.5 Simulation of an optimised bifacial system

After analysing the effects of various bifacial PV plant design parameters, it was possible to simulate and compare an optimised system with a non-optimised system. For the optimised system, the module height and row spac-

ing were set to 3 meters and 9 meters respectively while the albedo was enhanced to 0.6. The non-optimised system implemented a module height of 1.5 meters, row spacing of 5 meters and albedo of 0.2. The results showed that the average energy production can be increased by 29.82% with the necessary optimisation. The bifacial gain significantly increased by 17.4% when compared to the non-optimised system. It must be kept in mind that the optimisation of these specific parameters may lead to design intricacies such as: increased losses due to increased cable lengths, increased wind loading and maintenance complexities for higher mounting structures and the extra costs of maintaining a high ground surface albedo.

5.9.6 Comparison with commercial software

A comparison was done between the modelled irradiance and energy output of the ray tracing method with the effective one-diode model and *PVsyst*. Measured front and rear irradiance was compared with both modelled results and showed that the ray tracing method models the rear side irradiance more accurately with RMSE and MBE values of 3.23 W/m^2 and 1.37 W/m^2, compared to the RMSE and MBE values of 7.67 W/m^2 and -2.94 W/m^2 for *PVsyst*. However it was shown that *PVsyst* models the front side irradiance with greater accuracy with corresponding RMSE values of 46.98 W/m^2, where the ray tracing method yielded a RMSE of 64.29 W/m^2. The energy output of *PVsyst* was slightly less accurate when comparing it's RMSE of 1.62 kWh with the ray tracing and effective one-diode model RMSE of 1.32 kWh.

Chapter 6

Conclusions and recommendations

Unlike monofacial PV modules, bifacial PV modules can produce a higher power output by exposing PV cells to the irradiance incident on the rear side as well as the front side of modules. Bifacial PV's potential higher power output per unit area can significantly decrease the LCOE of PV modules which will play an important role in the growth of solar PV as renewable energy source. In order for bifacial PV to become the leading solar energy source, some uncertainties need to be clarified. This can be accomplished by accurate modelling and simulation software of which there is a shortage. The goal of this thesis was to address the problem of inaccurate modelling of bifacial PV modules by investigating and developing the techniques used to model irradiance and electrical behaviour of bifacial modules.

6.1 Irradiance model

Irradiance modelling of bifacial PV and more specifically the rear side irradiance of bifacial PV modules consists of many complexities. The irradiance model therefore formed the core of the research as proposed. It is known that view factor modelling falls short in accurately modelling the rear side irradiance. Ray tracing was therefore chosen as the modelling in order to increase the accuracy of rear side irradiance modelling. The irradiance model was developed by utilising the ray tracing capabilities of the open-source software tool named *Radiance*. In order to model front and rear side irradiance it was necessary to describe a virtual environment that closely represented a real world PV plant environment. The virtual environment consisted of three parts namely the sky model, ground model and the geometric description of bifacial PV modules.

The irradiance model was verified by comparing the modelled irradiance output with front and rear side irradiance as measured by commercial grade pyranometers on a bifacial PV test site. The irradiance model verification

respectively yielded an average RMSE and MBE of 24.01 W/m^2 and -9.825 W/m^2 for the front side irradiance which relates to an underestimation when compared with measured data. The focus of the ray tracing model was to accurately the model the complex rear side irradiance, which resulted in average RMSE and MBE values of 2.68 W/m^2 and 0.64 W/m^2 respectively. These errors show that the ray tracing model slightly overestimates the rear side irradiance. These results are accurate enough to conclude that the ray tracing algorithm was implemented successfully to model the irradiance distribution of bifacial PV modules. The ray tracing technique also proved to be effective to be integrated with a electrical model in order to further simulate bifacial PV modules.

6.2 Electrical model

The electrical model is responsible for providing some insight regarding bifacial PV performance in conjunction with the implemented irradiance model. The possibility of simulating bifacial modules accurately relies heavily on the validity of the electrical model as there are very little simulation tools available that can model bifacial PV in a electrical context.For this project, two $R_{sh}-R_s$ one-diode models were implemented. The effective irradiance $R_{sh}-R_s$ one-diode takes the bifaciality factor into account by adding the rear side irradiance to the total effective irradiance, as a fraction of the rear sides's performance relative to the front side. The total effective irradiance then determines the excited current which in effect determines the power output of a module. The parallel $R_{sh}-R_s$ one-diode model consists of two parallel circuits, each representing the front and the rear side respectively. Each of the two circuit's excited current output contributes to the total power output of a module.

The two electrical models were verified by comparing their modelled power outputs with power output as measured on the PV test site. A power logger was used to measure the bifacial power output of a single bifacial PV module. The on-site measured irradiance for a clear sky and intermittent day was given as input to the electrical models in order to make a valid comparison between modelled results and measurements. The test concluded that the effective irradiance $R_{sh}-R_s$ one-diode model is the most accurate in modelling the electrical behaviour of bifacial PV modules with an average energy output RMSE of 0.265 kWh and a MBE of 0.07 kWh which relates to a slight overall overestimation. The parallel $R_{sh}-R_s$ one-diode model underestimated the bifacial energy performance with an average MBE of -0.241 kWh for the clear sky and intermittent day.

6.3 Simulation software for bifacial PV

The simulation software for bifacial PV was realised by integrating the irradiance and electrical models with the *python* developing language. Additional miscellaneous features such as a backtracking algorithm, data file handling and a graphical user interface were added in order to expand the capabilities of the simulation software.

The integrated irradiance and electrical models were verified by comparing the modelled power output with measured power output as for the electrical model verification. The integration of the irradiance model with the effective irradiance $R_{sh} - R_s$ one-diode model delivered the most accurate results with an average RMSE of 0.155 kWh for the two days. The average MBE showed that the effective $R_{sh} - R_s$ one-diode model slightly underestimates with a value of -0.112 kWh. The integration of the irradiance model with the parallel $R_{sh} - R_s$ one-diode model resulted in average RMSE and MBE values of 0.545 kWh and -0.415 kWh respectively. After verifying the accuracy of the bifacial PV simulation software, it was possible to simulate the effects of various design parameters. These design parameters included fixed tilt versus tracking, module height above the ground, ground surface albedo and row spacing.

6.3.1 Optimal tilt angle

Before the fixed tilt system could be compared with a tracking system, it was necessary to obtain the optimal tilt angle for bifacial PV modules. By analysing the energy output, a tilt angle of 33° was observed to be the optimal tilt angle for the specific location. Although the bifacial gain increased with an increase in tilt angle, the same was not true for energy output.

6.3.2 Tracking versus fixed tilt

It was now possible to compare a 33° fixed tilt bifacial system with a single-axis tracking bifacial system which follows a backtracking algorithm. The results showed that a fixed tilt system leads to the highest average bifacial gain of 8.3%. However, when analysing the energy output for the two scenarios, the single-axis backtracking system produced the highest energy output with an average of 17.9 kWh when compared with the fixed tilt's average energy output of 15.4 kWh. It was therefore determined that the single-axis backtracking system outperforms the fixed tilt system with regards to bifacial energy output, and is thus the optimal solution.

6.3.3 Module height

The goal of this simulation was to show that an increased reflective surface area would lead to increased rear irradiance exposure and result in higher bifacial energy output and bifacial gain. Simulations were done by plotting the energy output and bifacial gain with an increase of module height from 1-3 meters for clear sky winter and summer days. The results showed that an average energy output increase of 4.1% is achievable by increasing the module height from 1-3 meters. An average bifacial gain of 8.8% is observed between winter and summer at a module height of 3 meters, where the bifacial gain also reaches a threshold and will have less significant effects with a further increase in module height.

6.3.3.1 Albedo

By increasing the ground surface albedo, it was expected that the energy production and bifacial gain will also increase. The simulations were done by increasing the albedo from 0.2-0.6. The results showed that significant linear increases in energy and bifacial gain are achievable by optimising the albedo. The increased albedo from 0.2-0.6 significantly increased the average bifacial gain from 6.6-17.8%. The average increase of 12.05% in energy output between winter and summer shows that the increased reflectivity of the ground has a great effect on the rear side irradiance and hence, the increased bifacial energy output. This shows that an optimisation of the reflective ground surface area can greatly enhance the performance of a bifacial PV system.

6.3.3.2 Row spacing

Another way of increasing the reflective surface area is to increase the spacing between adjacent rows in a PV plant. For this experiment, the row spacing (pitch) was increased from 5-9 meters. The average energy output increased by 3.8% with an increase of row spacing from 5-9 meters. The bifacial gain for summer initially decreased with an increase in row spacing. This is due to the fact that the front side irradiance also increases together with the rear side irradiance, which increases the monofacial energy output, hence a decreased bifacial gain. The average bifacial gain increased by only 0.3% with the increase in row spacing which shows that row spacing has the least effect on energy output and bifacial gain when compared with module height and albedo.

6.3.3.3 Optimal bifacial system simulation

After analysing the effects of various bifacial PV plant design parameters, it was possible to simulate and compare an optimised system with a non-optimised system. For the optimised system, the module height and row spacing were set to 3 meters and 9 meters respectively while the albedo was en-

hanced to 0.6. The non-optimised system implemented a module height of 1.5 meters, row spacing of 5 meters and albedo of 0.2. The results showed that the average energy production can be increased by 29.82% with the necessary optimisation. The bifacial gain significantly increased by 17.4% when compared to the non-optimised system.

6.3.3.4 Comparison with commercial software

A comparison was done between the modelled irradiance and energy output of the ray tracing method with the effective one-diode model and *PVsyst*. Measured front and rear irradiance was compared with both modelled results and showed that the ray tracing method models the rear side irradiance more accurately with RMSE and MBE values of 3.23 W/m^2 and 1.37 W/m^2, compared to the RMSE and MBE values of 7.67 W/m^2 and -2.94 W/m^2 for *PVsyst*. However it was shown that *PVsyst* models the front side irradiance with greater accuracy with corresponding RMSE values of 46.98 W/m^2, where the ray tracing method yielded a RMSE of 64.29 W/m^2. The energy output of *PVsyst* was less accurate when comparing it's RMSE of 1.62 kWh with the ray tracing and effective one-diode model RMSE of 1.32 kWh.

6.4 Bifacial PV design recommendations

After simulating various design parameters and analysing their effects on bifacial energy output and bifacial gain, it is possible to make some recommendations with regards to bifacial PV design. From the simulation results it is clear that the primary driver in maximising bifacial energy performance is the enhancement of the reflective surface surrounding the bifacial PV installation. This can be done by increasing the module height, ground surface albedo and row spacing. It would be very beneficial to study the overall financial benefits of such optimisation with regards to costs for additional structures, maintaining a certain albedo and losing effective surface area with an increase in row spacing. Some design consideration must kept in mind with regards to increased losses for increased cable lengths, increased wind loading and maintenance complexities for higher mounting structures etc.

Overall, it is of great importance to prevent obstructing the rear side of bifacial PV modules with wiring and other plant equipment such as mounting structure, combiner boxes and inverters. It must be kept in mind that the front side of a bifacial module remains the primary power source and care must be taken when optimising for the rear side irradiance. Rear side irradiance optimisation must be done without the expense of the front side irradiance. With regards to simulation of bifacial PV, it is evident that commercial tools such as *PVsyst* lacks in some areas of rear side irradiance modelling. It might

be of great interest to somehow combine the effectiveness of ray tracing's rear side irradiance modelling capabilities with the effectiveness of *PVsyst*'s front irradiance and electrical modelling.

6.5 Recommendations

As bifacial PV is a relatively new renewable energy source, there are many opportunities for further research and investigation into the technology. As it was shown that ray tracing can accurately model the rear side irradiance of bifacial modules, it lacks in accuracy with regards to the front side irradiance. It might be of interest to investigate the possibility of combining view factor modelling for the front side irradiance with ray tracing for the rear side irradiance. Another uncertainty regarding bifacial PV, is the effects of temperature on the performance of bifacial modules. By studying the temperature effects, it may be possible to improve the electrical modelling accuracy of bifacial PV modules. One question that begs to be answered: Is bifacial PV more profitable than monofacial PV? An in depth cost benefit analysis would be very beneficial for the future of bifacial PV.

Appendices

Appendix A

PVsyst simulation report

PVSYST V6.85	Scatec Solar (South Africa)	20/01/20	Page 1/6

Grid-Connected System: Simulation parameters

Project : **Bifacial**

Geographical Site	**SUN - Stellenbosch University**			Country	**South Africa**
Situation		Latitude	-33.93° S	Longitude	18.87° E
Time defined as		Legal Time	Time zone UT+2	Altitude	119 m
		Albedo	0.20		
Meteo data:		**Elsenburg**	Custom file - Imported		

Simulation variant : **Rear side irr**

	Simulation date	20/01/20 15h56

Simulation parameters		System type	**Trackers single array, with backtracking**		
Tracking plane, tilted Axis		Axis Tilt	0°	Axis Azimuth	0°
Rotation Limitations		Minimum Phi	-60°	Maximum Phi	60°
		Tracking algorithm	Astronomic calculation		
Backtracking strategy		Nb. of trackers	4	Single array	
		Tracker Spacing	5.00 m	Collector width	2.03 m
Inactive band		Left	0.02 m	Right	0.02 m
Backtracking limit angle		Phi limits	+/- 65.3°	Ground cov. Ratio (GCR)	40.6 %
Models used		Transposition	Perez	Diffuse	Perez, Meteonorm
Horizon		Free Horizon			
Near Shadings		Linear shadings			
Bifacial system		Model	Unlimited trackers, 2D calculation		
		Tracker Spacing	5.00 m	Tracker width	2.07 m
		Backtracking limit angle	65.4°	GCR	41.4 %
		Ground albedo	20.0 %	Axis height above ground	1.00 m
		Module bifaciality factor	75 %	Rear shading factor	0.0 %
		Module transparency	0.0 %	Rear mismatch loss	10.0 %
User's needs :		Unlimited load (grid)			

PV Array Characteristics

PV module	Si-mono	Model	**LR6-72 BP 355 M Bifacial**		
Original PVsyst database		Manufacturer	Longi Solar		
Number of PV modules		In series	12 modules	In parallel	4 strings
Total number of PV modules		Nb. modules	48	Unit Nom. Power	355 Wp
Array global power		Nominal (STC)	**17.04 kWp**	At operating cond.	15.46 kWp (50°C)
Array operating characteristics (50°C)		U mpp	424 V	I mpp	37 A
Total area		Module area	**94.5 m²**	Cell area	84.7 m²
Inverter		Model	**SUN2000_42KTL**		
Original PVsyst database		Manufacturer	Huawei Technologies		
Characteristics		Operating Voltage	200-1000 V	Unit Nom. Power	42.0 kWac
Inverter pack		Nb. of inverters	2 * MPPT 25 %	Total Power	21 kWac
				Pnom ratio	0.81

PV Array loss factors

Thermal Loss factor		Uc (const)	29.0 W/m²K	Uv (wind)	0.0 W/m²K / m/s
Wiring Ohmic Loss		Global array res.	194 mOhm	Loss Fraction	1.5 % at STC

List of References

[1] K. Ratshomo and R. Nembahe, "South african energy sector report," 11 2018.

[2] "Renewables 2018, global status report." REN21, 2018.

[3] R. K. Joris Libal, *Bifacial Photovoltaics: Technology, Applications and Economics*. IET, 2019.

[4] "Global market outlook for solar power (2018-2022)." SolarPower Europe, 2018.

[5] L. Kreinin, N. Bordin, A. Karsenty, A. Drori, D. Grobgeld, and N. Eisenberg, "Pv module power gain due to bifacial design. preliminary experimental and simulation data," in *2010 35th IEEE Photovoltaic Specialists Conference*. IEEE, 2010, pp. 002 171–002 175.

[6] R. Guerrero-Lemus, R. Vega, T. Kim, A. Kimm, and L. Shephard, "Bifacial solar photovoltaics–a technology review," *Renewable and sustainable energy reviews*, vol. 60, pp. 1533–1549, 2016.

[7] S. Wenham, M. Green, M. Watt, and R. Corkish, *Applied Photovoltaics*. Earthscan, 2007.

[8] A. Asgharzadeh, T. Lubenow, J. Sink, B. Marion, C. Deline, C. Hansen, J. Stein, and F. Toor, "Analysis of the impact of installation parameters and system size on bifacial gain and energy yield of pv systems," in *2017 IEEE 44th Photovoltaic Specialists Conference (PVSC)*, 2017.

[9] I. Shoukry, J. Libal, R. Kopecek, E. Wefringhaus, and J. Werner, "Modelling of bifacial gain for stand-alone and in-field installed bifacial pv modules," *Energy Procedia*, vol. 92, pp. 600–608, 2016.

[10] M. Chiodetti, "Bifacial pv plants: performance model development and optimization of their configuration," 2015.

[11] A. S. Glassner, *An introduction to ray tracing*. Elsevier, 1989.

[12] H. Holst, M. Winter, M. R. Vogt, K. Bothe, M. KÃ¶ntges, R. Brendel, and P. Altermatt, "Application of a new ray tracing framework to the analysis of extended regions in si solar cell modules," *Energy Procedia*, vol. 38, pp. 86–93, 12 2013.

[13] S. A. Pelaez, C. Deline, S. M. MacAlpine, B. Marion, J. S. Stein, and R. K. Kostuk, "Comparison of bifacial solar irradiance model predictions with field validation," *IEEE Journal of Photovoltaics*, vol. 9, no. 1, pp. 82–88, Jan 2019.

[14] J. P. Singh, A. G. Aberle, and T. M. Walsh, "Electrical characterization method for bifacial photovoltaic modules," *Solar Energy Materials and Solar Cells*, vol. 127, pp. 136 – 142, 2014. [Online]. Available: http://www.sciencedirect.com/science/article/pii/S0927024814002165

[15] C. W. Hansen, J. S. Stein, C. Deline, S. MacAlpine, B. Marion, A. Asgharzadeh, and F. Toor, "Analysis of irradiance models for bifacial pv modules," in *Photovoltaic Specialists Conference (PVSC), 2016 IEEE 43rd.* IEEE, 2016, pp. 0138–0143.

[16] U. A. Yusufoglu, T. M. Pletzer, L. J. Koduvelikulathu, C. Comparotto, R. Kopecek, and H. Kurz, "Analysis of the annual performance of bifacial modules and optimization methods," *IEEE Journal of Photovoltaics*, vol. 5, no. 1, pp. 320–328, 2015.

[17] D. Riley, C. Hansen, J. Stein, M. Lave, J. Marion, and F. Toor, "A performance model for bifacial pv modules," in *44th IEEE Photovoltaic Specialist Conference*, 2017.

[18] R. Perez, P. Ineichen, R. Seals, J. Michalsky, and R. Stewart, "Modeling daylight availability and irradiance components from direct and global irradiance," *Solar energy*, vol. 44, no. 5, pp. 271–289, 1990.

[19] P. Ineichen, O. Guisan, and R. Perez, "Ground-reflected radiation and albedo," *Solar Energy*, vol. 44, no. 4, pp. 207 – 214, 1990. [Online]. Available: http://www.sciencedirect.com/science/article/pii/0038092X90901497

[20] Y. A. Cengel, *Heat Transfer: A Practical Approach*, 2nd ed. McGraw-Hill, 2003.

[21] "Frequently asked question about curve tracing," 2019. [Online]. Available: http://www.seawardsolar.com/userfiles/curve-tracing.php

[22] "Measurement of photovoltaic current-voltage characteristics." IEC - International Electrotechnical Commission, 2006.

[23] N. Badcock and L. Santoni, "Technical briefing note - bifacial pv technology," 2019.

[24] G. Arnoux, N. Bassi, V. Fakhfouri, and R. Ambigapathy, "Toward the standardisation of the power rating of bifacial solar devices." Presentation at 5th bifi PV workshop 2018, Denver, Colorado, 2018.

[25] V. Fakhfouri, "Iec 60904-1-2 draft: Measurement of current-voltage characteristics of bifacial photovoltaic devices." Presentation at 4th bifi PV workshop 2017, Konstanz, Germany, 2017.

[26] V. J. Chin, Z. Salam, and K. Ishaque, "Cell modelling and model parameters estimation techniques for photovoltaic simulator application: A review," *Applied Energy*, vol. 154, pp. 500–519, 2015.

[27] W. D. Soto, S. Klein, and W. Beckman, "Improvement and validation of a model for photovoltaic array performance," *Solar Energy*, vol. 80, no. 1, pp. 78 – 88, 2006. [Online]. Available: http://www.sciencedirect.com/science/article/pii/S0038092X05002410

[28] "Release notes 6.6x - pvsyst," 2019. [Online]. Available: https://www.pvsyst.com/release-notes-6-6x/

[29] "Bifacial systems," 2019. [Online]. Available: https://files.pvsyst.com/help/bifacial-systems.htm

[30] "Enhanced energy yield for pv systems using bifacial modules: simulation and model verification," 2017. [Online]. Available: http://bifipv-workshop.com/fileadmin/layout/images/Konstanz-2017/3-L.-Kunath-POLYSUN-Enhanced-energy-harvest-simulation.pdf

[31] "Bifacial view factor," 2019. [Online]. Available: https://github.com/NREL/bifacialvf

[32] "Bifacial radiance," 2019. [Online]. Available: https://github.com/NREL/bifacial_radiance

[33] "Radiance cookbook." jaloxa, 2014.

[34] Y. A. Mahmoud, W. Xiao, and H. H. Zeineldin, "A parameterization approach for enhancing pv model accuracy," *IEEE Transactions on Industrial Electronics*, vol. 60, no. 12, pp. 5708–5716, Dec 2013.

[35] "Lr6-72bp 350-370m." Longi Solar, 2018.

[36] E. Skoplaki and J. Palyvos, "Operating temperature of photovoltaic modules: A survey of pertinent correlations," *Renewable Energy*, vol. 34, no. 1, pp. 23 – 29, 2009. [Online]. Available: http://www.sciencedirect.com/science/article/pii/S0960148108001353

[37] D. Schneider, "Control algorithms for large scale, single axis photovoltaic trackers," in *Proceedings of the 16th International Student Conference on Electrical Engineering POSTER 2012*, Prague, Czech Republic, May 17 2012.

[38] R. J. Hyndman and A. B. Koehler, "Another look at measures of forecast accuracy," *International Journal of Forecasting*, vol. 22, no. 4, pp. 679 – 688, 2006. [Online]. Available: http://www.sciencedirect.com/science/article/pii/S0169207006000239

[39] J. Shuda, A. Rix, and M. T. Booysen, "Module-level monitoring of solar pv plants using wireless sensor networks," 01 2018.